Annual Report
Jahresbericht

2018

Walther–Meißner–Institut
für Tieftemperaturforschung

Bayerische Akademie der Wissenschaften

Contact:

Prof. Dr. Rudolf Gross
Walther–Meißner–Institut für Tieftemperaturforschung
Bayerische Akademie der Wissenschaften
and
Lehrstuhl für Technische Physik – E23
Technische Universität München

Address:

Walther–Meißner–Str. 8
D - 85748 Garching
GERMANY

Phone: +49 – (0)89 289 14201
Fax: +49 – (0)89 289 14206
e–mail: Rudolf.Gross@wmi.badw.de
www: http://www.wmi.badw.de

Secretary's Office and Administration:

Emel Dönertas

Phone: +49 – (0)89 289 14202
Fax: +49 – (0)89 289 14206
e–mail: Emel.Doenertas@wmi.badw.de
Sekretariat@wmi.badw.de

Andrea Hamitaga

Phone: +49 – (0)89 289 14205
Fax: +49 – (0)89 289 14206
e–mail: Andrea.Hamitaga@wmi.badw.de
Verwaltung@wmi.badw.de

Preface

Dear colleagues, friends, partners, and alumni of the Walther-Meißner-Institute (WMI),

our ***Annual Report 2018*** intends to provide you with an overview of our last year's scientific activities. It also contains statistical data, an overview of our teaching and public engagement activities, and information on recent developments in infrastructure and experimental facilities.

The Annual Report always is an excellent opportunity to reflect on the past year. In the past year, the WMI could reap the benefits of the hard work done in the years before. First, after the tedious application procedure for a new Cluster of Excellence within the ***German Excellence Strategy***, the new Cluster of Excellence *«Munich Center for Quantum Science and Technology» (MCQST)* was granted in September 2018 with a total budget of more than 50 million euro for the first seven-year funding period. The MCQST will start in January 2019 (see report on page 21 – 28) and will play an important role for the future WMI research program. Together with Immanuel Bloch and Ignacio Circac, Rudolf Gross of WMI is one of the spokespersons of MCQST. The strong involvement of WMI in the MCQST is a natural continuation of its strong research focus on solid state based quantum systems and its active participation in several projects related to quantum science & technology (see page 34–34). Second, the *«Zentrum für QuantumEngineering» (ZQE)* of the Technical University of Munich was granted in 2018 with the German Federal Government and the Free State of Bavaria sharing the costs of around 40 million euro for the new building on the Research Campus Garching. The application for this new central facility of TUM was triggered by Rudolf Gross, who early pointed out that the translation of quantum technologies into practical applications requires the close collaboration of natural sciences and engineering disciplines under one roof. Third, the EU Quantum Flagship project *«Quantum Microwave Communication and Sensing» (QMiCS)* was granted and already started in October 2018 (see report on page 31 – 32). QMiCS is a three-year project in the basic science pillar of the *«European Quantum Flagship»* and is coordinated by Frank Deppe of WMI. Finally, in the past year a new DFG Research Project on *«Pure Spin Currents in Oxide-Based Epitaxial Heterostructures»* has been granted and a project on *«Spin Dynamics of Hybrid Skyrmion-Magnon Solitons»* has been acquired within the new *DFG Priority Program 2137 «Skyrmionics: Topological Spin Phenomena in Real-Space for Applications»*.

In 2018, we could also reap the benefits of the major reconstruction measure with a total budget of more than 6 million euro, which has been planned since 2015 and implemented within the last two years (see page 13–17). This measure has been supplemented by a complete renovation of the mechanical workshop within a so-called «Kleine Baumaßnahme» with a total budget of 400 kEuro (see page 18). Although the construction work was very perturbing and the associated noise and mess was wearing on the nerves, our research activities have been continued and resulted in a number of high level publications (see page 97). The high impact of our research work is documented by more than 2 000 citations of WMI publications in 2018 (ISI Web of Science) and a large number of invited conference, colloquium and seminar talks (see page 121). As in previous years, WMI was active in organizing symposia, workshops and conferences to increase its international visibility (see page 113).

We have been successful again regarding the improvement of the technological infrastructure via third party funding. In 2018, equipment worth more than 1 million euro could be installed. Most importantly, supported by the BMBF research network *«Quantum Communication (Q.com)»*, the versatile laser writing system *PicoMaster 200* of the company 4PICO could be obtained and taken into operation early in 2018 (see page 73–74). Moreover, a new UHV sputtering system for large area superconducting thin films and heterostructures was delivered by the company Mantis Deposition ltd in November 2018 (see page 69–72) and taken into operation.

Due to the considerable time delays in the construction work, the WMI staff strongly suffered from noise and unforseen rearrangements also in 2018. I would like to thank all members of WMI for their inexhaustible patience, understanding and support! Only due to the strong commitment and persistence of everybody most part of our ambitious research programs could be implemented despite the unfavorable circumstances. Moreover, 5 bachelor, 18 master and 5 PhD theses were completed, while 9 master and 17 PhD students as well as 3 habilitation candidates are still ongoing with their work (see page 103).

The research program of WMI relies on the continuous support by various funding agencies. To this end, we gratefully acknowledge financial support from the BAdW, the DFG, the Bavarian Ministry for Science and Arts, the BMBF and the EU. An important key to success is the recruitment of outstanding, scientifically independent group leaders with complementary research interests and technical expertise. This process is monitored by the Scientific Advisory Board of WMI which has a strong commitment to support and promote young scientists in their career.

Finally, I would like to express my deep thanks and gratitude to all colleagues, guests, students, postdocs and cooperating partners, who contributed to our research and teaching activities within the past year, and last but not least to all our friends and sponsors for their interest, trust and continuous support. I hope that our Annual Report 2018 inspires your interest in WMI.

Garching, December 2018

Rudolf Gross

Contents

The Walther–Meißner–Institute

General Information

The ***Walther-Meißner-Institute for Low Temperature Research (WMI)*** was originally operated by the Commission for Low Temperature Research of the ***Bavarian Academy of Sciences and Humanities (BAdW)***. Between 2013 and 2015, the Bavarian Academy of Sciences and Humanities with its more than 300 employees was reorganized. With the passing of the new statutes in October 2015, the 36 Commissions (Research Groups) of the Academy — they were originally set up in order to carry out long-term projects, which are too ambitious for the lifetime or capacity of any single researcher, or which require the collaboration of specialists in various disciplines — were abolished. The research program of BAdW is now implemented in Academy Institutes (such as the Walther-Meißner-Institute or the Leibniz Supercomputing Center) and Academy Projects. The Academy Institutes and Projects are managed by the Institute and Project Committees and supervised by the Institute and Project Advisory Boards, respectively. In this way a clear separation between the managing bodies of the institutes/projects (responsible for the implementation of the research programs) and the corresponding supervisory bodies (responsible for the quality control) was established. To this end, also the Commission for Low Temperature Research was dissolved and replaced by the WMI Committee and the WMI Advisory Board in 2015.

The historical roots of WMI go back to ***Walther Meißner***. He founded the Commission for Low Temperature Research in 1946 when he was president of BAdW (1946 – 1950). The first research activities then were started in 1946 in the Herrsching barracks. After the retirement of Walther Meißner in 1952, Heinz Maier-Leibnitz, who followed Walther Meißner on the Chair for Technical Physics of the Technische Universität München, became the new head of the Commission for Low Temperature Research. In 1967, the commission moved to the Garching research campus after the construction of the new *«Zentralinstitut für Tieftemperaturforschung»* (ZTTF) was completed (director: Prof. Heinz Maier-Leibnitz, technical director: Prof. Franz Xaver Eder). Until 1972, the theory group of the Institute Laue Langevin was hosted at the ZTTF with prominent members such as Peter Fulde. In 1980, Prof. Dr. Klaus Andres became the new director of the ZTTF again associated with the Chair for Technical Physics (E23) at the Technical University of Munich (TUM), followed by Prof. Dr. Rudolf Gross in 2000. In 1982, the ZTTF was renamed into Walther-Meißner-Institute for Low Temperature Research (WMI) on the occasion of Walther Meißner's 100. birthday.

Starting from 2000, the so far unused basement of the WMI building was made available for technical infrastructure (airconditioning, particulate airfilters, pure water system etc. for clean room) and additional laboratory space. Fortunately, in 2008 WMI succeeded in getting extra money from the state government within the so-called *«Konjunkturpaket II»*. This money has been used to establish the new *«WMI Quantum Science Laboratory»* in the basement of the building, providing about 150 m^2 additional laboratory space particularly suited for low temperature facilities and ultra-sensitive studies on solid state quantum systems. The WMI Quantum Science Laboratory was fully operational early in 2011 and meanwhile hosts three new mK systems and sophisticated experimental techniques for the study of solid state based quantum systems and circuits. In 2016, the Bavarian Ministry for Science and Arts granted more than 6 Mio. Euro for redevelopment measures regarding the technical infrastructure, safety requirements and energy efficiency. An important part of the building project implemented in 2017/18 was the reconstruction of the entrance area and the main staircase, providing now direct access to the new WMI Quantum Laboratories in the basement of the WMI building as well as additional communication areas and meeting rooms in the ground floor. Moreover, it included the replacement of all windows and doors, the upgrade of the technical

infrastructure for cooling water, air conditioning, liquid nitrogen and helium storage, as well as the complete redevelopment of the mechanical workshop and various safety measures.

As already mentioned, it is a long tradition that WMI hosts the Chair for Technical Physics (E 23) of TUM with the director of the WMI being a full professor at the Faculty of Physics of TUM. In general, WMI has established tight links to research groups of both Munich universities, joining technological and human resources in the fields of experimental and theoretical solid-state and condensed matter physics, low temperature techniques, materials science as well as thin film and nanotechnology. Noteworthy, the WMI supplies liquid helium to more than 25 research groups at both Munich universities and provides the technological basis for low temperature research.

Important Discoveries

The WMI looks back on a long history of successful research in low temperature physics. In the following we list some important discoveries as well as experimental and technical developments made at WMI:

- **1961: discovery of flux quantization in multiply connected superconductors**
  (R. Doll, M. Näbauer, *Experimental Proof of Magnetic Flux Quantization in a Superconducting Ring*, Phys. Rev. Lett. **7**, 51-52 (1961)).
- **1986: discovery of an anomalous temperature dependence of the penetration depth in UBe_{13}**
  (F. Gross, B.S. Chandrasekhar, D. Einzel, K. Andres, P.J. Hirschfeld, H.R. Ott, J. Beuers, Z. Fisk, J.L. Smith, *Anomalous Temperature Dependence of the Magnetic Field Penetration Depth in Superconducting UBe_{13}*, Z. Physik B - Condensed Matter **64**, 175-188 (1986)).
- **1992: discovery the intrinsic Josephson effect**
  (R. Kleiner, F. Steinmeyer, G. Kunkel, and P. Müller, *Intrinsic Josephson Effects in $Bi_2Sr_2CaCu_2O_8$ Single Crystals*, Phys. Rev. Lett. **68**, 2394-2397 (1992)).
- **2002: development of dilution refrigerators with pulse tube refrigerator precooling**
  (K. Uhlig, *$^3He/^4He$ Dilution Refrigerator with Pulse Tube Precooling*, Cryogenics **42**, 73-77 (2002)).
- **2010: first demonstration of ultrastrong coupling in superconducting circuit quantum electrodynamics**
  (T. Niemczyk, F. Deppe, H. Huebl, E. P. Menzel, F. Hocke, M. J. Schwarz, J. J. Garcia-Ripoll, D. Zueco, T. Hümmer, E. Solano, A. Marx, R. Gross, *Circuit Quantum Electrodynamics in the Ultrastrong-Coupling Regime*, Nature Physics **6**, 772-776 (2010)).
- **2010: development of dual path method for state tomography of propagating quantum microwaves**
  (E.P. Menzel, M. Mariantoni, F. Deppe, M.A. Araque Caballero, A. Baust, T. Niemczyk, E. Hoffmann, A. Marx, E. Solano, R. Gross, *Dual-Path State Reconstruction Scheme for Propagating Quantum Microwaves and Detector Noise Tomography* , Phys. Rev. Lett. **105**, 100401 (2010)).
- **2012: first realization of path entanglement of propagating quantum microwaves**
  (E. P. Menzel, R. Di Candia, F. Deppe, P. Eder, L. Zhong, M. Ihmig, M. Haeberlein, A. Baust, E. Hoffmann, D. Ballester, K. Inomata, T. Yamamoto, Y. Nakamura, E. Solano, A. Marx, R. Gross, *Path Entanglement of Continuous-Variable Quantum Microwaves*, Phys. Rev. Lett. **109**, 250502 (2012)).
- **2013: discovery of the spin Hall magnetoresistance** (jointly with partners at Tohoku University and TU Delft)
  (H. Nakayama, M. Althammer, Y.-T. Chen, K. Uchida, Y. Kajiwara, D. Kikuchi, T. Ohtani, S. Geprägs, M. Opel, S. Takahashi, R. Gross, G. E. W. Bauer, S. T. B. Goennenwein, E. Saitoh, *Spin Hall Magnetoresistance Induced by a Non-Equilibrium Proximity Effect*, Phys. Rev. Lett. **110**, 206601 (2013)).

- **2013: first demonstration of strong magnon-photon coupling**
  (H. Huebl, Ch. Zollitsch, J. Lotze, F. Hocke, M. Greifenstein, A. Marx, R. Gross, S.T.B. Goennenwein, *High Cooperativity in Coupled Microwave Resonator Ferrimagnetic Insulator Hybrids*, Phys. Rev. Lett. **111**, 127003 (2013)).
- **2017: first experimental observation of the spin Nernst effect**
  (S. Meyer, Yan-Ting Chen, S. Wimmer, M. Althammer, S. Geprägs, H. Huebl, D. Ködderitzsch, H. Ebert, G.E.W. Bauer, R. Gross, S.T.B. Goennenwein, *Observation of the spin Nernst effect*, Nature Materials **16**, 977-981 (2017)).

Present Research Activities

The research activities of the Walther-Meißner-Institute are focused on low temperature condensed matter physics (see reports below). The research program is devoted to both **fundamental** and **applied research** and also addresses **materials science, thin film and nanotechnology** aspects. With respect to **basic research** the main focus of the WMI is on

- quantum phenomena and quantum coherence in solid state systems,
- superconductivity and superfluidity,
- magnetism, including spin transport, spin dynamics, spin mechanics and spin caloritronics,
- circuit quantum electrodynamics and circuit electro-nanomechanics,
- ordering and emergent phenomena in correlated quantum matter,
- and the general properties of metallic systems at low and very low temperatures.

The WMI also conducts **applied research** in the fields of

- solid-state quantum information processing and quantum communication systems,
- superconducting and spin-based devices,
- multi-functional and multiferroic materials,
- and the development of low and ultra-low temperature systems and techniques.

With respect to **materials science, thin film and nanotechnology** the research program is focused on

- the synthesis of superconducting and magnetic materials,
- the single crystal growth of oxide materials,
- the thin film technology of complex superconducting and magnetic heterostructures, including multi-functional and multi-ferroic material systems,
- and the fabrication of superconducting, magnetic and hybrid nanostructures.

The WMI also develops and operates systems and techniques for low and ultra–low temperature experiments. A successful development have been dry mK-systems that can be operated without liquid helium by using a pulse-tube refrigerator for precooling. In the early 2000s, these systems have been successfully commercialized by the company VeriCold Technologies GmbH at Ismaning, Germany, which was taken over by Oxford Instruments in 2007. As a further typical example we mention very flexible dilution refrigerator inserts for temperatures down to about 20 mK fitting into a 2 inch bore. These systems have been engineered and fabricated at WMI. Within the last years, several dilution refrigerators have been provided to other research groups for various low temperature experiments. WMI also operates a helium liquifier with an annual capacity of above 180.000 liters and supplies both Munich universities with liquid helium. To optimize the transfer of liquid helium into transport containers, WMI has developed a pumping system for liquid helium that is commercialized in collaboration with a company.

To a large extent the research activities of WMI are integrated into national and international research projects such as Clusters of Excellence, Collaborative Research Centers, Research Units, or EU projects. The individual research groups of WMI offer a wide range of attractive research opportunities for bachelor and master students, Ph.D. students and postdoctoral fellows.

Experimental Facilities and Resources

The WMI is equipped with state of the art facilities for the preparation and characterization of superconducting and magnetic materials as well as for various low and ultra–low temperature experiments. The main experimental and technological resources of WMI are listed in the following.

Materials Preparation and Fabrication of Nanostructures

- Laser Molecular Beam Epitaxy (L-MBE) system for oxide heterostructures (equipped with in–situ RHEED, Omicron AFM/STM system, atomic oxygen/nitrogen source, infrared-laser heating system, metallization). The L-MBE systems is connected to a UHV magnetron sputtering systems for metals (e.g. Nb, Al, NiPd, ...) and an electron beam deposition system via a UHV transfer chamber
- molecular beam epitaxy (MBE) system for metals
- UHV cluster tool consisting of two magnetron sputter deposition systems for superconducting and magnetic heterostructures, respectively, and a load lock
- UHV magnetron sputtering system for large-area deposition of superconducting thin films and heterostructures
- reactive ion etching (RIE) system, Plasmalab 80 Plus with ICP plasma source, Oxford Instruments Plasma Technology
- ion beam etching (IBE) system equipped with a LN_2 cooled sample holder
- automated critical point dryer Leica EM CPD 300
- polishing machine for substrate preparation
- ultrasonic bonding machine
- 50 m^2 class 1000 clean room facility
- maskless lithography UV Direct Laser Writer, PicoMaster 200 UV of the company 4PICO, The Netherlands
- 100 kV nB5 Electron Beam Lithography System by NanoBeam Limited, UK, with 6 inch laser stage
- optical lithography (Süss maskaligner MJB 3 and projection lithography)
- four-mirror image furnace for crystal growth

Characterization

- 2–circle x–ray diffractometer (Bruker D8 Advance, sample temperature up to 1 600°C)
- high resolution 4–circle x–ray diffractometer with Göbel mirror and Ge monochromator (Bruker D8 Discover)
- Philips XL 30 SFEG scanning electron microscope with EDX analysis
- UHV room temperature AFM/STM system
- two Raman spectroscopy systems (1.5 to 300 K, in-situ sample preparation)
- tip-enhanced Raman spectroscopy (TERS) system
- SQUID magnetometer (Quantum Design, 1.5 to 700 K, up to 7 T)
- several high field magnet systems (up to 17 T Tesla) with variable temperature inserts

- 7 T split coil magnet systems with optical access and variable temperature insert
- 3D vector magnet (2/2/6 Tesla) with variable temperature inserts
- experimental set–ups for the measurement of noise including low noise SQUID amplifiers and signal analyzers
- high-frequency network analyzers (up to 40 GHz) and various microwave components (sources, mixers, circulators, attenuators) for the determination of high frequency parameters
- ultra-sensitive microwave receiver for state tomography of quantum microwaves (dual path method with FPGA signal processing)
- high-frequency cryogenic probing station (up to 20 GHz, $T > 4$ K)
- magnetooptical Kerr effect (MOKE) system
- broadband ferromagnetic resonance (FMR) system

Low temperature systems and techniques

- several ^{3}He/^{4}He dilution refrigerator inserts for temperatures down to 10 mK
- "dry" mK-cooler based on a dilution refrigerator with pulse-tube precooling and equipped with a large number of microwave lines and cold electronics (e.g. amplifiers, circulators, attenuators, directional couplers) for ultra-sensitive experiments on solid state quantum systems
- "dry" dilution refrigerator with a base temperature of about 10 mK equipped with a 3D vector magnet (1/1/6 Tesla)
- "wet" mK-cooler based on a dilution refrigerator liquid helium precooling and equipped with a large number of microwave lines and cold electronics (e.g. amplifiers, circulators, attenuators, beam splitters) for time-domain microwave experiments on solid state quantum systems
- experimental set–ups for the measurement of specific heat, magnetization, thermal expansion as well as electrical and thermal transport properties as a function of temperature, magnetic field and pressure

Building Projects

General Redevelopment of the WMI Building and Infrastructure

Rudolf Gross, Achim Marx

Figure 1: View on the cross-aisles and new main staircase of the WMI building as seen from the inner courtyard.

The Bavarian Ministry for Science and Arts granted in total about 6.5 Mio. Euro to the Walther-Meißner-Institute (WMI) for general redevelopment measures regarding the technical infrastructure, safety requirements and energy efficiency. The planning stage of this extensive building project was completed late in 2016 and the construction work started in May 2017. The initial plan was to finish the building project already until Christmas 2017. However, due to a significant lack in coordination, missing professionalism of the involved companies as well as unforseen delays due to technical reasons und the problem that several companies did not meet their time schedule, the redevelopment measure could not be completely implemented until Christmas 2018. Some minor residual work, such as the installation of a new transformer station, has to be shifted to 2019. The fact that the completion of the whole building project took more than three times as long as expected was very unfortunate for the WMI research activities. Laboratory rooms could not be used for an extended period of time and experiments have been often perturbed by the ongoing construction work. This was nerve-shattering and perturbing for everybody. However, meanwhile it becomes evident and also clearly visible that the redevelopment measure has been a large success and will have a large future benefit for WMI.

The building project included the following specific measures:

- extension of the main staircase of the WMI building to the basement and redesignment of the front entrance
- replacement of all windows and office/laboratory doors
- equipping the WMI laboratories with air conditioning systems, including the installation of a central refrigeration unit in the basement
- installation of a new chemical laboratory
- redevelopment and replacement of the helium recovery system and the liquid nitrogen tank
- installation of a new transformer station to increase the power handling capability of the electric power system.

Historical Context

The first redevelopment of the WMI building, which has been established in 1967, took place between 2000 and 2003. At that time besides the general renovation of most office and laboratory rooms the key measures have been

- the installation of the WMI clean room and thin film laboratories
- the installation of the WMI crystal growth laboratory
- the redevelopment of the WMI seminar and library rooms
- the replacement of the electrical power system
- the installation of a glas fibre network and server computers.

Starting from 2000, the so far unused basement of the WMI building was made available for technical infrastructure (airconditioning, particulate airfilters, pure water system etc. for the clean room) and additional laboratory space. However, the extension to the full basement – although originally planned – was not possible until 2003 due to the limited budget.

Fortunately, in 2008 WMI succeeded in getting extra money from the state government within the so-called «*Konjunkturpaket II*». These funds have been used to establish the new «*WMI Quantum Science Laboratory*» in the basement of the building, providing about 150 m^2 of additional laboratory space particularly suited for low temperature facilities and ultra-sensitive studies on solid state quantum systems. The WMI Quantum Science Laboratory was fully operational early in 2011 and meanwhile hosts three new mK systems and sophisticated experimental techniques for the study of solid state based quantum circuits and systems.

Extension of the Main Staircase and Redesignment of the Front Entrance

Since the completion of the «*WMI Quantum Science Laboratory*» in 2011, the basement of the WMI was fully usable and hosts a lot of laboratory space. Nevertheless, the access to the basement via the main staircase at the north side of the WMI building was not possible and only a temporary access was established via the safety exits at the east and west side of the building. Therefore, the extension of the main staircase down to the basement was urgently required. For the implementation of this measure the old staircase tower (see Fig. 2, top left) was torn down and replaced by a new structure (see Fig.2, top right).

Figure 2: The main staircase of WMI and the cross-aisles at the north side of the WMI building before and after the reconstruction.

Figure 3: Impressions from the new staircase, the cross-aisles and front entrance of WMI.

This major change of the building structure not only allowed us to combine the staircase extension with a general redesignment of the front entrance (see Fig.3) but also to change of the fire rescue path. Since the cross-aisles in the basement and the first floor are no longer part of the fire exit path, they can now be used for sitting areas or to show exhibits. In addition, the aisles along the long side of the building received new safety exits directly to the Walther-Meißner street and the main entrance was raised to avoid stairs inside the building and to adopt the entrance to the needs of people with disabilities.

As a particular benefit of the extension of the main staircase and redesignment of the front entrance WMI obtained a new communication area and a new meeting room on the ground floor level close to the front entrance. With the steadily increasing number of students and guests these rooms have been urgently needed. The meeting room has been named ***«Walther-Meißner»*** and is equipped with state-of-the-art media technology for presentations, teaching and web meetings. In addition, WMI obtained a new changing room with showers for the technical staff in the basement.

Figure 4: The new meeting room «Walther-Meißner» in the ground floor of the WMI building.

Figure 5: The new refrigerating compressor installed in the basement of the WMI building (left) and the cooling water distribution system (right).

Replacement of the Windows and Office/Laboratory Doors

The replacement of all windows as well as all doors of the laboratory and office rooms in the WMI building has been completed in 2018. Besides a better thermal insulation the new windows have integrated venetian blinds and a small window part allowing for a permanent ventilation (e.g. during the night) what is particularly important in the hot summer period. The new doors are equipped with an electronic locking system and meet the present safety standards.

Airconditioning Systems for the Laboratory Rooms

The laboratory rooms of WMI have been equipped with airconditioning systems. This measure was urgently required and has been fully completed in 2018. It was unavoidable since the increased installed electrical power in some laboratories resulted in intolerable temperatures over the summer period. Moreover, an increasing number of sensitive experiments requires temperature stabilization.

For supplying the required cooling power, a new refrigerating compressor has been installed in the basement at the south end of the WMI building (see Fig. 5). For this purpose the respective part of the basement has been completely redone and a new outside door has been introduced, which allows now for an easy direct access to the basement area. This is particularly useful for the installation of the refrigerating compressor and other big machines in the basement. Moreover, the old chiller has been removed from the inner courtyard and a new chiller has been installed on the roof of the WMI building. For this installation, the roof construction has been locally reinforced.

Installation of a New Chemical Laboratory

The chemical laboratory in the ground floor of the WMI building has been newly laid out and rebuilt from scratch.

Figure 6: The new liquid nitrogen tanks and new storage vessels for ultra-pure helium gas (left) as well as the new high pressure storage containers for the recovered helium gas (right).

Replacement of the Helium Recovery System and the Liquid Nitrogen Tank

The replacement of the high pressure storage containers for the recovered helium gas and the liquid nitrogen tank have been completed and both systems are already in operation. Furthermore, new storage vessels for ultra-pure helium gas needed for the starting phase of the liquifier have been installed and are also in use. With the new containers for the recovered helium gas we could increase the storage capacity of helium gas. This makes us less susceptible to supply shortages and strong fluctuations of the market price of liquid helium.

Installation of a New Transformer Station

The installation of a new transformer station for increasing the power handling capability of the WMI electric power system has been postponed several times due to planning mistakes of the Staatliches Bauamt München 2. Meanwhile, the transformer station and one of the required transformers have been delivered (see Fig. 7). The second transformer and the cables connecting to the power distribution box in the WMI building will be hopefully installed early in 2019. The change from a low to medium voltage connection reduces the required cross-sectional area of the underground cables considerably and removed the problem of missing space in the cable duct.

Figure 7: The new transformer station positioned at the south-west corner of the WMI building.

Renovation and Modernization of the Mechanical Workshop

Rudolf Gross, Achim Marx

The Mechanical Workshop of the Walther-Meißner-Institute has not been renovated since the completion of the WMI building in 1967. Therefore, it was high time to start redevelopment and modernization measures. Fortunately, the Bavarian Ministry for Science and Arts granted 400 kEuro for 2018 within a so-called *«Kleine Baumaßnahme»* to implement this plan. Besides some minor residual work, the redevelopment and modernization measures have been completed in 2018. The key parts have been

- the replacement of the workshop floor
- the complete replacement of the electrical power and lighting installation
- the movement of the stockroom to the basement
- the rearrangement of the machine park and the office of the workshop manager
- the almost complete replacement of the furnishings.

The measure also included the replacement of the floor in the aisle in front of the workshop area.

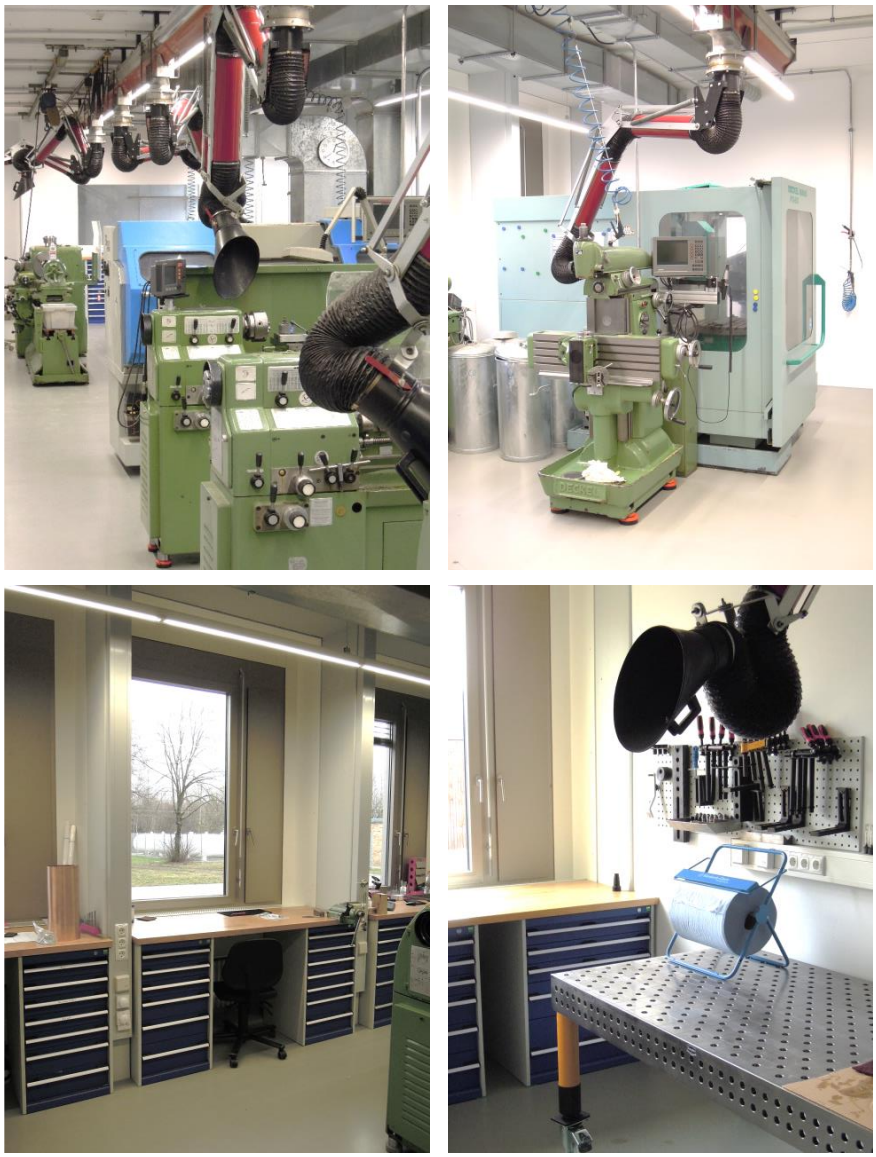

Figure 1: Some views of the mechanical workshop after the renovation and modernization measure.

Joint Research Projects

Clusters of Excellence

Rudolf Gross

From the «Excellence Initiative» to the «Excellence Strategy»

The past few years were considerably influenced by the discussion of new proposals for Clusters of Excellence within the *German Excellence Strategy*, which aims to strengthen Germany's position as an outstanding place for research and to further improve the international competitiveness of German universities. The *Excellence Strategy* was designed to continue the *German Excellence Initiative*, which has been started in 2005 by supporting research of the highest standard, enhancing research profiles, and facilitating cooperation in the research system. On the basis of the administrative agreement reached by the federal and state governments on 16 June 2016, the DFG and the German Council of Science and Humanities implemented the *Excellence Strategy* in two funding lines:

1. **Clusters of Excellence** for project-based funding in internationally competitive fields of research at universities or university consortia,
2. **Universities of Excellence** to strengthen universities as individual institutions or as university consortia in the long term and further develop their leading international role on the basis of successful Clusters of Excellence.

The WMI has been a founding member and one of the key institutions of the Cluster of Excellence *«Nanosystems Initiative Munich» (NIM)* since it was established in 2006 within the *Excellence Initiative*. The WMI has been also a key player in establishing the new Cluster of Excellence ***«Munich Center for Quantum Science and Technology» (MCQST)***. The first seven-year funding period of MCQST has been granted in September 2018.

A. The «Nanosystems Initiative Munich» (NIM)

The second funding period of the Cluster of Excellence *«Nanosystems Initiative Munich» (NIM)* ended in December 2018. NIM will not receive further funding within the new program named *«Excellence Strategy»* starting in 2019.

NIM was established in 2006 within the *Excellence Initiative*. After a successful first funding period (10/2006 – 09/2012), a second five-year funding period (10/2012 – 09/2017) was granted. This second funding period has been further extended until December 2018. The NIM Cluster of Excellence developed into one of the world's leading nanoscience research centers and, without any doubt, was a big success. NIM researchers were able to design, fabricate and control multi-functional nanosystems for applications in information technology, energy conversion and medical technologies. NIM brought together researchers from the Munich area specialized in physics, biophysics, physical chemistry, biochemistry, pharmacy, biology, electrical engineering and medicine. The WMI was

permanently contributing to the highly successful NIM cluster mainly in the NIM Research Areas on «*Quantum Nanophysics*» and «*Hybrid Nanophysics*» . Hans Hübl and Sebastian Gönnenwein of WMI were Principal Investigators and Frank Deppe was an Associate Member. Rudolf Gross was both member of the NIM Executive Board and coordinator of the Research Area 1 on «*Quantum Nanophysics*» over the full twelve-year funding period of NIM.

As already discussed in the Annual Report 2017, the NIM Executive Board decided not to submit a proposal for a third funding period of NIM within the Excellence Strategy. Instead, it was decided to support the creation of three new and much more focussed cluster initiatives emerging out of the NIM Research Areas 1, 3 and 4 with the focus on quantum science & technology, energy conversion, and synthetic biology, respectively. After a lengthy internal selection procedure all three cluster initiatives created out of NIM were considered promising by the university boards of both Munich universities and letters of intent for joint initiatives have been submitted to the German Research Foundation in November 2016. In turn, three draft proposals were emerging out of the NIM Research Areas 1, 3 and 4 and have been submitted to the DFG Head Office until the cut-off date of 3 April 2017:

1. **Munich Center for Quantum Science and Technology (MCQST)**
2. **e-conversion**
3. **BioDesign**.

In total, 195 draft proposals for Clusters of Excellence (Munich: 3 TUM, 5 LMU, 5 joint TUM/LMU proposals) have been submitted and reviewed by international expert panels. The comparative assessment of the review results formed the basis for the decisions made by a Committee of Experts in September 2017 as to which 88 cluster initiatives (Munich: 1 TUM, 1 LMU, 4 joint TUM/LMU proposals) have been invited to submit full proposals. Two of the tree NIM-emerging proposals made it to the next round. Only the proposal «Biodesign» failed. This means that NIM provided the scientific basis and key PIs to one third of the successful clusters proposals of the two Munich universities. The full proposals for the first seven-year funding period of MCQST and e-conversion have been reviewed in 2018 and fortunately both clusters were granted on 27th September 2018. The first funding period will start on 1st January 2019.

Although the nanoscience oriented cluster «*Nanosystems Initiative Munich*» will no longer receive funding within the Excellence Strategy, there is still strong interest in nanoscience and nanotechnology at both Munich universities and also at WMI. At all institutions the core research activities on nanoscience and nanotechnology will be continued and the key research facilities of NIM will be maintained. Most importantly, the nanoscience facilities represent a key infrastructure for the new clusters MCQST and e-conversion. Besides a transition phase funding provided by DFG until October 2019, NIM will receive further support from the State of Bavaria and both Munich universities (25% of the original budget) to keep the Munich nanotechnology platform alive and maintain the state-of-the-art nanotechnology facilities build up within NIM.

NIM Seed Funding

The WMI was successful in attracting NIM seed funding for two high-risk projects. The seed funding proposals have been reviewed by the NIM Scientific Advisory Board in November 2017 and started in 2018.

Within the project «***Multi-Photon Scattering Tomography with Propagating Quantum Microwaves***» (Gross, Deppe) we started to do multi-photon scattering on quantum systems. As superconducting quantum circuits based on nanoscale Josephson junctions have developed

into a key hardware platform in the field of quantum science and technology, the quantum properties of the microwave signals emitted from these circuits have become an important research field. The related experiments can be subdivided into two major groups. In one of them, the focus is put onto the implementation of continuous-variable quantum protocols. This field has been pioneered by WMI within the past decade and led to the recently granted EU Quantum Technology Flagship Project «***Quantum Microwave Communication and Sensing***», which is coordinated by WMI (see report on page 31). The second group of experiments aims at realizing scattering experiments on a quantum system using either microwave photons in a discrete-variable description or quasi-classical coherent states as probe signals. This set of experiments is strongly related to the concepts governing the generation, manipulation, and detection of photons in the optical regime and is therefore often referred to as microwave quantum photonics. In this context, WMI started to study the scattering properties of artificial superconducting atoms (superconducting quantum bits) in a transmission line and in a superconducting Mach-Zehnder interferometer (see Fig. 1). In both cases, the qubit has been successfully used to extract information about the broadband, but controlled environment.

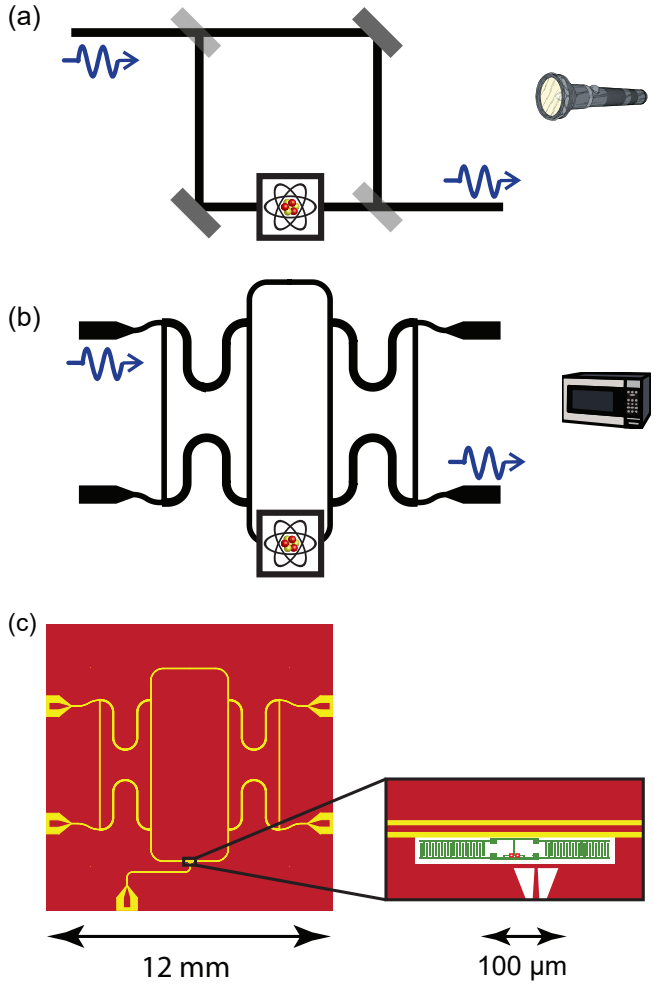

Figure 1: Schematics of (a) an optical and (b) a microwave Mach–Zehnder interferometer with an artificial atom placed in one of the interferometer arms. (c) Layout of the composite chip. The close-up on the right shows the transmon qubit with a tuneable Josephson junction formed by a dc-SQUID. The positions of the two SQUID junctions are marked with red rectangles.

So far all experiments on quantum scatterers are well described by resonant (single photon) scattering theory. Within the NIM seed funding project we move beyond such simple scenarios and towards fundamentally novel grounds: The investigation of multi-photon scattering at a quantum system, where each photon is strongly off-resonant. Specifically, we aim at the experimentally relevant challenge of determining multi-photon scattering matrix elements using only coherent states as inputs and simple quadrature measurements at the outputs. To this end, we combine already existing platforms and techniques, namely our superconducting on-chip interferometer with the correlation-based dual-path detector developed at WMI. In the simplest case, the scatterer placed in one of the interferometer arms is a single transmon qubit. In such a scenario, theory predicts that one can directly measure the two-photon scattering matrix element, essentially by recording the first-order correlation function between the two interferometer outputs. It is a key goal of this seed-funding project to measure such scattering matrix element for the first time.

Since direct reconstructions of the multi-photon scattering matrix elements have not even been realized in the optical regime yet, our experiments promise to add a fundamentally new tool to photonics in general. With respect to superconducting circuits, the proposed project presents an

important step towards more advanced scenarios such as quantum computing with propagating microwaves in the spirit of all-optical quantum computing. Here, gates based on two-photon scattering promise a deterministic approach with a strongly reduced loss of photon indistinguishability due to the distortion of the propagating wave packet.

In a second seed funding project «***Quantum Sounds on Nanostrings***» (Hübl, Gross) we combine a circuit QED setup with a nano-mechanical, doubly-clamped string resonator to (i) swap non-classical photonic states to the nano-string resonator, (ii) store complex phononic quantum states in the mechanical element, and (iii) determine the mechanical lifetime of the phononic quantum state by swapping it back to the microwave domain. Realizing this approach represents a major step towards generating/storing quantum states in mechanical elements and will have an important impact for the realization of quantum-enhanced mechanical sensing applications. A key requirement for implementing this approach is to establish strong coupling between the mechanical and the circuit QED subsystems, allowing for fast state swapping. It is the key goal of this seed-funding project to establish such strong coupling and thereby pave the way to a variety of interesting quantum experiments and sensing applications.

NIM Conference «The Future of Nanoscience»

The conference *«The Future of Nanoscience»* took place at the Evangelische Akademie Tutzing from September 4 to 6, 2018. It was is intended to celebrate the successes of twelve years of NIM and to look into the future of nanosciences. To this end we invited leading protagonists of all research areas of NIM as speakers. In addition, successful NIM alumni provided their input. Moreover, we also organized a poster session for PhD students. In a technology transfer session, we provided a forum for NIM spin-off companies. Finally, an evening panel discussion entitled *«Quo Vadis Nanoscience»* with the well-known opinion leaders Christian Kehrt (TU Braunschweig), Harald Lesch (LMU Munich), Robert Schlögl (MPI CEC Mühlheim), and Petra Schwille (MPI Biochemistry Munich) was arranged for the public. The discussion was presented by Jörg P. Kotthaus (LMU Munich) and Gerhard Abstreiter (TUM). The event was complemented by a boat tour with conference dinner on the picturesque Starnberger See.

NIM Research Activities

As in previous years, also in 2018 the WMI research activities strongly profited from NIM. Some of our recent results are presented in several contributions to this Annual Report. They range from the field of superconducting quantum circuits, hybrid quantum systems, electro-nanomechanical systems, to spin dynamics, spin caloritronics and the study of physics related to pure spin currents.

B. The «Munich Center for Quantum Science and Technology» (MCQST)

The new Cluster of Excellence ***«Munich Center for Quantum Science and Technology» (MCQST)*** has been granted on 27th September 2018 within the ***German Excellence Strategy***. The first seven-year funding period will start on 1st January 2019. The cluster will be coordinated by the three spokespersons Immanuel Bloch (LMU Munich and MPQ), Ignacio Cirac (MPQ and TUM) and Rudolf Gross (TUM and BAdW) and joins groups from the LMU Munich, the Technical University of Munich, the Max Planck Institute of Quantum Optics, the Walther-Meißner-Institute and the German Science Museum. The acquisition of the new Cluster of Excellence has been a great success and will push the Munich research activities on quantum science and technology to a new level. It allows Munich to become an internationally leading center in one of the most interesting research and technology field.

The application procedure for the new cluster has been lengthy and time-consuming. The first proposal for a new excellence cluster with the preliminary title *«Quantum Science, Technology & Matter»* was submitted by Rudolf Gross to the university board of TUM already in August 2015, after the very successful Collaborative Research Center 631 on *«Solid State Quantum Information Processing»* (07/2003 – 06/2015) came to an end. It was already evident from the beginning that all Munich institutions working in the field on quantum science and technology have to join forces to be successful in the application of a new cluster of excellence within the ***German Excellence Strategy***. Therefore, a draft proposal was submitted to the German Research Foundation jointly by LMU and TUM on 3 April 2017. After a positive review by an expert panel and a comparative assessment by the Committee of Experts appointed by the Joint Science Conference (GWK) the preparation of the full proposal was started. The full proposal (front page is shown on the right) was submitted to the DFG Head Office until the cut-off date of 21 February 2018.

Figure 2: The MCQST team representing the Cluster of Excellence MCQST at the review meeting on 12 June 2018. From left to right: Wolfgang Heckl, Thomas Hofmann, Tatjana Wilk, Michael Greiner, Ulrich Schollwöck, Christian Pfleiderer, Rudolf Gross, Wolfgang Herrmann, Immanuel Bloch, Bernd Huber, Jonathan Finley, Simone Warzel, Ignacio Cirac, Harald Weinfurter, Monika Aidelsburger, Mari-Carmen Bañuls. The picture was taken after the review meeting in front of the DFG head office.

The full proposal has been reviewed by an international expert panel on 12 June 2018 at the DFG Head Office in Bonn. The research program and structural measures planned within MCQST have been presented by the three spokespersons (Immanuel Bloch, Ignacio Cirac, Rudolf Gross) supported by the president of LMU Munich (Bernd Huber) as well as Monika Aidelsburger (physics, LMU) and Simone Warzel (mathematics, TUM). The full team representing MCQST at the review meeting is shown in Fig. 2.

Figure 3: The MCQST team chatting just before the presentation of the MCQST proposal to the review panel.

The rationale for a cluster initiative focussing on quantum science and technology is straightforward. Quantum Mechanics has revolutionized our understanding of nature and has enabled the development of ground-breaking new technologies during the last century. Today, we are witnessing a «***second quantum revolution***», in which information theory and quantum physics are uniting, thereby providing radically new ways of communication and computation as well as a general new framework for our understanding of nature. The exceptional level of controlling and engineering individual quantum objects achieved in recent years makes the area of Quantum Science and Technology (QST) one of the most active fields of science today. MCQST aims

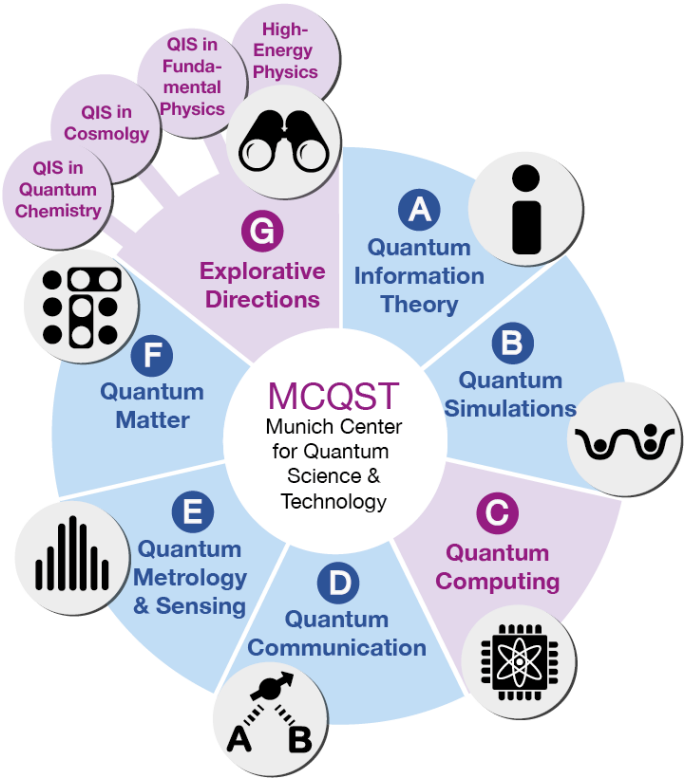

Figure 4: Schematic of the focus Research Units A-G of MCQST, connecting fundamental science and technological applications. Purple fields/circles indicate either topics to be strengthened (RU-C) or new, explorative fields of research (RU-G) that will significantly extend the reach of the MCQST and connect Quantum Information Science (QIS) to other fields of science.

at discovering and understanding the novel and unifying concepts in the interdisciplinary research fields of QST, and finally will make them tangible and practical, in order to develop the extraordinary applications being in reach through next generation quantum devices. MCQST will build a world-leading center in Quantum Science and Technology with a highly multidisciplinary profile.

The research strategy of MCQST is guided by the expectation that the second quantum revolution will have a transformative impact on science, technology and ultimately on society. Quantum computers are expected to solve problems that could never be addressed even by the most powerful supercomputers. This opens up unforeseen possibilities of designing and developing new materials with unparalleled properties, of discovering chemical compounds for materials science and drug design, or powerful algorithms that will transform machine learning and artificial intelligence. Quantum communication will eventually replace the way we interact remotely in the future, providing us with secure and efficient platforms ultimately immune against cyberattacks. Quantum technologies will also lead to ultraprecise sensors and clocks, with impact in medicine, biology and transportation.

To probe and understand the dynamics of entanglement in quantum many-body systems and to explore the intimate connection to information propagation or scrambling is at the heart of the research program of MCQST. Based on entanglement, Quantum Information Theory is already providing original perspectives to other fields of science that study quantum systems of many particles, for example to Quantum Chemistry, Condensed Matter and High Energy Physics or even to Cosmology. It has already been realized that the difficulty of answering some key questions in these fields is rooted in the amount of entanglement they possess. This has led to new and entirely unanticipated connections among those fields and converted Quantum Science and Technology into a vibrant and multidisciplinary field of research that transcends Physics, Computer Science, Mathematics, Materials Science, Electrical Engineering and Chemistry.

On the applied and technological level, MCQST strives to develop dedicated quantum de-

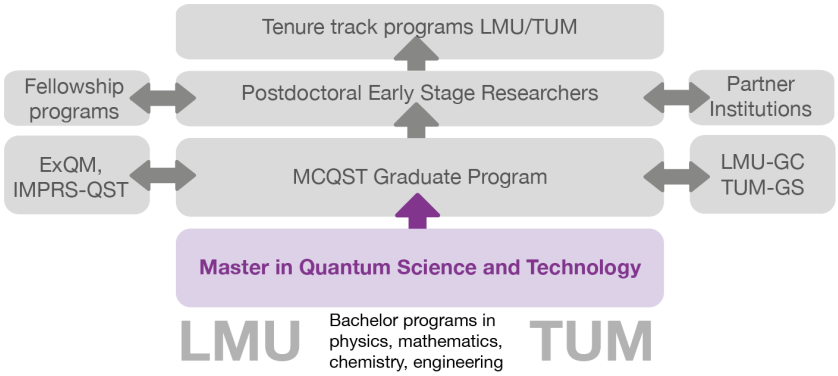

Figure 5: A dedicated Master's program in Quantum Science and Technology co-organized by both LMU and TUM will provide an advanced education in QST and link students in physics, mathematics, chemistry and engineering to the MCQST graduate program. It will thus provide a broad education in QST, foster interdisciplinary collaboration from an early stage and provide students skill sets in QST of relevance for both academia and industry.

vices and quantum hardware and software for prototypes of quantum computers and simulators as well as of quantum communication networks. We will develop quantum sensors and techniques to measure electric fields at the nanoscale and frequency or gravitation with unprecedented sensitivity and resolution for sciences ranging from biology to astronomy. New techniques for quantum control of quantum devices and materials will lead to novel applications ranging from atomic systems, through chemistry all the way to medical systems. An important structural goal will be to link ground-breaking research with industrial partners and to generate a communication hub for scientists and engineers working in research institutions and industry.

An important educational component of MCQST will be to establish a dedicated Master's program on Quantum Science and Technology for top students from all over the world. This is urgently required to educate the new generation of scientists, engineers and entrepreneurs well trained for the QST revolution to come. The PhD program of MCQST will build on the existing excellence graduate schools (***Ph.D. School of Excellence «Exploring Quantum Matter» (ExQM)*** and ***International Max Planck Research School «Quantum Science and Technology» (IMPRS-QST)***), providing PhD students with a rich variety of research topics, while engaging them directly in a unique environment.

In order to generate an optimal research environment, an important structural measure of MCQST will be to develop the existing (since 2014) ***«Munich Quantum Center» (MQC)*** into a long-term internationally leading center for cutting edge research, technology development and education in QST with the mission of fostering and promoting collaborations between different disciplines and researchers.

Strong public engagement will be achieved by several measures. On the one hand, MCQST will raise the awareness for the specific QST research in Munich by a dedicated public relations office and, on the other hand, through our partner the Deutsches Museum, one of the most prominent science and technology museums worldwide. In collaboration with this partner we will develop joint outreach activities such as a series of temporary and permanent exhibitions on QST to make the public aware of QST and introduce them to this new and fascinating research field.

The «Zentrum für QuantumEngineering» (ZQE)

Rudolf Gross


Vorschlag zur Errichtung eines Forschungsneubaus
an der
Technischen Universität München
in Garching mit fakultätsübergreifender Ausrichtung
gemäß Art. 91b, Abs. 1 Satz 1 Nr. 3 GG
Center for Quantum Technologies (CQT)
Zentrum für Quantentechnologien
(Rudolf Gross, 15.01.2017)

Triggered by a draft proposal (see right) for a new Center for Quantum Technologies sent by Rudolf Gross to the university board of the Technical University of Munich in January 2017, TUM applied for a new research building. Later on, the name of this new central institute of TUM has been slightly changed to ***«Zentrum für QuantumEngineering» (ZQE)*** to clearly separate between the ZQE and the Cluster of Excellence ***«Munich Center for Quantum Science and Technology» (MCQST)***. Whereas the MCQST focuses on fundamental aspects of quantum science and technology, the key focus of the ZQE will be rather on linking research in natural sciences and engineering faculties to promote translation of quantum technologies to industrial applications. Only by joining quantum science experts from mathematics, physics and chemistry with those in computer sciences and electrical engineering under one roof, a rapid transfer of scientific findings from basic science to real-world applications is possible. To implement this goal, the ZQE aims to create a strong network with industry partners and a fruitful environment for startup companies.

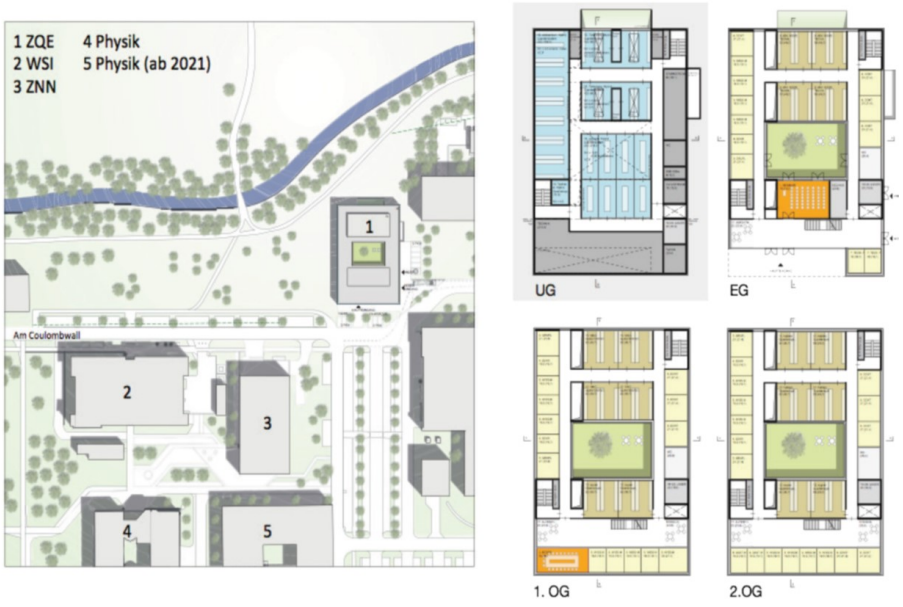

Figure 1: Left: The planned location of the ZQE on the Garching Research Campus close to the Center of Nanoscience and Nanotechnology (ZNN) and the Walter Schottky Institute (WSI). Right: The floor-level structure of the ZQE.

A draft proposal for the ZQE has been sent to the Bavarian Ministry for Science and Arts in August 2017 and the full proposal has been submitted to the German Council of Science and Humanities (Wissenschaftsrat) in January 2018. The German Council of Science and Humanities recommended funding of the ZQE in his meeting from 27 April 2018 and the Joint Science Conference (GWK) followed this recommendation on 29 June 2018. Besides the ZQE of TUM, the Regensburg Center for Ultrafast Nanoscopy (RUN) has been

granted. The German Federal Government and the Free State of Bavaria will share the costs of around 80 million euro for both buildings equally.

The new Center for Quantum Engineering will be placed on the Garching Research Campus next to the Center for Nanoscience and Nanomaterials of TUM (ZNN) and hopefully completed until end of 2022. It will be headed by Christian Pfleiderer (physics) and Holger Boche (electrical and computer engineering). The ZQE will strongly profit from the immediate vicinity to the Walter Schottky Institute for Semiconductor Physics (WSI), which is also a collaborative facility of the Department of Physics and the Department of Electrical and Computer Engineering, and from the close ties to the WMI and the Max Planck Institute for Quantum Optics. It will also profit from the long-standing, very successful preliminary studies and already established collaborations within the Collaborative Research Center 631 on «*Solid State Quantum Information Processing*» (2003–2015) and the Cluster of Excellence «*Nanosystems Initiative Munich*» (2006–2018). Furthermore, the basic research-oriented cluster MCQST starting in 2019 will be a key partner of ZQE. WMI not only triggered the application of the ZQE but will be one the key players of ZQE and will help to make the ZQE a success.

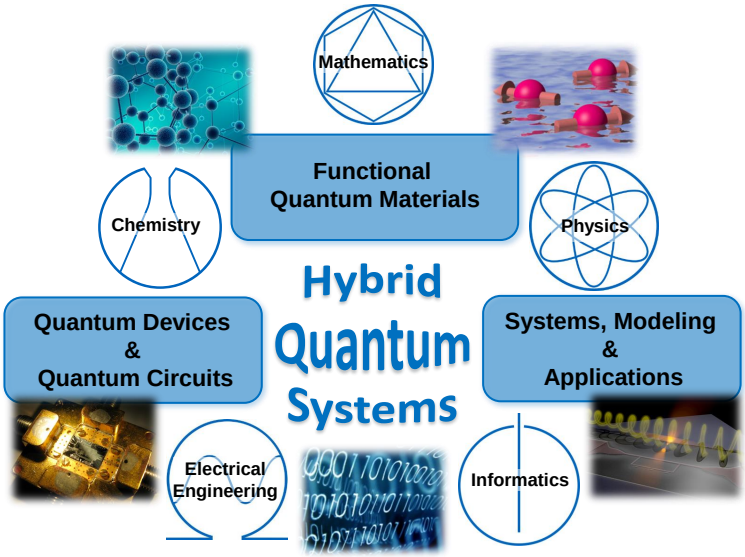

The ZQE will focus on three interdisciplinary research domains: (i) hybrid quantum devices and quantum circuits, (ii) functional quantum materials, and (iii) aspects related to complex quantum systems aspects and modeling. The key scientific goal of ZQE is to combine different methodological approaches and already well studied quantum systems such as charge and spin qubits in semiconductors, defects in diamond, superconducting quantum circuits, nanomechanical systems or molecular magnets. In this way hybrid quantum systems with tailor-made properties for specific applications shall be developed. The key strategic goal of ZQE is to link the already successful research work in quantum science with the development and commercial application of quantum technology. To achieve this goal, the long-standing work of individual groups will be concentrated at ZQE and a network with industrial partners will be established. In this way ZQE will become an important national center in a technology field with high relevance and economical potential.

There are of coarse strong scientific synergies of the ZQE with the EU flagship project ***«Quantum Technology»***, which has just been started. WMI is already coordinating the EU Quantum Technology Flagship Project ***«Quantum Microwave Communication and Sensing»*** (see report on page 31), which aims at developing the world-wide first quantum local area network (QLAN) in the microwave regime. Such a QLAN is important for distributed quantum computing with superconducting quantum processors. The announcement by the Bavarian Prime Minister Söder to commence building a quantum computer in Bavaria (government statement of 18 April 2018) is a reference to the successes of the actors in the greater Munich area brought together through the Munich Quantum Center (MQC).

The EU Quantum Flagship Project «Quantum Microwave Communication and Sensing» (QMiCS)

Frank Deppe, Kirill G. Fedorov, Achim Marx, Rudolf Gross [1]

The ***«European Quantum Flagship»*** was launched in 2018 as one of the largest and most ambitious research initiatives of the European Union. With a budget of about 1 billion euro and a duration of 10 years, the flagship brings together research institutions, academia, industry, enterprises, and policy makers, in a joint and collaborative initiative on an unprecedented scale. The main objective of the Quantum Flagship is to consolidate and expand European scientific leadership and excellence in this research area as well as to transfer quantum physics research from the lab to the market by means of commercial applications and disruptive technologies. With over 5000 researchers from academia and industry involved in this initiative throughout its lifetime, it aims to create the next generation of disruptive technologies that will impact Europe's society, placing the region as a worldwide knowledge-based industry and technological leader in this field.

In the first call for proposals within the Quantum Flagship, 140 proposals were submitted and only 20 projects were granted. Among the successful projects is one led by the Walther-Meißner-Institute (coordinator: Frank Deppe). The project is entitled ***«Quantum Microwave Communication and Sensing» (QMiCS)***. Scientific project partners are Aalto University (Finland), École Normale Supérieure de Lyon (France), Instituto de Telecomunicações (Portugal), Universidad del País Vasco/Euskal Herriko Unibertsitatea Bilbao (Spain), and the VTT Technical Research Centre of Finland Ltd. (Finland). Active industry partner are Oxford Instruments Nanotechnology Ltd. (United Kingdom) and TTI Norte S.L. (Spain). WMI is very happy about the success in the very competitive Quantum Flagship program. This success underlines the leadership of WMI in the field of physics and technology of propagating quantum microwaves, a field pushed by the WMI since almost 10 years.

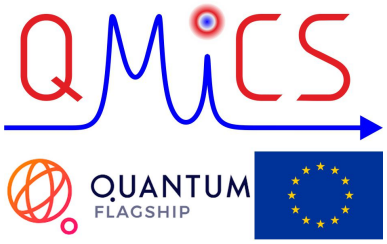

Figure 1: Logos of EU Quantum Flagship Project QMiCS (top) together with the logos of the EU Quantum Flagship (bottom left), and the European Union (bottom right).

QMiCS is a three-year project in the basic science pillar of the EU Quantum Flagship and has started on 1 October 2018. On 22 and 23 November 2018, the involved scientists celebrated the project start at the Walther-Meißner-Institute in the framework of the kick-off meeting. A group photo is shown in Fig. 2. The mission of QMiCS is to combine European expertise and lead the efforts in developing novel components, experimental techniques, and theory models building on the quantum properties of continuous-variable propagating microwaves. The long-term visions of QMiCS are

- the realization of distributed quantum computing & communication via microwave quantum local area networks (QLANs) and
- the implementation of sensing applications based on the illumination of an object with quantum microwaves (quantum radar).

With respect to key quantum computing technology platforms (superconducting quantum circuits, NV centers, semiconductor quantum dots), microwaves intrinsically allow for zero frequency conversion loss since they are the natural frequency scale. They can be distributed via superconducting cables with surprisingly little losses, eventually allowing for quantum

[1] The authors acknowledge support from the EU Quantum Flagship within the Project QMiCS under the grant agreement No. 820505.

Figure 2: Group photo of the QMiCS team taken during the kick-off meeting on 23 November 2018 at WMI.

communication and cryptography applications. Radar works at gigahertz frequencies because of the atmospheric transparency windows anyways. Scientifically, QMiCS targets are

- the development of a QLAN via quantum teleportation,
- the demonstration of a quantum advantage in microwave illumination,
- the development of a roadmap to real-life applications for the second/third phase of the QT Flagship.

Beneath these three grand goals lies a strong component of disruptive enabling technology provided by two full and one external industry partner: the development of a microwave QLAN cable connecting the millikevin stages of two dilution refrigerators, improved cryogenic semiconductor amplifiers, and packaged pre-quantum ultrasensitive microwave detectors. The resulting "enabling" commercial products are beneficial for quantum technologies at microwave frequencies in general. In addition, QMiCS fosters awareness in industry about the revolutionary business potential of quantum microwave technologies, especially via the advisory third parties Airbus Defence and Space Ltd and Cisco Systems GmbH. In this way, QMiCS helps placing Europe at the forefront of the second quantum revolution and kick-starting a competitive European quantum industry.

The EU Project «Magnetomechanical Platforms for Quantum Experiments and Quantum Enabled Sensing Technologies» (MaQSens)

Hans Hübl, Natalie Segercratz, Rudolf Gross [1]

The EU Project ***«Magnetomechanical Platforms for Quantum Experiments and Quantum Enabled Sensing Technologies» (MaQSens)*** (coordinator: Markus Aspelmeyer, University of Vienna) started in January 2017. Within this project, WMI collaborates with partners from the University of Vienna, the Technical University of Vienna, the Austrian Academy of Sciences, and the Universitat Autonòma de Barcelona as well as the industry partners Airbus DS GmbH and attocube systems AG.

MaQSens seeks to establish a radically new technology platform for experiments in macroscopic quantum physics and for quantum enabled sensing. It exploits magnetic coupling between superconducting quantum circuits and superconducting mechanical resonators – both levitated and suspended – to enter a hitherto inaccessible parameter regime of both unprecedented force sensitivity and full quantum control of massive, macroscopic objects. The approach followed by MaQSens combines, in a new way, techniques from different research areas (magnetic levitation, superconducting circuits, atom-chip technology, cavity opto-mechanics and quantum optics) and is set up as a joint collaborative effort between expert European teams from academia and industry. The technology developed in MaQSens will enable quantum experiments of otherwise unachievable coherence times and masses, which has immediate implications for testing fundamental physical questions, for performing hybrid quantum information processing and, on the applied side, for ultrasensitive force sensing applications.

The WMI contributes to this project by testing and developing ultra-low vibration platforms for cryogenic environments. Here, the long-standing and established know-how of WMI in cryo-engineering is a key ingredient to overcome the key challenges. WMI contributes to the project by designing and manufacturing vibration isolation stages which are compatible with low-temperature cryostats. In addition, there is a strong joint effort in tailoring and performing initial test experiments with levitated superconducing spheres. For this project part, guest researchers have spent significant periods of frames at WMI during the startup phase of the project. Moreover, with the strong expertise of the WMI in the fabrication and characterization of superconducting quantum circuits and nano-electromechanical circuits, the group at the WMI designs, develops and implements inductive detection techniques for mechanical objects. These developments are of key relevance for achieving the scientific goals and implementing the technology platforms of the project.

[1]This project has received funding from the European Unions Horizon 2020 research and innovation programme under grant agreement No. 736943, and from the European Research Council (ERC) under the European Union's Horizon 2020 research and innovation programme under grant agreement No. 649008.

Coordinated Projects in Quantum Science and Technology

Rudolf Gross

The Walther-Meißner-Institute (WMI) participates in several coordinated research programs, centers, graduate schools and initiatives in the field of Quantum Science and Technology (QST). Besides the already ending Cluster of Excellence ***«Nanosystems Initiative Munich»*** with its Research Area 1 on Quantum Nanophysics and the upcoming new cluster ***«Munich Center for Quantum Science and Technology»*** (see page 21–28), as well as the the EU Quantum Flagship Project ***«Quantum Microwave Communication and Sensing» (QMiCS)*** (see page 31–32) and the EU Project ***«Magnetomechanical Platforms for Quantum Experiments and Quantum Enabled Sensing Technologies» (MaQSens)*** (see page 33) these are

- the **Munich Quantum Center (MQC)**
- the **Ph.D. School of Excellence «Exploring Quantum Matter» (ExQM)**
- the **International Max Planck Research School «Quantum Science and Technology» (IMPRS-QST)**

The focus of MQC, ExQM and IMPRS-QST has been outlined already in our Annual Report 2017 and will not be repeated here. However, we would like to point out that they are important for WMI to continue its ambitious research program in QST, which started already in 2003 with the Collaborative Research Center 631 «Solid State Quantum Information Processing Systems».

WMI is particularly pleased that the ***«Munich Quantum Center» (MQC)***, which was founded in 2014 as a 'virtual center', gets persistent financial support from both Munich universities starting from 2019. MQC hosts all scientists and engineers in the greater Munich area working in the field of quantum science and technology and therefore the number of people in MQC by far exceeds the number of Principal Investigators in MCQST or some Munich based BMBF or EU projects. Of course, the activities of MQC will be closely coordinated with those of the cluster MCQST. Meanwhile, MQC gathers more than 40 research groups of TUM, LMU, MPQ and WMI. The members of the MQC research groups meet up regularly at common workshops and seminars to create a very interactive ambience for quantum science in Munich. In this way, MQC aims at communicating recent advances and developments in the field of QST. Furthermore, MQC is a successful platform to enhance the outside visibility of the Munich research activities in the field of QST. To this end, MQC is very successful in organizing workshops and schools as well as in stimulating new coordinated research projects.

Basic Research

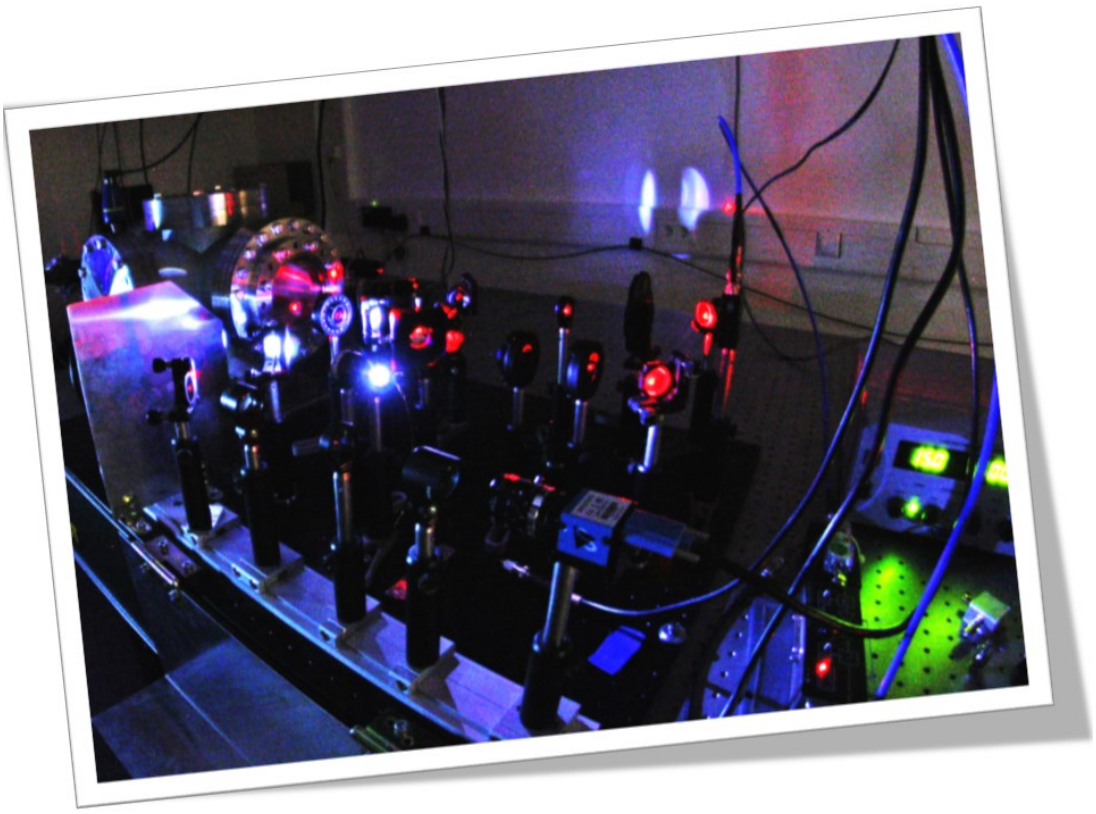

Phonon Anomalies as a Probe for Magnetic Order in Fe-Based Superconductors

A. Baum, D. Jost, F. Löffler, M. Mitschek, M. Opel, B. Muschler, T. Böhm, R. Hackl [1]
Ying Li, M. Tomić, R. Valentí, [2] *I. I. Mazin,* [3] *N. Lazarević, A. Milosavljević, M. Šćepanović, M. Grujić-Brojčin,* [4] *M. M. Radonjić,* [5] *B. Nikolić,* [6] *N. Stojilović,* [4,7] *Z. V. Popović,* [4,8]
Aifeng Wang, C. Petrovic, [9] *J.-H. Chu* [10,11,12] *I. R. Fisher* [11,12]

Magnetic order in the vicinity of superconductivity appears to be a universal feature of unconventional superconductors. Yet, for many materials the interplay of magnetism and the nearby ordering phenomena are not well understood. In iron based superconductors (IBS) the magnetic phase is accompanied or preceded by a transition to an orthorhombic or nematic phase and the related fluctuations above the ordering temperature [1–4]. Pinning down the driving force behind these transitions and their interrelation with superconductivity remains challenging [5–7]. This interrelation of lattice, orbital and spin degrees of freedom makes phonons a natural choice as probes.

Anomalies of the four phonon modes Raman-active in the IBS [8] have been observed at the onset of magnetic order in materials based on $BaFe_2As_2$ (Ba-122) [9–11] and in FeTe [12], while their temperature dependences are conventional in systems without magnetic order [13, 14].

For clarifying the leading instability in the IBSs we performed systematic Raman studies of the phonon anomalies in selected compounds and analyzed the data in collaboration with theorists [8, 15]. Here we briefly summarize the main results in FeS and de-twinned Ba-122 and outline the more general point of view emerging from the entire study.

FeS is superconducting below $T_c \approx 5\,\mathrm{K}$ [16] and remains tetragonal down to the lowest temperatures [17]. Whether FeS hosts magnetic order is still under debate [18–21]. Here, phonons can be used as sensitive probes. Fig. 1 shows Raman spectra of FeS at four light polarizations. Out of the three peaks, the mode at $215\,\mathrm{cm}^{-1}$ can be identified as out-of-phase vibration of iron atoms [8, 15]. The peak centered at $305\,\mathrm{cm}^{-1}$ is a superposition of two unresolved modes. The strongest mode at $305\,\mathrm{cm}^{-1}$ has A_{1g} symmetry and is identified as the in-phase vibration of sulfur atoms. Peaks P1 and P2 obey A_{1g} and mixed $A_{1g} + B_{1g}$ selection rules, respectively.

By fitting Voigt profiles to the phonons the temperature dependencies of their peak energies $\Omega_{\mathrm{ph}}(T)$ and linewidths $\Gamma_{\mathrm{L}}(T)$ can be extracted and are shown in Fig. 2. The overall temperature dependencies can be well described by lattice contraction [22] and anharmonic decay [23]

[1]The project was funded by DFG via the Priority Program SPP 1458 (grant-no. Ha2071/7) and the TRR 80. The collaborations with Stanford University and the Institute of Physics Belgrade were supported, respectively, by BaCaTeC (grant-no. A5[2012-2]) and DAAD (grant nos. 57142964 and 57335339).

[2]Goethe-Universität Frankfurt, Germany. The work was supported via TRR 49 and by the Centre for Scientific Computing (CSC) in Frankfurt.

[3]Code 6393, Naval Research Laboratory, Washington DC, USA. The work was supported by the ONR through the NRL basic research program and by the AvH foundation.

[4]University of Belgrade, Serbia. The work was supported by the Serbian Ministry of Education, Science and Technological Development under Project III45018.

[5]University of Belgrade, Serbia. Simulations were performed at the PARADOX supercomputing facility at the Scientific Computing Laboratory of the Institute of Physics, Belgrade.

[6]Faculty of Physics, University of Belgrade, Studentski trg 12, Belgrade, Serbia

[7]University of Wisconsin, USA. The work was supported by grant FDS498 from UW Oshkosh.

[8]Serbian Academy of Sciences and Arts, Belgrade, Serbia

[9]Brookhaven National Laboratory, USA. The work was supported by the Center for Emergent Superconductivity, an Energy Frontier Research Center funded by the U.S. DOE, Office of Basic Energy Sciences.

[10]University of Washington, Seattle, USA

[11]SLAC National Accelerator Laboratory, Menlo Park, USA

[12]Geballe Laboratory for Advanced Materials & Dept. of Applied Physics, Stanford University, USA

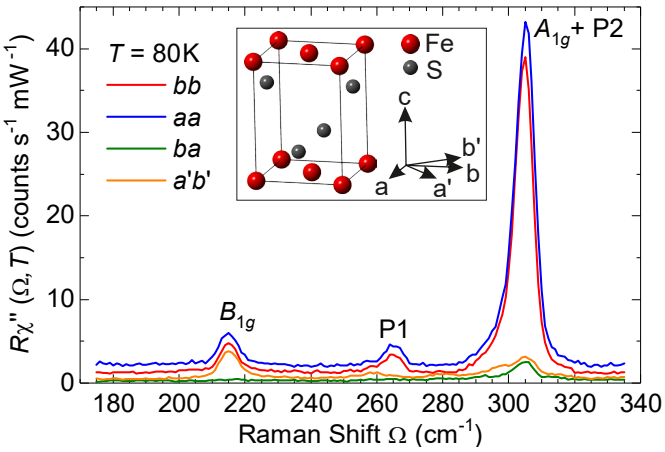

Figure 1: Raman spectra of tetragonal FeS at $T = 80\,\mathrm{K}$ for light polarizations as indicated. The inset shows the crystal structure of FeS and the polarization directions with respect to the crystal orientation.

(red solid and dashed lines, respectively) where the volume data are taken from Ref. [17]. Deviations from the conventional behavior occur at 50 K and below 20 K. The temperature dependencies (Fig. 2) of P1 and P2 are nearly identical to those of the Raman-active phonons thus indicating their phononic origin. Calculations of the phonon density of states (PDOS) [15] predict a gap in the PDOS in the energy range around P1. Therefore, P1 presumably originates from a second order scattering process where, in agreement with the PDOS, two acoustic zone-boundary modes are excited simultaneously. Two-phonon scattering indicates strong phonon-phonon coupling, which in turn suggests enhanced electron-phonon coupling in metallic FeS. P2 concurs with a maximum of the PDOS and may be traced back to defect-induced first-order scattering.

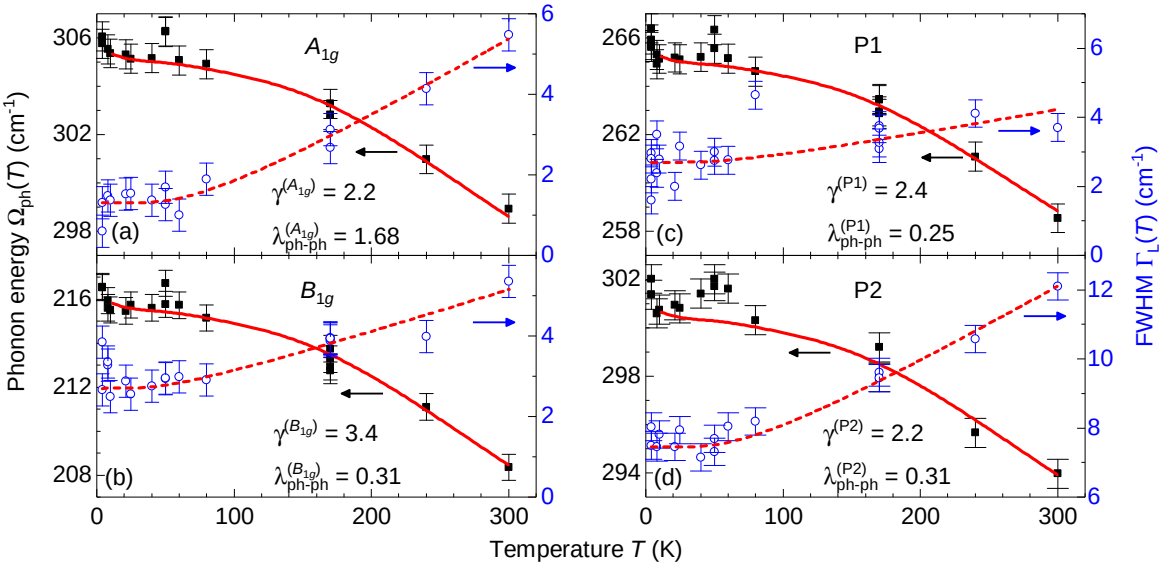

Figure 2: Temperature dependence of the phonon energies $\Omega_{\mathrm{ph}}(T)$ and line widths $\Gamma_{\mathrm{L}}(T)$ in FeS. Black squares show the phonon energies Ω_{ph}, blue open circles denote the line width Γ_{L}. Solid and dashed red lines represent the temperature dependence of Ω_{ph} and Γ_{L} based on volume contraction and anharmonic decay [22, 23].

Anomalies in the temperature dependence of phonons are typically found at phase transitions or incipient order. (i) At 50 K the energies of all four modes show a sudden increase while the linewidths remain unaffected. So far neither the lattice constants [17] nor any other quantity indicate a phase transition at 50 K. This makes it currently very difficult to identify the origin of this anomaly. (ii) Below $T^* \approx 20\,\mathrm{K}$ all four modes harden by typically $1\,\mathrm{cm}^{-1}$ along with the decrease in the unit cell volume [17]. We studied the magnetization of FeS in detail in the range of 20 K and below but could not find an indication of a phase transition. However, T^* coincides with the onset of short-range magnetism reported by μSR [19]. Obviously, FeS has some similarities with FeSe which is also close to a magnetic instability but orders only with applied pressure.

$BaFe_2As_2$ undergoes a magneto-structural transition at $T_m = T_s \approx 135\,K$. Unexpectedly, the fully-symmetric As phonon can be observed below T_m in the Raman spectra measured with crossed polarizations and the electric fields oriented along the axes of the pseudo-tetragonal 2 Fe unit cell [11]. As expected and shown in Fig. 3(a) the As phonon is the strongest line in the spectra with parallel light polarizations (RR) and gains intensity upon cooling. In spectra with crossed polarizations [Fig 3(b)] the phonon is absent above T_m as expected, but appears at temperatures below T_m (blue spectrum) with an intensity comparable to that in parallel polarizations. Upon de-twinning the sample, the phonon's spectral weight $A_{IS}^{(As)}$ can be measured separately for parallel light polarizations oriented either along the antiferromagnetic ($\tilde{a}\tilde{a}$) or ferromagnetic axis ($\tilde{b}\tilde{b}$). $A_{\tilde{a}\tilde{a}}^{(As)}$ and $A_{\tilde{b}\tilde{b}}^{(As)}$ are plotted as a function of the excitation energy $\hbar\omega_I$ in Fig. 4(a). For $\tilde{a}\tilde{a}$ configuration (red squares) the spectral weight shows a continuous increase with energy while for $\tilde{b}\tilde{b}$ configuration the intensity is virtually constant for $\hbar\omega_I < 2.7\,eV$ followed by a steep increase towards higher energies.

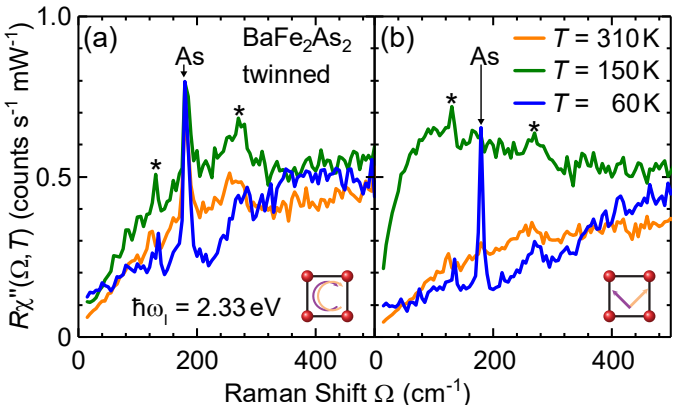

Figure 3: Electronic continua and As phonon in $BaFe_2As_2$. (a) In parallel RR polarization configuration (see inset), the As phonon appears at all temperatures. (b) For crossed light polarizations (ab), the As phonon is present only below the magneto-structural transition at $T_s = 135\,K$. Asterisks mark the E_g modes.

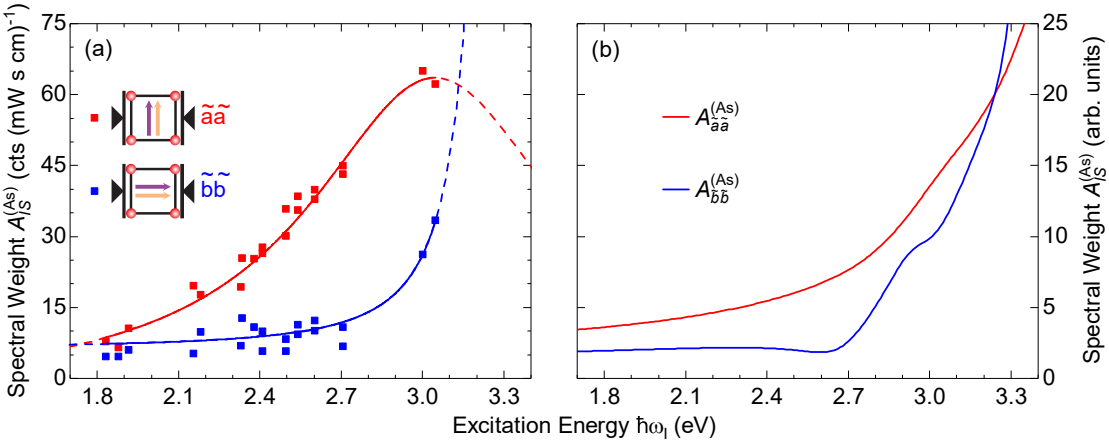

Figure 4: Spectral weight $A_{IS}^{(As)}$ of the As phonon in $BaFe_2As_2$ as a function of excitation energy $\hbar\omega_I$ and polarization IS. (a) Experimental data. The variation of $A_{\tilde{b}\tilde{b}}^{(As)}$ (ferromagnetic axis, blue squares) is distinctly different from $A_{\tilde{a}\tilde{a}}^{(As)}$ (antiferromagnetic axis, red squares). The solid lines are Lorentzian functions whose extrapolations beyond the measured energy interval are shown as dashes. (b) Theoretical prediction of $A_{\tilde{a}\tilde{a}}^{(As)}$ (red) and $A_{\tilde{b}\tilde{b}}^{(As)}$ (blue). The curves qualitatively reproduce the experimental data shown in panel (a).

Both polarizations display typical resonance behavior which occurs when the intermediate state of the Raman process is an eigenstate of the electronic system. Hence, the resonance profile reflects the band structure. In turn, the spectral weight can be calculated from a model band structure *via* the derivative of the dielectric function with respect to the normal coordinate of a given vibration. We obtained the band structure using local density approximation (LDA) [8] for the magnetically ordered state. The predicted spectral weight, as shown in Fig 4(b), qualitatively captures the resonance behavior and relative intensities if an orbital-dependent renormalization of the band structure is applied as follows [8]: (i) The bands near

the Fermi energy E_F stemming predominantly from iron $3d$ orbitals are renormalized by a factor $2 \ldots 3$. (ii) Bands below $-2.7\,\mathrm{eV}$ being derived predominantly from As $4p$ orbitals remain unchanged. (iii) Bands between $-2.7\,\mathrm{eV}$ and E_F having mixed character cannot be renormalized by rescaling and are disregarded in the calculations of the dielectric function. The experimental and theoretical results indicate that resonance effects are the main source of the As phonon anomaly below T_m and originate from the reconstruction of the band structure induced by the magnetic order.

This conclusion can be tested independently by scrutinizing compounds having transitions at separate temperatures, $T_m < T_s$, such as $Ba(Fe_{1-x}Co_x)_2As_2$ for $x > 0$ or FeSe having only a structural transition [8]. For $x = 0.025$ the anomaly appears only below T_m. For $x = 0.051$ the anomalous intensity starts appearing at T_s, increases linearly (not like an order parameter) and saturates instantaneously at T_m. In FeSe the temperature dependence of the anomalous intensity is similar to that in $Ba(Fe_{0.949}Co_{0.051})_2As_2$ but no saturation is observed down to 20 K, and the magnitude of $A^{(As)}(T \to 0)$ is an order of magnitude smaller than in Ba-122. Obviously, the magnetic correlation length starts to increase smoothly below T_s, and thus magnetism does not leave an imprint on the spin relaxation time [2] although magnetism is the leading instability.

References

[1] D. Johrendt, J. Mater. Chem. **21**, 13726–13736 (2011).
[2] S.-H. Baek, D. V. Efremov, J. M. Ok, J. S. Kim, J. van den Brink, and B. Büchner, Nat. Mater. **14**, 210–214 (2015).
[3] K. Matsuura, Y. Mizukami, Y. Arai, Y. Sugimura, N. Maejima, A. Machida, T. Watanuki, T. Fukuda, T. Yajima, Z. Hiroi, K. Y. Yip, Y. C. Chan, Q. Niu, S. Hosoi, K. Ishida, K. Mukasa, S. Kasahara, J.-G. Cheng, S. K. Goh, Y. Matsuda, Y. Uwatoko, and T. Shibauchi, Nat. Commun. **8**, 1143 (2017).
[4] J.-H. Chu, J. G. Analytis, C. Kucharczyk, and I. R. Fisher, Phys. Rev. B **79**, 014506 (2009).
[5] R. M. Fernandes, A. V. Chubukov, and J. Schmalian, Nat. Phys. **10**, 97–104 (2014).
[6] A. E. Böhmer, F. Hardy, L. Wang, T. Wolf, P. Schweiss, and C. Meingast, Nat. Commun. **6**, 7911 (2015).
[7] S. Lederer, Y. Schattner, E. Berg, and S. A. Kivelson, Phys. Rev. Lett. **114**, 097001 (2015).
[8] A. Baum, Y. Li, M. Tomić, N. Lazarević, D. Jost, F. Löffler, B. Muschler, T. Böhm, J.-H. Chu, I. R. Fisher, R. Valentí, I. I. Mazin, and R. Hackl, Phys. Rev. B **98**, 075113 (2018).
[9] M. Rahlenbeck, G. L. Sun, D. L. Sun, C. T. Lin, B. Keimer, and C. Ulrich, Phys. Rev. B **80**, 064509 (2009).
[10] L. Chauvière, Y. Gallais, M. Cazayous, A. Sacuto, M. A. Measson, D. Colson, and A. Forget, Phys. Rev. B **80**, 094504 (2009).
[11] L. Chauvière, Y. Gallais, M. Cazayous, M. A. Méasson, A. Sacuto, D. Colson, and A. Forget, Phys. Rev. B **84**, 104508 (2011).
[12] Y. J. Um, A. Subedi, P. Toulemonde, A. Y. Ganin, L. Boeri, M. Rahlenbeck, Y. Liu, C. T. Lin, S. J. E. Carlsson, A. Sulpice, M. J. Rosseinsky, B. Keimer, and M. Le Tacon, Phys. Rev. B **85**, 064519 (2012).
[13] Y. J. Um, J. T. Park, B. H. Min, Y. J. Song, Y. S. Kwon, B. Keimer, and M. Le Tacon, Phys. Rev. B **85**, 012501 (2012).
[14] V. Gnezdilov, Y. G. Pashkevich, P. Lemmens, D. Wulferding, T. Shevtsova, A. Gusev, D. Chareev, and A. Vasiliev, Phys. Rev. B **87**, 144508 (2013).
[15] A. Baum, A. Milosavljević, N. Lazarević, M. M. Radonjić, B. Nikolić, M. Mitschek, Z. I. Maranloo, M. Šćepanović, M. Grujić-Brojčin, N. Stojilović, M. Opel, A. Wang, C. Petrovic, Z. V. Popović, and R. Hackl, Phys. Rev. B **97**, 054306 (2018).
[16] X. Lai, H. Zhang, Y. Wang, X. Wang, X. Zhang, J. Lin, and F. Huang, J. Am. Chem. Soc. **137**, 10148–10151 (2015).
[17] U. Pachmayr, N. Fehn, and D. Johrendt, Chem. Commun. **52**, 194–197 (2016).
[18] D. Vaughan, and M. Ridout, J. Inorg. Nucl. Chem. **33**, 741–746 (1971).
[19] S. Holenstein, U. Pachmayr, Z. Guguchia, S. Kamusella, R. Khasanov, A. Amato, C. Baines, H.-H. Klauss, E. Morenzoni, D. Johrendt, and H. Luetkens, Phys. Rev. B **93**, 140506 (2016).
[20] F. K. K. Kirschner, F. Lang, C. V. Topping, P. J. Baker, F. L. Pratt, S. E. Wright, D. N. Woodruff, S. J. Clarke, and S. J. Blundell, Phys. Rev. B **94**, 134509 (2016).
[21] S. Kuhn, M. Kidder, D. Parker, C. dela Cruz, M. McGuire, W. Chance, L. Li, L. Debeer-Schmitt, J. Ermentrout, K. Littrell, M. Eskildsen, and A. Sefat, Physica C **534**, 29–36 (2017).
[22] H.-M. Eiter, P. Jaschke, R. Hackl, A. Bauer, M. Gangl, and C. Pfleiderer, Phys. Rev. B **90**, 024411 (2014).
[23] P. G. Klemens, Phys. Rev. **148**, 845–848 (1966).

On the Diffusive Thermal Conductivity of BCS Superfluids

D. Einzel

Introduction. This contribution is devoted to an analytic treatment of the transport properties in a pair–correlated (BCS–) superfluid. Generally speaking, transport and relaxation in such a superfluid can be traced back to the existence of a gas of thermal excitations, the so called Bogoliubov–Valatin quasiparticles (BVQP). In particular, we wish to reconsider the diffusive thermal conductivity of the BVQP gas in the B–phase of superfluid ^{3}He [1, 2]. In contrast to earlier treatments of this thermal transport problem, we aim at an analytic approach [3] by using a very accurate interpolation scheme for the involved temperature–dependent functions. Since transport in the BCS superfluid ^{3}He–B is characterized (in the absence of impurities and lattice phonons) exclusively by inelastic two–particle collisions, the temperature–dependence of the inelasic scattering rate $I(T)$ is the main focus of this work. We present a very accurate analytic interpolation scheme also for the quantity $I(T)$. Finally, we estimate for the first time, what can be expected, when the thermal mean free path becomes comparable with the size of the experimental apparatus. As a result, at this so–called Knudsen transition, $\kappa(T)$ develops a maximum structure, followed by an exponential decrease, instead of increasing $\propto T^{-1}$ in the low temperature limit.

Basic definitions. The temperature–dependent functions occuring in the BCS description are generally seen to depend on temperature via the quantity $z = \Delta(T)/k_{\rm B}T$. As an example, the energy gap $\Delta(T)$ may be written in the form [4]

$$\Delta(T) \;=\; k_{\rm B}T_{\rm c} z {\rm e}^{-b(z)} \;;\; b(z) = 2\sum_{n=0}^{\infty}\left\{\frac{1}{2n+1} - \frac{1}{\sqrt{(2n+1)^2+\frac{z^2}{\pi^2}}}\right\} \tag{1}$$

The conversion between the $T/T_{\rm c}$ scale and the z–scale is possible via the relation $T/T_{\rm c} = \exp[-b(z)]$. Both in the zero–$T$ limit and in the Ginzburg–Landau regime ($T \to T_{\rm c}$) there emerge two universal so–called BCS–Mühlschlegel parameters from the BCS theory [5], namely $\delta_{\rm sc} = \Delta(0)/k_{\rm B}T_{\rm c} = \pi/{\rm e}^{\gamma}$ and $\Delta C/C_{\rm N} = 12/7\zeta(3)$, with $\gamma = 0.557721\ldots$ the Euler constant and $\zeta(3)$ the Riemann ζ function. Let us now turn to the diffusive thermal conductivity of superfluid ^{3}He–B, which has extensively been discussed in Refs. [1, 2]:

$$\kappa T \;=\; \frac{n}{m^*}\left(k_{\rm B}T\right)^2\tau_\kappa \;;\; \tau_\kappa = \bar{\tau}\frac{\pi^2}{3}\frac{y_\sigma}{1-\frac{\lambda_1^-}{3}g_\sigma} \;;\; g_\sigma = \frac{y_\sigma}{y_\sigma + \frac{3z^2}{\pi^2}y_0} \tag{2}$$

with n the total density and m^* the effective mass of the ^{3}He atoms. In (2) the quantity λ_1^- represents a pressure–dependent scattering parameter, which is theoretically not too well accessible. Therefore we may treat λ_1^- as an open parameter, which can in principle be adapted to the experimental observation. It has been shown in Refs. [1, 3] that the diffusive thermal conductivity $\kappa(T)$ can be elegantly expressed by two generalized z–dependent Yosida functions y_0 and y_σ:

$$y_0 \;=\; \int_0^\infty \frac{dt}{\cosh^2\sqrt{t^2+\frac{z^2}{4}}} \;;\; y_\sigma = \frac{12}{\pi^2}\int_0^\infty \frac{dt\,t^2}{\cosh^2\sqrt{t^2+\frac{z^2}{4}}} \tag{3}$$

Note that $y_\sigma = \sigma(T)/\sigma_N(T)$ can be expressed by the BVQP entropy density $\sigma(T)$ in the superfluid state.

Analytic treatment. In Ref. [3] the author has introduced a very accurate interpolation procedure which connects exact results available both in the low temperature limit ($T \to 0$) and in the Ginzburg–Landau regime ($T \to T_c$). Defining the reduced temperature $r = T/T_c$, one may write explicitly [3]:

$$y_0^{\rm int}(r) = y_{00}\left(1 - r^{\beta_0}\right) + e^{\delta_{sc}} e^{-\frac{\delta_{sc}}{r}} r^{\beta_0 - \frac{1}{2}} \; ; \; y_{00}(r) = \sqrt{\frac{2\pi\delta_{sc}}{r}} e^{-\frac{\delta_{sc}}{r}} \tag{4}$$

$$y_\sigma^{\rm int}(r) = y_{\sigma 0}(r)\left(1 - r^{\beta_\sigma}\right) + e^{\delta_{sc}} e^{-\frac{\delta_{sc}}{r}} r^{\beta_\sigma - \frac{3}{2}} \; ; \; y_{\sigma 0}(r) = \frac{3}{\pi^2}\sqrt{2\pi\left(\frac{\delta_{sc}}{r}\right)^3} e^{-\frac{\delta_{sc}}{r}}$$

In Eq. (4) we have defined the exponents $\beta_0 = [5/2 - \delta_{sc}]/[1 - y_{00}(1)]$ and $\beta_\sigma = (\Delta C/C_N + 3/2 - \delta_{sc})/[1 - y_{\sigma 0}(1)]$. The BVQP relaxation time, that characterizes $\kappa(T)$, is given by $\bar{\tau}(T) = \tau_N^0(T_c)/r^2 I(T)$. Here we present a new interpolation procedure for the averaged BVQP scattering rate $I(T)$ ($r = T/T_c$):

$$I_{\rm int}(r) = I_0(r)(1 - r^{\beta_I}) + \frac{4}{3} e^{\delta_{sc}} e^{-\frac{\delta_{sc}}{r}} r^{\beta_I - \frac{3}{2}} \; ; \; I_0(r) = \frac{3w_0}{\sqrt{2\pi}}\sqrt{\left(\frac{\delta_{sc}}{r}\right)^3} e^{-\frac{\delta_{sc}}{r}} \tag{5}$$

In Eq. (5) we have defined $\beta_I = \left[2\pi^2/5\zeta(3) + 3/2 - \delta_{sc}\right]/[1 - 3I_0(1)/4]$. The quantity w_0 is defined as $w_0 = 1 - 2\gamma_0/3 + \delta_0$, with γ_0 and δ_0 two weakly pressure–dependent scattering parameters.

As a next step, let us define the thermal transport mean free path λ_κ:

$$\lambda_\kappa(T) = \lambda_c \frac{T_c^2}{T^2 I(T)} \frac{\sqrt{g_\sigma}}{1 - \frac{\lambda_1^-}{3} g_\sigma} \; ; \; \lambda_c = v_F \tau_N^0(T_c) \tag{6}$$

While in the bulk result (2) for the thermal conductivity $\kappa(T)$, the thermal mean free path λ_κ can increase without limitation, the existence of measuring cells, flow channels etc. prevents this increase in that λ_κ gets replaced by the characteristic cell size d. This fact eventually allows for taking into account mean free path effects and the possibility of a Knudsen transition, at least on a phenomenological level, through the replacement: $\kappa \to \kappa_{\rm eff}$ with

$$\kappa_{\rm eff}(T) = \frac{\kappa(T) d}{d + \lambda_\kappa} = \frac{\kappa(T)}{1 + \frac{\lambda_c}{d}\frac{T_c^2}{T^2 I(T)}\frac{\sqrt{g_\sigma}}{1 - \frac{\lambda_1^-}{3} g_\sigma}} \tag{7}$$

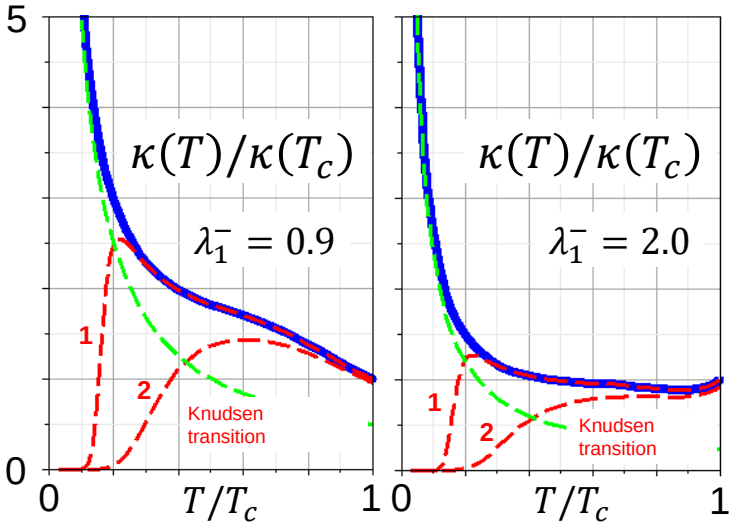

Figure 1: The normalized diffusive thermal conductivity of ^{3}He–B vs reduced temperature T/T_c. The values $\gamma_0 = 0.14$ and $\delta_0 = 0.28$ for the scattering parameters were used. The dashed green line indicates the bulk low–T–behavior of $\kappa(T) \propto T^{-1}$. The dashed red lines mark the Knudsen transitions expected for $\lambda_c/d = 0.0001$ (curves 1) and $\lambda_c/d = 0.03$ (curves 2), respectively.

Results. In Fig. 1 we show the results for the normalized thermal conductivity $\kappa(T)/\kappa(T_c)$ for two values of the scattering parameter $\lambda_1^- = 0.9$ and $\lambda_1^- = 2$. Furthermore we used the values for the scattering parameters $\gamma_0 = 0.14$ and $\delta_0 = 0.28$. Depending on these parameters, $\kappa(T)$ is seen to first increase or decrease below T_c. In the low temperature limit, the green dashed line indicates the increase of $\kappa(T) \propto T^{-1}$. Mean free path effects are seen to show up as pronounced deviations from the T^{-1}–behavior (maximum structure), the details of which depend on the ratio of $v_F\tau_N^0(T_c)$ to the sample size d.

Conclusions. In summary, we have reinvestigated the diffusive thermal conductivity of BVQP in superfluid ^{3}He–B. A very accurate interpolation procedure, applied to the generalized Yosida functions $y_0(T)$ and $y_\sigma(T)$ as well as for the averaged BVQP scattering rate $I(T)$ allows for an analytic investigation of the temperature dependence of $\kappa(T)$ at *all* temperatures below T_c. As a result, $\kappa(T)$ shows (i) either an increase or decrease below T_c and (ii) a Knudsen transition, the position of which depends on the thermal mean free path at the transition $\lambda_\kappa(T_c)$ and the size d of the measuring apparatus.

References

[1] D. Einzel, J. Low Temp. Phys. **54**, 427–474 (1983).
[2] D. Vollhardt, and P. Wölfle (eds.) *The Superfluid Phases of Helium 3* (Taylor and Francis, London, 1990).
[3] D. Einzel, J. Low Temp. Phys. **130**, 493–508 (2002).
[4] B. Mühlschlegel, Z. Phys. **155**, 313–327 (1959).
[5] D. Einzel, J. Low Temp. Phys. **126**, 867–879 (2002).

Superconductivity in Stoichiometric $CaKFe_4As_4$

D. Jost, J.-R. Scholz, U. Zweck, R. Hackl [1]
W. R. Meier, A. E. Böhmer, P. C. Canfield[2,3]
N. Lazarević [4]

In unconventional superconductors such as the Fe-based pnictides or chalcogenides the pairing mechanism is not well understood. Yet, revealing the interactions in these materials may enable an educated guess or predictions similarly successful as for the hydride LaH_{10+x} ($-1 < x < 2$) [1] shown to become superconducting at a T_c close to room temperature.

Inelastic light (Raman) scattering may pave the way to access details of the interaction potential at the origin of Cooper pairing. Studies of $Ba_{1-x}K_xFe_2As_2$ in a wide range of doping x substantiated this expectation [2, 3] and demonstrated that a hierarchy of pairing instabilities can be observed. In $Ba_{1-x}K_xFe_2As_2$ two subdominant pairing channels having $d_{x^2-y^2}$ symmetry compete with the s-wave ground state and manifest themselves as Raman-active modes below twice the gap energy. Several criteria support the interpretation in terms of Bardasis-Schrieffer (BS) excitons [3]. The ground state and the two sub-leading channels could be reproduced theoretically using two independent methods. Both a functional Renormalization Group (fRG) and a Random Phase Approximation (RPA) analysis correctly predict the hierarchy of pairing states and their doping dependence [4].

Given this agreement between theory and experiment in $Ba_{1-x}K_xFe_2As_2$ the confirmation in a different material would be highly desirable for demonstrating that the in-gap modes are generic and not just accidental. However, most of the known pnictides or chalcogenides have rather anisotropic gaps on the relevant bands thus hampering the observation of undamped modes below the maximal gap. Therefore, the discovery of $CaKFe_4As_4$ was very useful [5]. $CaKFe_4As_4$ is similar to $Ba_{1-x}K_xFe_2As_2$ concerning T_c, the gap [6], and the thermodynamic and transport properties [7]. In addition it is stoichiometric since Ca and K reside on alternating layers and is thus virtually free of defects.

As shown in Fig. 1, spectral changes upon entering the superconducting state can be observed in $CaKFe_4As_4$ in all symmetries. The differences are considerably smaller in A_{1g} and B_{2g} [Fig. 1 (a) and (c)] than in B_{1g} [Fig. 1(b)] symmetry. The results from angle-resolved photoemission spectroscopy (ARPES) are indicated in Fig. 1 (a) as horizontal bars for the four bands of $CaKFe_4As_4$ where α, β, and γ denote the hole bands in the Brillouin zone center and δ stands for the electron band. ARPES and Raman results are consistent. As expected, the A_{1g} spectra reflect the entire range of gaps, whereas the B_{2g} spectra are more sensitive to the gap on the electron bands. The change of the B_{1g} spectra upon entering the superconducting state is substantial as highlighted in the difference spectra (orange). The onset is relatively sharp, and the peak has a clear maximum at $134\,cm^{-1}$ accompanied by a hump on the high energy side at approximately $165\,cm^{-1}$. All relevant B_{1g} energies are well below the maximum gap $2\Delta \approx 220 \pm 20\,cm^{-1}$.

Fig. 1(d) and (e) show difference spectra obtained at two elevated temperatures clearly displaying the double peak structure and, possibly, the existence of another peak in the range

[1]The project was funded by DFG via TRR 80, the Friedrich-Ebert-Foundation (FES), and by DAAD (grant nos. 57142964 and 57335339).

[2]Department of Physics and Astronomy, Iowa State University, USA

[3]Division of Materials Science and Engineering, Ames Laboratory, USA. Work at Ames Laboratory was supported by the U.S. Department of Energy under Contract No. DE-AC02- 07CH11358. W.R.M. was supported by the Gordon and Betty Moore Foundationś EPiQS Initiative through Grant No. GBMF4411.

[4]University of Belgrade, Serbia. The work was funded by the Serbian Ministry of Education, Science and Technological Development under Project III45018.

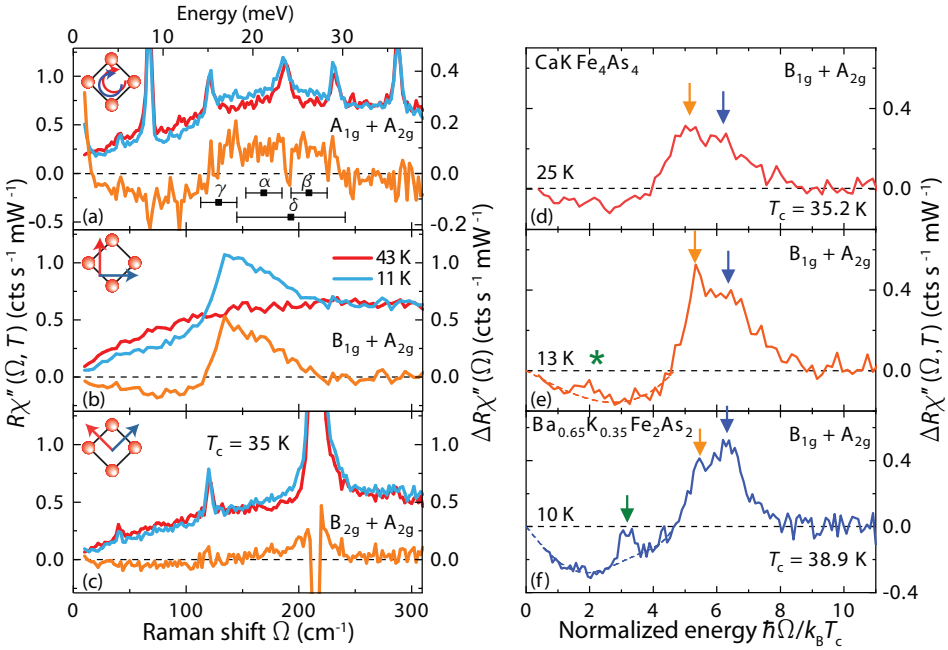

Figure 1: Raman response in $CaKFe_4As_4$ at symmetries and polarizations as indicated. (a)-(c) The normal state spectra (red) are subtracted from the superconducting spectra (blue) to highlight the electronic contribution in the difference spectra (orange). (a) The pair-breaking effect can be observed in the spectral range where the gap energies $2\Delta_i$ of the four bands $i = \alpha, \beta, \gamma, \delta$ are observed by ARPES [6] (horizontal bars). (d) and (e) B_{1g} difference spectra at 13 and 25 K. Blue and orange arrows mark the remainder of the pair-breaking peak and the Bardasis-Schrieffer (BS) mode, respectively. The very weak maximum at $2\,k_BT_c$ (asterisk) may be a second BS mode similar to that in (f) $Ba_{0.65}K_{0.35}Fe_2As_2$ (green arrow). Adopted from Ref. [8].

$2\,k_BT_c$ corresponding to $50\,cm^{-1}$ in absolute units. Both sub-structures of the main peak remain distinguishable even for higher temperatures [Fig. 1 (d) and (e)]. The response is remarkably similar to that of $Ba_{1-x}K_xFe_2As_2$ [Fig. 1 (f)] where the doping dependence for higher x strongly supports the BS scenario at $x = 0.35$ [4]. Even the mode at lower energy [green arrow in Fig. 1 (f)] may have a corresponding structure in $CaKFe_4As_4$ [green asterisk in Fig. 1 (d)] although more experiments are need here for confirmation. Thus, the results in $CaKFe_4As_4$ support the conclusions found for $Ba_{1-x}K_xFe_2As_2$ and provide further evidence for spin fluctuations at the origin of Cooper pairing in at least a subgroup of the pnictides.

References

[1] A. P. Drozdov, V. S. Minkov, S. P. Besedin, P. P. Kong, M. A. Kuzovnikov, D. A. Knyazev, and M. I. Eremets, ArXiv e-prints (2018).

[2] F. Kretzschmar, B. Muschler, T. Böhm, A. Baum, R. Hackl, H.-H. Wen, V. Tsurkan, J. Deisenhofer, and A. Loidl, Phys. Rev. Lett. **110**, 187002 (2013).

[3] T. Böhm, A. F. Kemper, B. Moritz, F. Kretzschmar, B. Muschler, H.-M. Eiter, R. Hackl, T. P. Devereaux, D. J. Scalapino, and H.-H. Wen, Phys. Rev. X **4**, 041046 (2014).

[4] T. Böhm, F. Kretzschmar, A. Baum, M. Rehm, D. Jost, R. Hosseinian Ahangharnejhad, R. Thomale, C. Platt, T. A. Maier, W. Hanke, B. Moritz, T. P. Devereaux, D. J. Scalapino, S. Maiti, P. J. Hirschfeld, P. Adelmann, T. Wolf, H.-H. Wen, and R. Hackl, npj Quantum Materials **3**, 48 (2018).

[5] A. Iyo, K. Kawashima, T. Kinjo, T. Nishio, S. Ishida, H. Fujihisa, Y. Gotoh, K. Kihou, H. Eisaki, and Y. Yoshida, Journal of the American Chemical Society **138**, 3410–3415 (2016).

[6] D. Mou, T. Kong, W. R. Meier, F. Lochner, L.-L. Wang, Q. Lin, Y. Wu, S. L. Bud'ko, I. Eremin, D. D. Johnson, P. C. Canfield, and A. Kaminski, Phys. Rev. Lett. **117**, 277001 (2016).

[7] W. R. Meier, T. Kong, U. S. Kaluarachchi, V. Taufour, N. H. Jo, G. Drachuck, A. E. Böhmer, S. M. Saunders, A. Sapkota, A. Kreyssig, M. A. Tanatar, R. Prozorov, A. I. Goldman, F. F. Balakirev, A. Gurevich, S. L. Bud'ko, and P. C. Canfield, Phys. Rev. B **94**, 064501 (2016).

[8] D. Jost, J.-R. Scholz, U. Zweck, W. R. Meier, A. E. Böhmer, P. C. Canfield, N. Lazarević, and R. Hackl, Phys. Rev. B **98**, 020504(R) (2018).

Fermi Surface and Momentum-Dependent Electronic Correlations in a Layered Organic Conductor Near the Mott Transition

M.V. Kartsovnik, W. Biberacher, S. Oberbauer [1]
V.N. Zverev [2]

The layered molecular charge-transfer salt κ-$(BETS)_2Mn[N(CN)_2]_3$ is a bandwidth-controlled Mott insulator, which can be driven to a metallic state by applying a very moderate pressure, $\sim 1\,\mathrm{kbar}$ [1, 2]. Similarly to other correlated-electron materials of topical interest, the compound exhibits superconductivity in a direct neighborhood to the insulating state. Moreover, it is a hybrid material composed of two-dimensional conducting and magnetic subsystems alternating in a regular manner on a subnanometer scale [2]. Thus, it is very interesting in the context of interplay between electronic correlations and magnetic instabilities.

Recently, we have found quantum (Shubnikov-de Haas, SdH) oscillations in the interlayer magnetoresistance of a κ-$(BETS)_2Mn[N(CN)_2]_3$ crystal pressurized to the metallic state [3]. The oscillation spectrum showed two fundamental frequencies attributed, respectively, to a classical and magnetic-breakdown (MB) orbit on the Fermi surface. The effective cyclotron mass on the classical orbit was found to be unusually high. In order to clarify the reason for this, we have carried out further high-field magnetotransport measurements and compared the results with new first-principles band structure calculations [4]. The experiment was done under a pressure of 1.4 kbar, which drives the compound into the fully metallic state, but not far away from the metal-insulator phase boundary [1].

In addition to the SdH oscillations, classical angle-dependent magnetoresistance oscillations (AMRO) [5] were found at $T \leq 1.5\,\mathrm{K}$. Based on a thorough analysis of both oscillatory phenomena we determined the size and shape of the in-plane Fermi surface as shown in Fig. 1 by a thick green line [4]. From the SdH oscillations the size of the classical orbit α and MB orbit β as well as the MB gap at the intersection of the Fermi surface with the Brillouin zone boundary have been evaluated. The gap in **k**-space is $\sim 1.5 \times 10^{-2}\,\mathrm{nm}^{-1}$, which is hardly resolvable in the scale of Fig. 1. The classical AMRO were observed at the highest field, $B = 28\,\mathrm{T}$, corresponding to an almost full MB regime. Therefore, only the MB orbit β was seen in those measurements. A very good agreement is found between the experimentally determined Fermi surface and the results of band structure calculations. In particular, the existence of almost flat segments of the α pocket is confirmed.

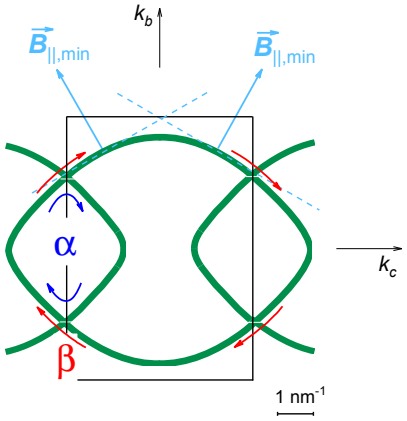

Figure 1: Fermi surface of κ-$(BETS)_2Mn[N(CN)_2]_3$ in the plane of conducting layers [4]. Thin black lines are the first Brillouin zone boundaries. The blue and red arrows show schematically the directions of the cyclotron motion on the classical orbit α and MB orbit β, respectively, in a field normal to the layers. The light-blue arrows show the in-plane field directions corresponding to the minima in $R(\varphi)$, see Fig. 2.

The effective cyclotron masses obtained from the T-dependence of the SdH amplitudes are $m_\alpha \approx 5.6m_0$ and $m_\beta \approx 7.0m_0$ for the α and β orbits, respectively (m_0 is the free electron mass). Comparing these values with the calculated band cyclotron masses $m_\alpha^b = 1.93m_0$ and $m_\beta^b = 2.89m_0$, we find that the many-body renormalization factors are notably different for the two orbits: $r_\alpha = 2.9$ and $r_\beta = 2.4$. While similarly strong many-body effects have been

[1]The work was supported in part by the German Research Foundation grant No. KA 1652/4-1 and by the LNCMI-CNRS, the member of the European Magnetic Field Laboratory (EMFL).
[2]Institute of Solid State Physics, Chernogolovka, Russia

reported for some other κ-type salts of BEDT-TTF and BETS, they are usually uniform over the Fermi surface [6, 7]. The stronger enhancement of many-body effects on the α pocket is most likely caused by an increased one-particle partial density of states associated with this pocket [4]. The corresponding effective reduction of the bandwidth may place this part of the conduction system more close to the Mott-insulating state, resulting in a relative enhancement of electron correlations. Additionally, the flat parts of the α Fermi pocket are subject to a "nesting" instability, that is, a strongly enhanced scattering at the wave vector connecting the opposite flat segments of the pocket. This may further contribute to the many-body renormalization factor for the effective mass. To check the role of the proximity to the insulating state, we have repeated the SdH experiment at an elevated pressure, $p = 4.1$ kbar, moving the material far away from the metal-insulator phase boundary. At these conditions the mass renormalization factors reduced and, importantly, became the same for both orbits, $r_\alpha = r_\beta = 1.78 \pm 0.05$.

The stronger impact of electronic correlations on the α Fermi pocket is also manifested in the angle dependence of the classical magnetoresistance in fields parallel to conducting layers [4]. Figure 2 shows the interlayer resistance of κ-$(BETS)_2Mn[N(CN)_2]_3$ as a function of the angle φ between the inplane field and crystallographic b-axis. Qualitatively, the shape of the φ-dependence is very similar to what is observed on other layered metals with an anisotropic inplane Fermi surface. The magnetoresistance is largely determined by the inplane curvature of the Fermi surface, showing minima at the field directions perpendicular to its flattest segments [5]. For the Fermi surface in Fig. 1 one would expect magnetoresistance minima at $|\varphi| \approx 42°$, when the field is perpendicular to the flat sides of the rhombus-like α pocket. However, in Fig. 2 the minima are in fact at $|\varphi| \approx 30°$. The discrepancy, $\gtrsim 10°$, definitely exceeds the experimental error bar. This result implies a suppressed contribution of carriers on the α pocket to the total interlayer conductivity. The most likely reason for that is a reduced mobility caused by the enhanced electronic correlations on this part of the Fermi surface.

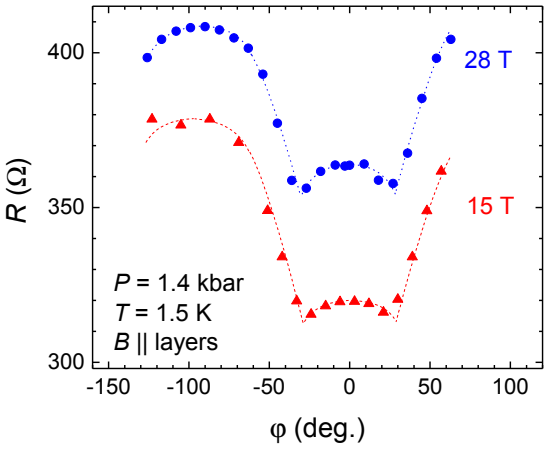

Figure 2: Angular dependence of the resistance in a field parallel to the conducting layers, at $B = 15$ and 28 T [4]. Dotted lines are guides to the eye.

In summary, both the quantum oscillations and classical magnetoresistance anisotropy in κ-$(BETS)_2Mn[N(CN)_2]_3$ point to a particular enhancement of electronic correlations on the α pocket of the Fermi surface in proximity to the Mott-insulating transition.

References

[1] V. N. Zverev, M. V. Kartsovnik, W. Biberacher, S. S. Khasanov, R. P. Shibaeva, L. Ouahab, L. Toupet, N. D. Kushch, E. B. Yagubskii, and E. Canadell, Phys. Rev. B **82**, 155123 (2010).
[2] N. D. Kushch, E. B. Yagubskii, M. V. Kartsovnik, L. I. Buravov, A. D. Dubrovskii, A. N. Chekhlov, and W. Biberacher, J. Am. Chem. Soc. **130**, 7238–7240 (2008).
[3] M. V. Kartsovnik, V. N. Zverev, W. Biberacher, S. V. Simonov, I. Sheikin, N. D. Kushch, and E. B. Yagubskii, Low Temp. Phys. **43**, 239–243 (2017).
[4] V. N. Zverev, W. Biberacher, S. Oberbauer, I. Sheikin, P. Alemany, E. Canadell, and M. V. Kartsovnik. Fermi surface properties of the bifunctional organic metal κ-$(BETS)_2Mn[N(CN)_2]_3$ near the metal–insulator transition. arXiv:1811.10265 (2018).
[5] M. V. Kartsovnik, Chem. Rev. **104**, 5737 (2004).
[6] J. Merino, and R. H. McKenzie, Phys. Rev. B **62**, 2416–2423 (2000).
[7] T. Kawamoto, and T. Mori, Phys. Rev. B **74**, 212502 (2006).

Quantum Discord in Squeezed Microwaves

K. G. Fedorov, S. Pogorzalek, M. Xu, Q. Chen, M. Renger, M. Fischer, E. Xie, A. Marx, F. Deppe, R. Gross [1]

Quantum discord is known as a general measure for quantum correlations in bipartite systems. It encompasses all nonclassical correlations including entanglement. Quantum discord has multiple intriguing fundamental properties with many of them requiring experimental verification such as the asymptotic robustness towards environmental noise. We experimentally investigate quantum discord in propagating two-mode squeezed (TMS) microwave states generated with the help of superconducting Josephson parametric amplifiers (JPAs) [1]. Here, we exploit an asymmetric noise injection into the TMS states to demonstrate the robustness of quantum discord against noise as opposed to the sudden death of entanglement.

We use two superconducting flux-driven JPAs operated at the frequency of $f_0 = 5.323\,\mathrm{GHz}$ for the generation of orthogonal squeezed microwave states. The task of each JPA is to perform a squeezing operation on the incident vacuum state. As shown in Fig. 1(a), generation of symmetric propagating two-mode squeezed states is achieved with a microwave beam splitter by superimposing two orthogonally squeezed microwave states [2–4]. In the TMS microwave states, entanglement is expressed by strong correlations between two nonlocal field quadratures. The state tomography is based on correlation measurements of paths 1&2 which can be used to derive the covariance

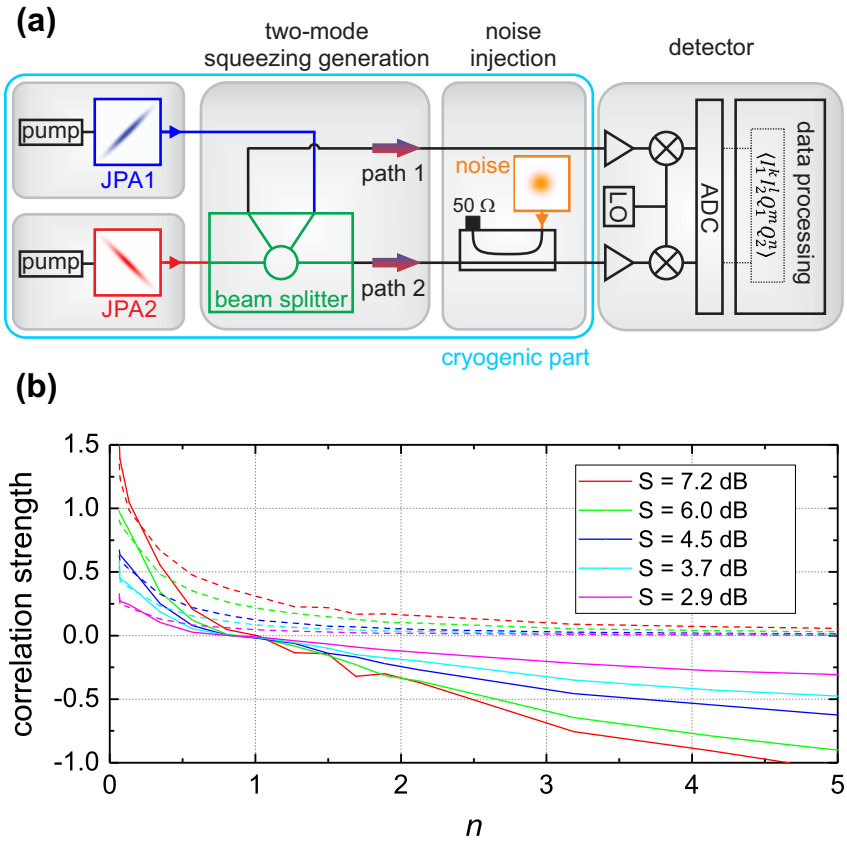

Figure 1: **(a)** Scheme for the experimental entanglement generation and noise injection into propagating two-mode squeezed microwave states. **(b)** Quantum discord (QD) and entanglement of formation (EoF) are plotted versus the injected noise photon number n for various squeezing levels from JPA1 and JPA2 under the condition $S_1 = S_2 = S$. Solid lines depict EoF and dashed lines depict QD. The sudden death of entanglement is reflected by negative EoF for $n \geq 1$, independent of the input squeezing level S, while QD is asymptotically resistant to external noise.

[1]The authors acknowledge support from the German Research Foundation through FE 1564/1-1, the doctorate program ExQM of the Elite Network of Bavaria, the EU Quantum Flagship project 'Quantum Microwaves for Communication and Sensing (QMiCS)', as well as the German Excellence Initiative via the 'Nanosystems Initiative Munich' (NIM) and the 'Munich Center for Quantum Science and Technology (MCQST)'. We also acknowledge the productive collaboration with the groups of Y. Nakamura and E. Solano.

matrix of the entangled beams [2–4]. By using this covariance matrix, one can calculate both entanglement of formation (EoF) and quantum discord (QD) which allow one to experimentally verify presence of path entanglement and general nonclassical correlations, respectively [5, 6]. Physically, the entanglement of formation quantifies the minimum amount of two-mode squeezing needed to prepare an entangled state starting from a classical one.

In order to test the robustness of these nonclassical correlations with respect to environmental noise, one has to perform a controlled noise injection into one of the entangled paths. The noise generation is performed by means of a Keysight 81160A arbitrary function generator (AFG) which produces a low-frequency white noise with a specified bandwidth of 160 MHz. The latter is then up-converted to the JPA frequency f_0 and sent to the cryogenic setup. We implement the actual noise injection in one of the entangled paths with a directional coupler as shown in Fig. 1(a). By varying the noise power emitted from the AFG, we probe entanglement of formation and quantum discord as a function of the injected noise photon number n for different JPA squeezing levels. The latter is defined as $S = -10\log_2[(\Delta X_{\mathrm{sq}})^2/0.25]$, where $(\Delta X_{\mathrm{sq}})^2$ is the variance of the squeezed quadrature and the chosen vacuum reference is $(\Delta X_{\mathrm{vac}})^2 \equiv 0.25$. Figure 1(b) shows the experimental results. They clearly demonstrate the sudden death of entanglement at $n = 1$ characterized by the negative values of EoF independent from the initial level of squeezing. This is an important fundamental threshold for the two-mode squeezed light. At the same time, QD remains positive in the whole range of noise photon numbers. This observation confirms the asymptotic robustness of QD to the noise.

The experimentally verified robustness quantum discord against noise strongly motivates the search for quantum communication and sensing protocols exploiting QD as a quantum resource. Such protocols would be inherently resistant to noise in contrast to entanglement-based approaches. The indirect role of QD has been already uncovered for some known applications such as the DQC1 quantum computation model [7] or quantum illumination protocols [8].

References

[1] S. Pogorzalek, K. G. Fedorov, L. Zhong, J. Goetz, F. Wulschner, M. Fischer, P. Eder, E. Xie, K. Inomata, T. Yamamoto, Y. Nakamura, A. Marx, F. Deppe, and R. Gross, Phys. Rev. Applied **8**, 024012 (2017).

[2] E. P. Menzel, R. Di Candia, F. Deppe, P. Eder, L. Zhong, M. Ihmig, M. Haeberlein, A. Baust, E. Hoffmann, D. Ballester, K. Inomata, T. Yamamoto, Y. Nakamura, E. Solano, A. Marx, and R. Gross, Phys. Rev. Lett. **109**, 250502 (2012).

[3] K. G. Fedorov, L. Zhong, S. Pogorzalek, P. Eder, M. Fischer, J. Goetz, E. Xie, F. Wulschner, K. Inomata, T. Yamamoto, Y. Nakamura, R. Di Candia, U. Las Heras, M. Sanz, E. Solano, E. P. Menzel, F. Deppe, A. Marx, and R. Gross, Phys. Rev. Lett. **117**, 020502 (2016).

[4] K. G. Fedorov, S. Pogorzalek, U. Las Heras, M. Sanz, P. Yard, P. Eder, M. Fischer, J. Goetz, E. Xie, K. Inomata, Y. Nakamura, R. Di Candia, E. Solano, A. Marx, F. Deppe, and R. Gross, Sci. Rep. **8**, 6416 (2018).

[5] S. Tserkis, and T. C. Ralph, Phys. Rev. A **96**, 062338 (2017).

[6] P. Giorda, and M. G. A. Paris, Phys. Rev. Lett. **105**, 020503 (2010).

[7] A. Datta, A. Shaji, and C. M. Caves, Phys. Rev. Lett. **100**, 050502 (2008).

[8] C. Weedbrook, S. Pirandola, J. Thompson, V. Vedral, and M. Gu, New J. Phys. **18**, 043027 (2016).

Quantum Vernam Cipher with Propagating Squeezed Microwaves

S. Pogorzalek, K. G. Fedorov, M. Xu, Q. Chen, M. Fischer, M. Renger, E. Xie, A. Marx, F. Deppe, R. Gross [1]

Quantum communication protocols employ nonclassical correlations as a resource for a more efficient transfer of quantum states when compared to their classical counterparts. The closely related field of quantum cryptography deals with the secure transfer of information by exploiting quantum correlations. As a fundamental quantum communication protocol, remote state preparation (RSP) achieves both an efficient and secure transfer of a quantum state. We focus on the latter property by relating the RSP scheme to an extension of the cryptographic protocol known as the Vernam cipher to the quantum regime. In particular, we achieve the transfer of a quantum squeezed state with 1.6 dB of squeezing below the vacuum over a distance of 35 cm of superconducting cable. At the same time, the classically communicated signal reveals nearly no information about the transferred quantum state.

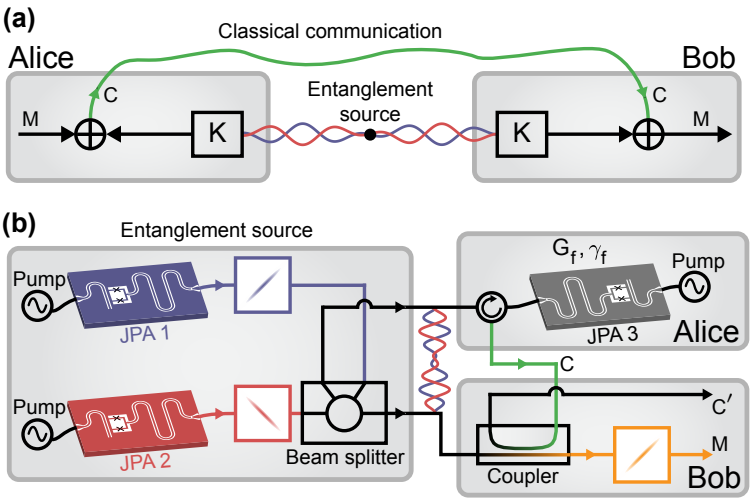

Figure 1: **(a)** Concept of the quantum Vernam cipher: an entangled resource and classical communication (encoded in the cipher C) are used to securely transfer a quantum state M. The key K is provided by the entangled state. **(b)** Experimentally implemented scheme: two JPAs and a beam splitter are used for the entanglement generation. On Alice's side, the message M is defined by the amplification properties of JPA 3. Bob uses a directional coupler to decipher the communicated signal by utilizing the initial entangled signal.

The principle of the quantum Vernam cipher is depicted in Fig. 1(a). Here, Alice wants to securely send a quantum state M to Bob by exploiting classical communication of a cipher C over an insecure channel. An entangled state provides the random key K in the form of quantum fluctuations to both parties. Note that K is essential for the Vernam cipher since it is used by Alice and Bob to encode and decode M. The key K needs to be a uniform random variable for secure communication, such that an eavesdropper with knowledge about C does not gain any information about M. Mathematically, this is expressed as

$$H(M) - H(M|C) = 0\,, \tag{1}$$

where $H(M)$ is the von Neumann entropy of the remotely prepared state and $H(M|C) = H(M,C) - H(C)$ is the conditional entropy of M given the feedforward signal C.

The experimentally implemented Vernam cipher is shown in Fig. 1(b). Multiple flux-driven Josephson parametric amplifiers (JPAs) [1] are used for either the generation of squeezed states (JPA 1 and JPA 2) or phase-sensitive amplification (JPA 3). The JPAs are placed inside magnetically shielded sample holders in a dry dilution refrigerator and are operated at $f_0 = 5.435\,\mathrm{GHz}$

[1] The authors acknowledge support from the German Research Foundation through project FE 1564/1-1, the doctorate program ExQM of the Elite Network of Bavaria; the EU Quantum Flagship project 'Quantum Microwaves for Communication and Sensing' (QMiCS), as well as the German Excellence Initiative via the 'Nanosystems Initiative Munich' (NIM) and the 'Munich Center for Quantum Science and Technology' (MCQST). We also acknowledge the productive collaboration with the groups of Y. Nakamura and E. Solano.

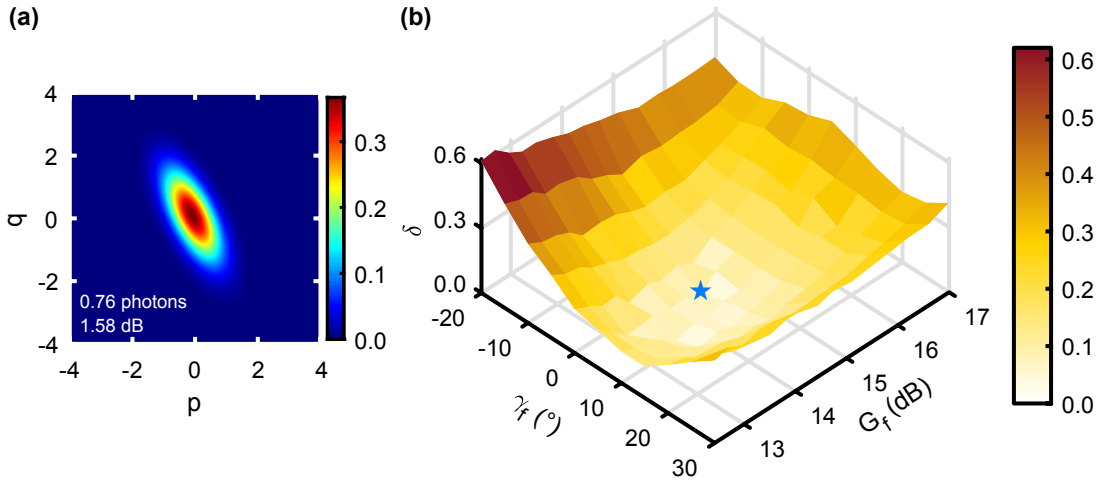

Figure 2: (a) Wigner function of the transferred state M on Bob's side at the optimal point. **(b)** Entropy difference $\delta = H(M) - H(M|C')$ as a function of the JPA 3 amplification parameters G_f and γ_f. The optimal point is marked by the blue star.

at a temperature of 50 mK. JPA 1 and JPA 2 generate squeezed states which are incident to an entangling beam splitter. The resulting two-mode squeezed (TMS) state, providing the key K, has an entanglement strength characterized by the negativity criterion of $N = 2.2$ [2] and is distributed to Alice and Bob. On Alice's side, her part of the entangled state is phase-sensitively amplified by JPA 3 in order to generate the cipher C. The to-be-transmitted message M is encoded by the degenerate gain G_f and amplification angle γ_f of JPA 3. C contains the essential classical information about M in the amplified field quadrature. After receiving C, Bob uses it to displace his part of the entangled state by utilizing a directional coupler with a fixed coupling $\beta \simeq -15\,\mathrm{dB}$ [3] and finally obtains M.

At the optimal point of the protocol ($G_f \simeq 14\,\mathrm{dB}$, $\gamma_f \simeq 5°$), we obtained a squeezed state M on Bob's side with a squeezing level of 1.6 dB below the vacuum as shown in Fig. 2(a). The security of the protocol can be evaluated by additionally detecting the signal C' from the second directional coupler output. With that, one can compute $\delta = H(M) - H(M|C')$ to verify Eq. (1) under the reasonable approximation of $C' \approx C$ (due to the low coupling β) using state tomography. In Fig. 2(b), we observe a decrease in δ when moving towards the optimal point where the smallest value $\delta = 0.06 \pm 0.04$ is reached. At this point, the entropy of the prepared state is $H(M) = 0.80$. This indicates that an eavesdropper in the classical communication can only gain a small amount of information on the transferred quantum state since $\delta \ll H(M)$.

In summary, we have successfully demonstrated that the RSP protocol can be related to the quantum Vernam cipher near the optimal point of the protocol. Here, a squeezed state is securely transferred from Alice to Bob. The demonstrated protocol provides the basis for various quantum communication protocols with microwaves and is a fundamental building block for local quantum networks in the microwave range.

References

[1] S. Pogorzalek, K. G. Fedorov, L. Zhong, J. Goetz, F. Wulschner, M. Fischer, P. Eder, E. Xie, K. Inomata, T. Yamamoto, Y. Nakamura, A. Marx, F. Deppe, and R. Gross, Phys. Rev. Appl. **8**, 024012 (2017).

[2] K. G. Fedorov, S. Pogorzalek, U. Las Heras, M. Sanz, P. Yard, P. Eder, M. Fischer, J. Goetz, E. Xie, K. Inomata, Y. Nakamura, R. Di Candia, E. Solano, A. Marx, F. Deppe, and R. Gross, Sci. Rep. **8**, 6416 (2018).

[3] K. G. Fedorov, L. Zhong, S. Pogorzalek, P. Eder, M. Fischer, J. Goetz, E. Xie, F. Wulschner, K. Inomata, T. Yamamoto, Y. Nakamura, R. Di Candia, U. Las Heras, M. Sanz, E. Solano, E. P. Menzel, F. Deppe, A. Marx, and R. Gross, Phys. Rev. Lett. **117**, 020502 (2016).

Quantum Process Tomography and Time Resolved Tomography

M. Renger, E. Xie, F. Deppe, Q. Chen, M. Fischer, S. Pogorzalek, K.G. Fedorov, A. Marx, R. Gross [1]

The experimental reconstruction of quantum processes is a key element in quantum information processing. It is particularly important for benchmarking quantum gates and quantum error correction [1]. A commonly used technique to solve this task is quantum process tomography (QPT) which allows one to gain full knowledge about a quantum process by performing a sufficient amount of projective measurements. In order to characterize single qubit operations, we implement a QPT protocol [2] which can be scaled up to large quantum systems in a straightforward manner.

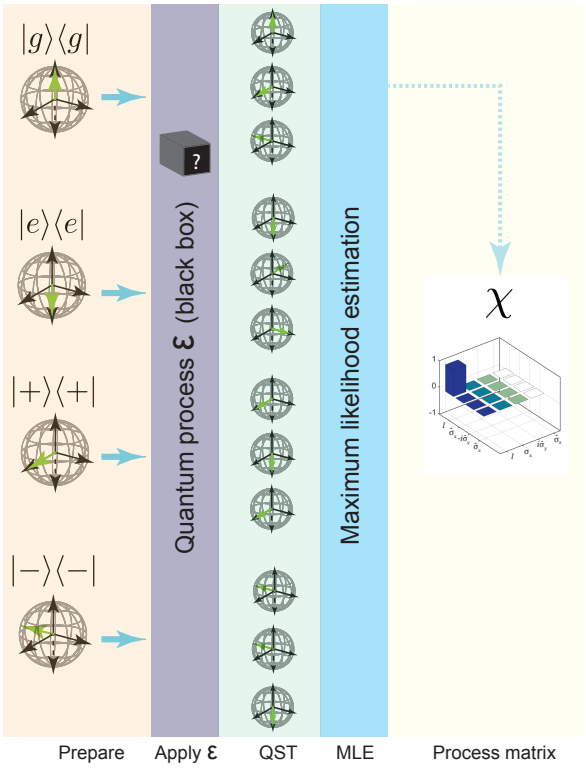

Figure 1: Schematic illustration of single qubit QPT. Four distinct input states are reconstructed with quantum state tomography. A MLE enforces physicality of the reconstructed process.

A quantum process $\mathcal{E}$ on a d-dimensional quantum system can be considered as a map between two density operators which can be expressed as $\mathcal{E}(\rho) = \sum_{m,n}^{d^2} B_m \rho B_n^\dagger \chi_{mn}$, where $\{B_m\}$ is a fixed operator basis [3]. As a result, all information about $\mathcal{E}$ is encoded in the evolution coefficients χ_{mn}, which can be rearranged as a $(d^2 \times d^2)$ process matrix χ. Single qubit processes ($d = 2$) can be interpreted as a translation, followed by a rotation and deformation of the Bloch sphere. For convenience, we use a modified Pauli basis $B_m \in \{I, \hat{\sigma}_x, -i\hat{\sigma}_y, \hat{\sigma}_z\}$. To obtain χ, we apply $\mathcal{E}$ to the qubit ground state $|g\rangle$, to the excited state $|e\rangle$ and to the superposition states $|+\rangle \equiv 1/\sqrt{2}(|g\rangle + |e\rangle)$ and $|-\rangle \equiv 1/\sqrt{2}(|g\rangle + i|e\rangle)$, and reconstruct the resulting states with quantum state tomography. Since the experimental setup adds noise to the system, it is not guaranteed that χ represents a physically valid process. We use a maximum-likelihood-estimation (MLE) and enforce physicality by parametrizing a valid $\tilde{\chi}(t_i)$ [4]. Subsequently, we calculate the process fidelity $f(\chi_1, \chi_2) = \mathrm{Tr}\sqrt{\sqrt{\chi_1}\chi_2\sqrt{\chi_1}}$ which allows us to compare the reconstructed process matrix with the expected result.

Our single qubit QPT protocol is summarized in Fig. 1. We use QPT to characterize the quantum memory experiment that has been implemented at the WMI [5], where we realize the quantum memory by coupling a transmon qubit to a rectangular 3D cavity resonator (see report on page 63). As described in [2, 5, 6], we exploit the multimode structure of the 3D cavity and combine readout and storage in one single device, thereby significantly enhancing scalability perspectives of this approach. Compared to the bare qubit energy decay time

[1] The authors acknowledge support from the German Research Foundation through FE 1564/1-1, the doctorate program ExQM of the Elite Network of Bavaria, the IMPRS 'Quantum Science and Technology', the EU Quantum Flagship project 'Quantum Microwaves for Communication and Sensing' (QMiCS), as well as the German Excellence Initiative via the 'Nanosystems Initiative Munich'(NIM) and the 'Munich Center for Quantum Science and Technology' (MCQST).

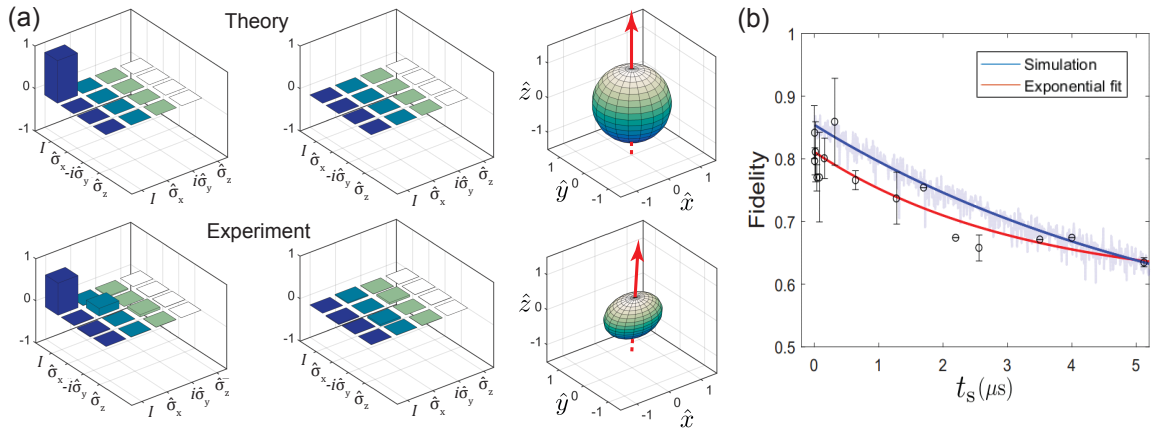

Figure 2: (a) Process matrix and Bloch sphere for the quantum memory protocol. Ideally, the memory process is an identity. Depolarization yields a contraction of the Bloch sphere. (b) Process fidelity as a function of the storage time t_s. The red curve is a fit to the measured data points (black circles), the blue curve is obtained by the simulation. Temporal variations of the decay times result in fluctuations of the fidelity (light blue).

$T_1 = 1.32\,\mu s$, we achieve an enhancement by a factor of 6 [6]. Using QPT, we measure a process fidelity $f = 87.6 \pm 2.5\,\%$ [2]. The corresponding process matrix as well as the reconstructed Bloch sphere are depicted in Fig. 2(a). When correcting for T_1-decay during the memory protocol, we obtain the corrected fidelity $f_c \simeq 96.6\,\%$. The experiment is carried out at 40 mK, yielding a thermal qubit population of 0.06 % and a thermal fidelity reduction of only 0.04 %. We attribute the remaining difference to 100 % to state leakage resulting from the low transmon anharmonicity of 2.6 %, dephasing, and inaccurate state preparation. As it is apparent from Fig. 2(a), the memory process can be written as $\mathcal{E}(\rho) \simeq (1-p)\rho + p\hat{\sigma}_x\rho\hat{\sigma}_x$. We interpret p as a Markovian probability for depolarization in the yz-plane, yielding a contraction of the Bloch sphere towards the $\hat{x}$-axis, probably caused by linear phase trends or IQ-sensitive noise.

In order to get access to the dynamical behavior of the system, we vary the storage time t_s and perform QPT for discrete time steps. Figure 2(b) shows the measured fidelities and a corresponding exponential fit. Error bars are obtained for a selection of data points. We simulate the memory protocol using a Lindblad master equation approach [3]. The resulting decay of the process fidelity is depicted in Fig. 2(b). We observe that the fidelities extracted from the simulation are larger than the measured values and assign this to the fact that we neglect the state leakage in the master equation. We observe a better coincidence of experiment and simulation for large t_s which can be explained by the asymmetric behavior of the measured depolarization in Fig. 2(a) which is not reproduced by the simulation. For increasing t_s, this difference in asymmetry decreases. In summary, we have successfully investigated the dynamics of a compact 3D quantum memory by means of QPT.

References

[1] J. Chiaverini, D. Leibfried, T. Schaetz, M. D. Barrett, R. B. Blakestad, J. Britton, W. M. Itano, J. D. Jost, E. Knill, C. Langer, R. Ozeri, and D. J. Wineland, Nature **432**, 602 EP – (2004).

[2] M. Renger. *Quantum Process Tomography of a 3D Quantum Memory*. Master's thesis, Technische Universität München (2018).

[3] M. A. Nielsen, and I. L. Chuang. *Quantum Computation and Quantum Information: 10th Anniversary Edition* (Cambridge University Press, New York, NY, USA, 2011), 10th edn.

[4] M. Howard, J. Twamley, C. Wittmann, T. Gaebel, F. Jelezko, and J. Wrachtrup, New Journal of Physics **8**, 33 (2006).

[5] E. Xie, F. Deppe, M. Renger, D. Repp, P. Eder, M. Fischer, J. Goetz, S. Pogorzalek, K. G. Fedorov, A. Marx, and R. Gross, Applied Physics Letters **112**, 202601 (2018).

[6] E. Xie. *A scalable 3D quantum memory*. Ph.D. thesis, TU München (2018).

Finite Size Effect of the Magnetic Correlation Length in Sr_2IrO_4

S. Geprägs, M. Opel, R. Gross [1]
D. Mannix [2]

The Ruddlesden-Popper series $Sr_{n+1}Ir_nO_{3n+1}$ has attracted considerable scientific attention as the strong spin-orbit coupling in these compounds may allow to generate materials with novel physical properties. In the first member of the series, the layered Sr_2IrO_4 (SIO) ($n = 1$) compound, the large spin-orbit coupling combined with a large crystal field splitting results in a Mott insulating ground state, in which the local electronic state of the Ir ions is represented by an effective total angular momentum $J_{\text{eff}} = 1/2$ [1]. Below the Néel temperature of around $T_N = 240\,\text{K}$, this pseudo-1/2-spins order in a layered, canted antiferromagnetic structure with a canting angle of around 12.2°. The magnetic structure of SIO is very similar to that of the seminal high T_c superconducting parent compound La_2CuO_4 (LCO). Therefore, SIO and LCO could represent model systems to investigate the physical effects which promote or suppress superconductivity in oxide materials, especially if these materials can be manipulated to mimic each other more closely using external perturbations.

Due to the strong magnetoelastic locking of the Ir moments to the rotation of the oxygen octahedra, epitaxial strain in SIO thin films represents an interesting possibility to tune the ground state of SIO. To this end, we fabricated tensile and compressive strained epitaxial SIO thin films with thicknesses between 30 and 120 nm on (001)-oriented $SrTiO_3$ (STO) and (110)-oriented $NdGaO_3$ (NGO) substrates by pulsed laser deposition (PLD) [2]. The crystalline structure of the SIO thin films were investigated by x-ray diffraction (XRD) measurements. A typical XRD Q_z-scan (L-scan) is shown in Fig. 1(a). In all SIO thin films, we found strong and pronounced Laue oscillations, indicating a coherent growth throughout the entire thickness of the thin films. The full width at half maximum (FWHM) of the rocking curves around the SIO (0 0 12) reflection of less than 0.04° reveals a low mosaic spread and an excellent crystalline quality of all SIO thin films (cf. inset of Fig. 1(a)). The epitaxial relations between the SIO thin films and the respective substrate was investigated by recording reciprocal space maps (RSM). Typical RSMs are shown in Fig. 1(b)-(e), where the SIO (1 1 18) reflections appear almost at the same in-plane Q_x position as the STO (1 0 3) and NGO (3 3 2) substrate reflections, respectively. This result demonstrates that even the 108 nm thick SIO film is still fully strained and therefore has the same in-plane lattice parameters as the STO substrate.

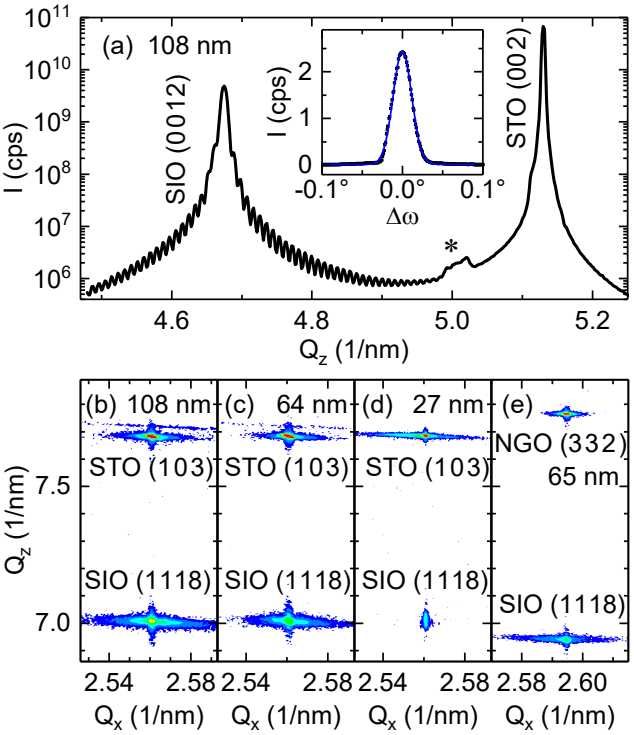

Figure 1: (a) X-ray diffraction of a 108 nm thick SIO film on STO. The powder reflections marked by the asterisks are caused by the beryllium dome used for the measurement. The inset shows the rocking curve around the SIO (0 0 12) reflection. A full width at half maximum of 0.03° is obtained. (b)-(d) Reciprocal space maps of SIO thin films around the STO (1 0 3) and (e) the NGO (3 3 2) reflections, indicating that all SIO thin films are fully strained.

[1] This work was supported by the European Synchrotron Radiation Facility (ESRF) via HC-1821.
[2] Department of Physics, Lund University, Sweden.

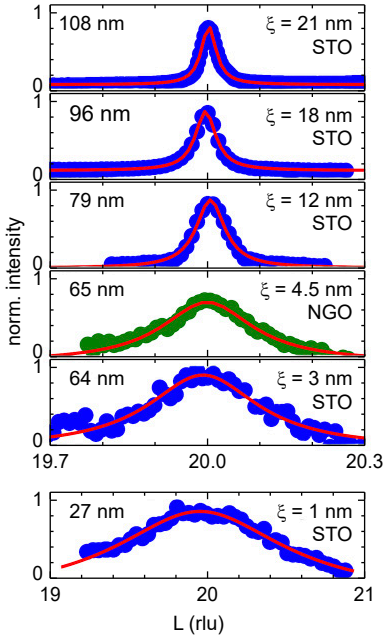

Figure 2: L-scans around the (1 0 20) magnetic reflection of SIO thin films with different thickness. The c-axis magnetic correlation length ξ is extracted from Lorentzian fits to the data (red lines).

To investigate the basal-plane antiferromagnetic (AFM) structure of the SIO thin films, we have employed polarized X-ray resonant scattering (XRS) measurements at the Ir $L_{2,3}$ absorption edges at the XMaS bending magnet beamline of the European Synchrotron Radiation Facility and at the I16 insertion device beamline of the Diamond Light Source. In such diffraction experiments, the AFM basal-plane gives rise to magnetic Bragg reflections below T_N, indexed by $(1\,0\,4n)$ and $(0\,1\,4n{+}2)$. From L-scans around the magnetic reflection $(1\,0\,20)$, we extract the magnetic correlation length ξ along the c-axis as the inverse of the half width at half maximum of the Lorentzian fits to the data. As obvious from Fig. 2, ξ is strongly dependent on the film thickness. We find a large correlation length of 21 nm for the 108 nm thick SIO film, which decreases to 1 nm for the 27 nm thick SIO thin film on STO. Since all SIO thin films on STO are fully strained, as was shown above, the difference in ξ cannot be ascribed to different strain states of the SIO thin films. This is further confirmed by the similar ξ values of the tensile-strained SIO thin film on STO with a thickness of 64 nm and the compressive-strained 65 nm thick SIO thin film on NGO. The thickness dependence of the magnetic correlation lengths is plotted in Fig. 3. Two regimes can be clearly identified: For $d \lesssim 62$ nm low ξ values are observed indicating a very short range magnetic order, whereas $d \gtrsim 62$ nm, the magnetic correlation length is found to strongly increase with increasing d. In this regime, a power-law fit to the data reveals a critical thickness of $d_c = 62.5$ nm (cf. black line in Fig. 3).

Interestingly, the ξ value of a 50 nm SIO thin film on STO reported in a previous XRS study by Lupascu *et al.* [3] (red symbol in Fig. 3) fits well into the thickness dependence of our SIO thin films. Therefore, our data strongly suggest that the magnetic correlation length ξ along the c-axis is independent of the strain state of the SIO films, but highly thickness dependent with a critical thickness of 62.5 nm, separating regions with short and long range magnetic order. Our results thus demonstrate that the magnetic order in SIO can be strongly tuned by varying the thickness of SIO thin films.

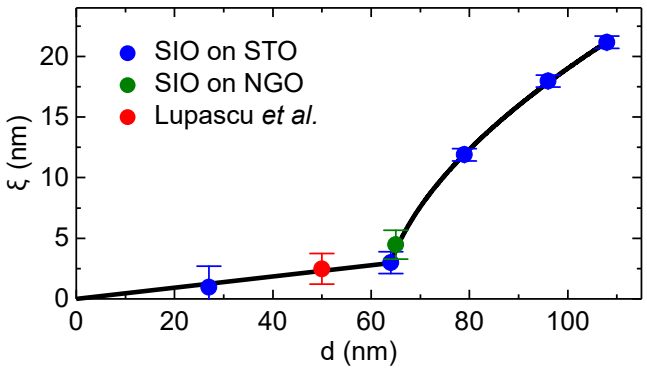

Figure 3: Magnetic correlation length ξ as a function of film thickness d of tensile-strained (blue symbols) and compressive-strained (green symbol) SIO thin films. The red symbol denotes the ξ-value reported by Lupascu *et al.* for a SIO thin film on STO [3]. The solid black line is a power-law fit, revealing a critical thickness of d_c=62.5 nm.

References

[1] B. J. Kim, H. Ohsumi, T. Komesu, S. Sakai, T. Morita, H. Takagi, and T. Arima, Science **323**, 1329–1332 (2009).
[2] S. Geprägs, J. Fischer, M. Opel, R. Gross, B. Skovdal, and D. Mannix, WMI Ann. Rep. **2012**, 75–76 (2015).
[3] A. Lupascu, J. P. Clancy, H. Gretarsson, Z. Nie, J. Nichols, J. Terzic, G. Cao, S. S. A. Seo, Z. Islam, M. H. Upton, J. Kim, D. Casa, T. Gog, A. H. Said, V. M. Katukuri, H. Stoll, L. Hozoi, J. van den Brink, and Y.-J. Kim, Phys. Rev. Lett. **112**, 147201 (2014).

Spin-Torque Excitation of Nanoscale Spin Waves

M. Weiler, S. Klingler, S. Geprägs, K. Ganzhorn, H. Maier-Flaig, M. Althammer, H. Huebl, R. Gross [1]
S.T.B. Goennenwein [2,3] *, V. Amin, R.D. McMichael, M. Stiles* [4]

Magnon logic devices use spin waves for computation purposes [1]. Practical magnon logic devices require operation with short-wavelength spin waves to profit from isotropic spin wave dispersion and miniaturized device dimensions [2]. However, an excitation of nanoscale spin waves by microwave magnetic fields requires nanolithographically defined microwave antennas that have poor efficiency due to high ohmic losses and impedance mismatch.

Here, we show that the interfacial nature of spin torques in magnetic heterostructures can be exploited for the efficient generation of spin waves with wavelengths shorter than 100 nm in yttrium iron garnet (YIG) [3]. With its long magnon propagation length, YIG is the material of choice for magnon logic. A 50 nm thick Co film is deposited on top of a YIG film with 1 µm thickness. The substrate is (111)-oriented gadolinium gallium garnet. We furthermore fabricate YIG/Cu(5 nm)/Co(50 nm) and YIG/AlO_x(1.5 nm)/Co(50 nm) thin film trilayers, where the YIG thickness is always 1 µm.

We test the static magnetic properties of these heterostructures using SQUID magnetometry. Fig. 1(a) shows magnetization versus external magnetic field loops for all three samples. For the YIG/Cu/Co and YIG/AlO_x/Co samples, qualitatively identical behavior is found, with two clearly separated switching fields, corresponding to the switching of uncoupled YIG and Co magnetizations. For the YIG/Co sample, a more continuous re-orientation of the magnetizations is observed, with full hysteresis closure at about ±4 mT. This behavior is indicative of static exchange coupling between the Co and YIG magnetizations as schematically illustrated in the inset of Fig. 1(a).

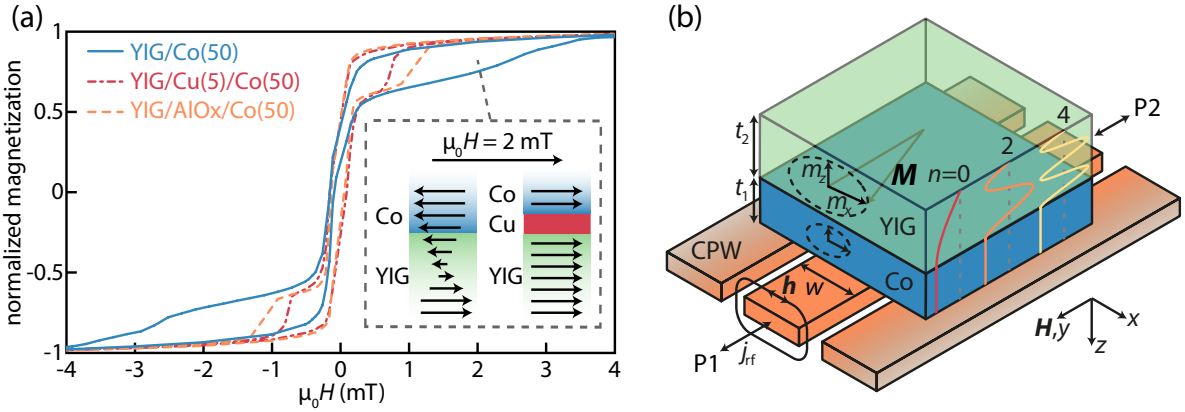

Figure 1: (a) Normalized magnetization of YIG/Co(50) (solid), YIG/Cu(5)/Co(50) (dash-dotted) and YIG/AlO_x(1.5)/Co(50) (dashed). The inset shows a possible static magnetization distribution in coupled YIG/Co and uncoupled YIG/Cu/Co. (b) Schematic depiction of YIG/Co bilayer on CPW. (Figure taken from Ref. [3]).

For the determination of the hybrid magnetization dynamics of our heterostructures, we place the samples on a coplanar waveguide (CPW) with center conductor width of $w = 300\,\mu m$ as depicted in Fig. 1(b). The two ports P1 and P2 of a vector network analyzer (VNA) are connected to the CPW and a static external magnetic field $\boldsymbol{H}$ is applied within the film plane. We measure the transmission S_{21} through the CPW as a function of frequency f and H for

[1] Financial support by the DFG via SPP 1538, project GR 1132/18 is gratefully acknowledged.
[2] Institut für Festkörperphysik, TU Dresden, Germany
[3] Financial support by the DFG via SPP 1538, project GO 944/4 is gratefully acknowledged.
[4] National Institute of Standards and Technology, Gaithersburg, MD, USA

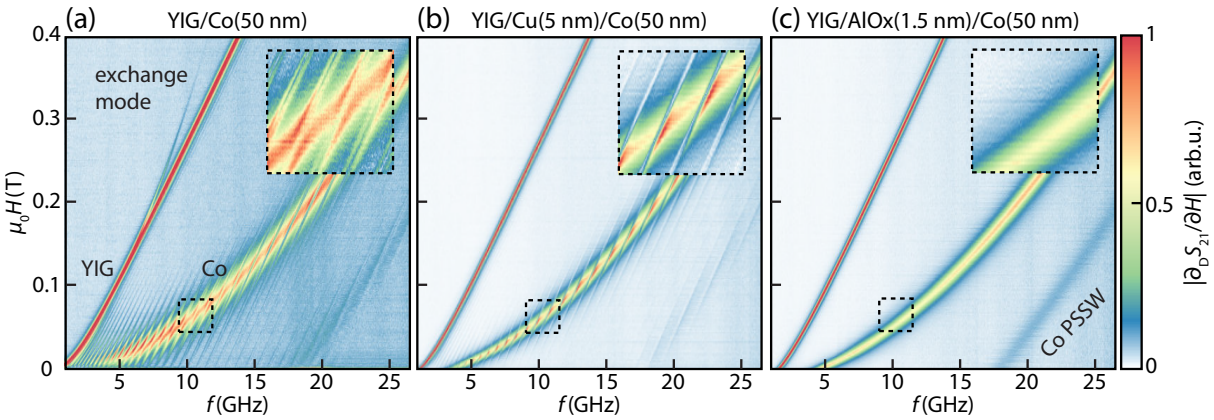

Figure 2: Microwave transmission through CPW loaded with YIG/Co(50) (a), YIG/Cu(5)/Co(50) (b) and YIG/AlO_x(1.5)/Co(50) (c). PSSWs in YIG are observed close to the Co FMR for YIG/Co(50) and YIG/Cu(5)/Co(50). No PSSWs are excited at the Co FMR in YIG/AlO_x(1.5)/Co(50). (Figure taken from Ref. [3]).

all three samples. Experimental results, corresponding to the normalized field-derivative [4] of S_{21} are shown in Fig. 2. For all three samples, two pronounced resonance dispersions are observed, corresponding to the uniform ferromagnetic resonance (FMR) modes of YIG and Co. For YIG/Co [Fig. 2(a)] and YIG/Cu/Co [Fig. 2(b)] we observe a series of further resonances close to the Co FMR mode. They are attributed to the excitation of perpendicular standing spin waves (PSSWs) in YIG. Pronounced anticrossing of the PSSW modes in YIG and the FMR mode in Co is observed for YIG/Co, best visible in the inset in Fig. 2(a). Notably, these features are completely absent in the YIG/AlO_x/Co sample [cf. Fig. 2(c)].

In total, we observe strong PSSW excitation in the YIG/Co sample with static exchange coupling. Slightly less pronounced PSSW excitation is observed in YIG/Cu/Co and the excitation is completely suppressed in YIG/AlO_x/Co. We thus conclude that the excitation mechanism is due to a combination of spin torques arising from static exchange coupling and spin current transport. Importantly, all torques arise at the YIG interface, allowing us to excite short-wavelength spinwaves from a uniform excitation. The static exchange coupling in YIG/Co furthermore results in an exchange mode [5], faintly visible in Fig. 2(a). Our experimental results are fully supported by a theoretical model based on the Landau-Lifshitz-Gilbert equation with spin torques [3] and are qualitatively different to those previously observed in all metallic Fe/Au/Fe trilayers [6]. We observe excitation of spin-waves with wavelengths as short as 50 nm in YIG/Co and YIG/Cu/Co. Our approach has recently been independently confirmed [7] and is very promising for applications in magnon logic devices.

References

[1] A. V. Chumak, V. I. Vasyuchka, A. A. Serga, and B. Hillebrands, Nat. Phys. **11**, 453 (2015).
[2] H. Yu, O. d' Allivy Kelly, V. Cros, R. Bernard, P. Bortolotti, A. Anane, F. Brandl, F. Heimbach, and D. Grundler, Nat. Comm. **7**, 11255 (2016).
[3] S. Klingler, V. Amin, S. Geprägs, K. Ganzhorn, H. Maier-Flaig, M. Althammer, H. Huebl, R. Gross, R. D. McMichael, M. D. Stiles, S. T. B. Goennenwein, and M. Weiler, Phys. Rev. Lett. **120**, 127201 (2018).
[4] H. Maier-Flaig, S. T. B. Goennenwein, R. Ohshima, M. Shiraishi, R. Gross, H. Huebl, and M. Weiler, Rev. Sci. Inst. **89**, 076101 (2018).
[5] D. C. Crew, K. J. Kennewell, M. J. Lwin, R. C. Woodward, S. Prasad, and R. L. Stamps, J. Appl. Phys. **97** (2005).
[6] B. Heinrich, Y. Tserkovnyak, G. Woltersdorf, A. Brataas, R. Urban, and G. E. W. Bauer, Phys. Rev. Lett. **90**, 187601 (2003).
[7] H. Qin, S. J. Hämäläinen, and S. van Dijken, Sci. Rep. **8**, 5755 (2018).

Echo Trains in Pulsed Electron Spin Resonance of a Strongly Coupled Spin Ensemble

S. Weichselbaumer, C. W. Zollitsch, R. Gross, H. Huebl [1]
M. S. Brandt [2]

Pulsed electron spin resonance (ESR) is a widely used spectroscopy technique which is used in many fields of science, e.g. in chemistry, materials science as well as in quantum sensing and information applications. A vast repertoire of pulse sequences has been developed and tailored to explore a specific spin property of the system under investigation. However, the majority of these pulse sequences is based on a Hahn echo [1], which consists of two microwave pulses, separated by a time delay τ. In the context of quantum information processing, the so-called strong coupling regime promises a coherent exchange of quantum information as well as an enhanced readout sensitivity for ESR applications. First seminal experiments revealed new physical effects, however, a thorough investigation of Hahn echos in the context of a strongly coupled spin ensemble is still missing.

For our experiments, we employ a planar superconducting lumped element resonator [2], patterned into a 150 nm thick Nb film. A microscope image of the resonator is shown in Fig. 1 (b). Panel (c) schematically shows the mounting of a thin slab of phosphorus doped ($[P] = 1 \times 10^{17}\,\mathrm{cm}^{-3}$) ^{28}Si containing the spin ensemble in a flip-chip geometry. The sample is mounted in a cryogen-free dilution refrigerator and cooled to $T = 50$ mK.

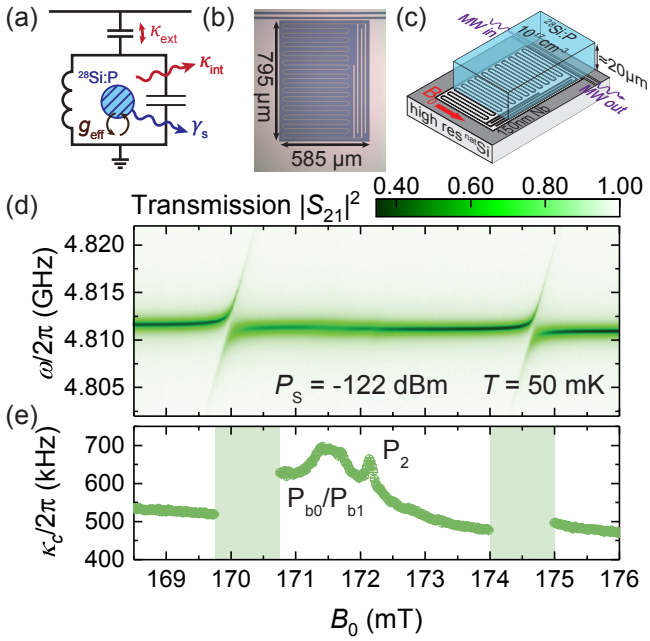

Figure 1: (a) Circuit diagram and (b) microscope image of the LER. The resonator is placed next to a microwave feedline. (c) Schematic of the thin ^{28}Si:P sample mounted in flip-chip geometry. (d) Transmission $|S_{21}|^2$ as a function of frequency and field showing two avoided level crossings, where the phosphorus hyperfine transitions are in resonance with the microwave resonator. (e) Extracted linewidth $\kappa/2\pi$ (HWHM) as a function of magnetic field indicating two additional spectroscopic features.

We first perform continuous-wave ESR by measuring the complex microwave transmission of the sample. We plot $|S_{21}|^2$ as a function of magnetic field in Fig. 1 (d). The observation of avoided crossings at $B_0 = 170.1$ mT and $B_0 = 174.3$ mT, respectively, indicates strong coupling between the hyperfine transitions of the phosphorus donors and the microwave resonator. An analysis of the linewidth $\kappa_c/2\pi$ in Fig. 1 (e) shows two additional spectroscopic features: (i) $B_0 = 171.5$ mT, indicating dangling bond defects at the (100)Si/SiO_2 interface as well as (ii) $B_0 = 172.2$ mT, indicating exchange-coupled donor pairs called P_2 dimers. Here, $[P_2] \ll [P]$, resulting only in a weak coupling of the P_2 dimers to the microwave resonators and therefore allowing a direct comparison of a strong and weakly coupled spin ensemble.

[1] The authors acknowledge financial support by the DFG via the priority program SPP 1601 (HU 1896/2-1) and the Nanosystems Initiative Munich (NIM).

[2] Walter Schottky Institut and Physik Department, Technische Universität München

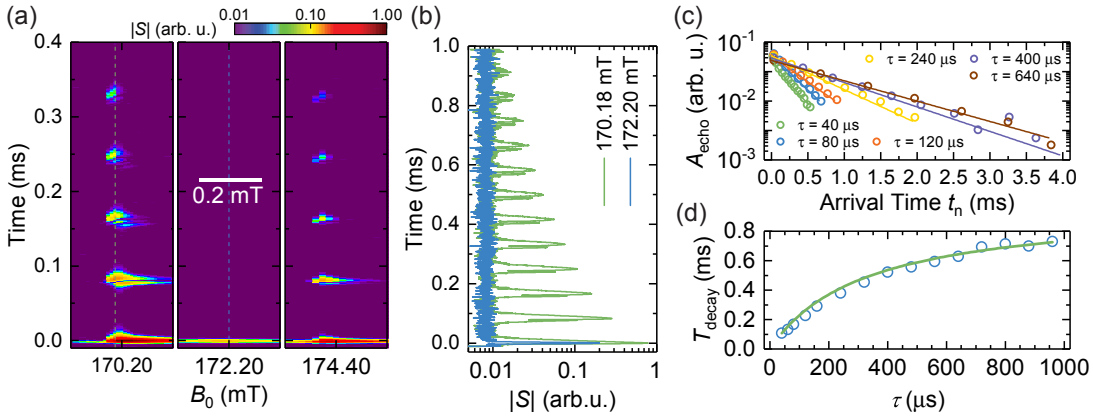

Figure 2: (a) Echo traces of Hahn echo experiments in three different field regimes, corresponding to strong (left and right panel) as well as weak coupling (center panel). (b) Time traces for fixed magnetic field. In the strong coupling regime, we observe echo trains with up to 13 echo signatures. (c) Analysis of the decay time T_{decay} of the echo trains using exponential fits (solid lines). (d) Dependence of the decay time on the echo spacing τ. T_{decay} increases with increasing τ, in accordance with the theory curve (solid green line).

In the next step, we apply Hahn echo pulse sequences at the microwave resonator frequency with pulse times of 1 µs and 2 µs, spaced by $\tau = 80\,\mu\mathrm{s}$. Fig. 2 (a) shows the recorded signal magnitude for three magnetic field ranges. The left and right panel correspond to the field regime of the strongly coupled hyperfine transitions (cf. Fig. 1). Here, we observe the first conventional Hahn echo at $t = 0$, followed by several consecutive echo signals at intervals corresponding to τ. In contrast, in the center panel, where the magnetic field range corresponds to the weakly coupled P_2 dimers, we only observe the first conventional Hahn echo. In Fig. 2 (b) we show time traces at a fixed magnetic field, corresponding to the dashed lines in panel (a). Here, the echo train compared to the single conventional Hahn echo is clearly visible. We attribute the presence of the echo train to the strong coupling between the spin ensemble and the microwave resonator. The photons generated in the resonator during a spin echo can act on the spin ensemble again, acting as an additional microwave pulse and therefore leading to a revival of the ESR signal.

To further analyze the decay of the echo train we perform Hahn echo experiments with varying echo spacing τ at fixed $B_0 = 170.18\,\mathrm{mT}$. We integrate the area of each echo and plot it against the arrival time $t_n = n\tau$ in Fig. 2 (c). Using an exponential fit, we can extract the characteristic time constant T_{decay}, which we plot against τ in Fig. 2 (d). To model $T_{\mathrm{decay}}(\tau)$, we use a phenomenological rate equation model, taking two loss channels into account: (i) losses via T_2 processes and (ii) losses via signal coupling out of the resonator (characterized by the resonator and spin loss rates, κ_c and γ_s, respectively). Using only T_2 as a fit parameter, we obtain a good agreement between our model and the data (solid green line in Fig. 2 (d)).

In conclusion, we found that Hahn echos performed on a strongly coupled spin ensemble lead to the formation of echo trains. We analyzed the decay of the echo train using a rate equation model and found a good agreement between theory and experiment. For more details we refer the interested reader to Ref. [3].

References

[1] E. L. Hahn, Physical Review **80**, 580–594 (1950).
[2] S. Weichselbaumer, P. Natzkin, C. W. Zollitsch, M. Weiler, R. Gross, and H. Huebl (2018). Submitted for publication, arXiv:1811.02971.
[3] S. Weichselbaumer, C. W. Zollitsch, M. S. Brandt, R. Gross, and H. Huebl (2018). Submitted for publication, arXiv:1809.10116.

Application–Oriented Research

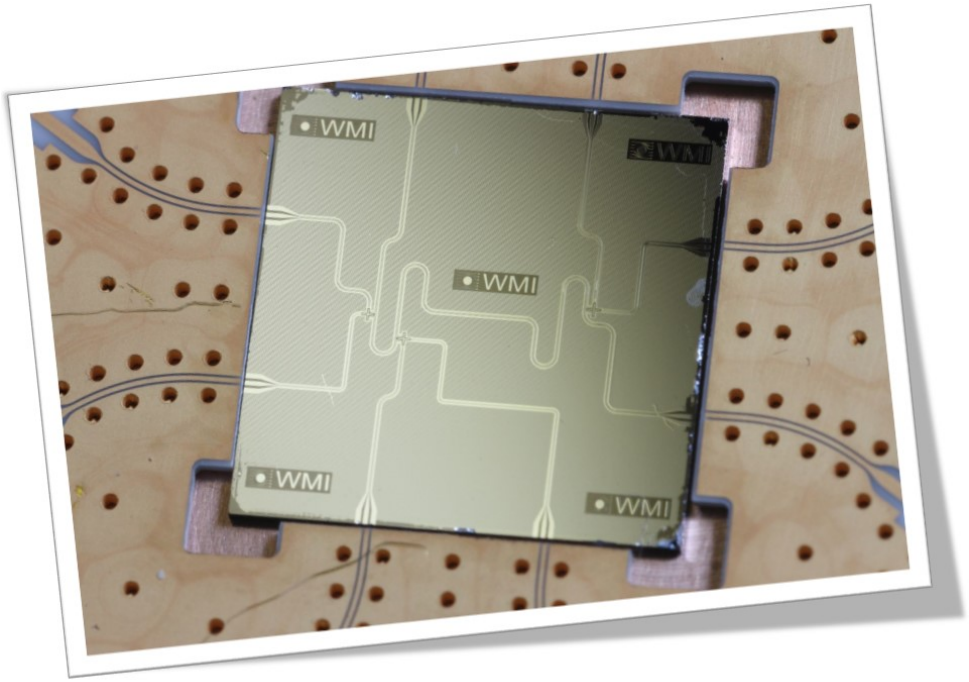

Optimized Antenna Designs for a 3D Quantum Memory

E. Xie, F. Deppe, M. Fischer, S. Pogorzalek, M. Renger, K. G. Fedorov, A. Marx, R. Gross [1]

In the ongoing race of constructing the first quantum computer, one important aspect is the storage of quantum information. In contrast to classical information, quantum information cannot be cloned, which raises the demands on a quantum of memory. For superconducting quantum circuits, it has turned out that 3D waveguide cavities are suitable for storing quantum information in the form of microwave photons. Beside the ability to store quantum information with a high fidelity, an ideal memory is required to have a fast information readout rate. We successfully demonstrate such a device (for details, see Ref. [1]) in a compact form utilizing the multimode structure of a 3D aluminum cavity. In such a cavity, a long-lived mode serves as the storage and a well-coupled mode as the readout mode. By proper design of the cavity, the storage time can be made 100 times longer than the readout time. Moreover, we find the quantum process fidelity of the storage and retrieval operation to be 78 % (see report on page 52).

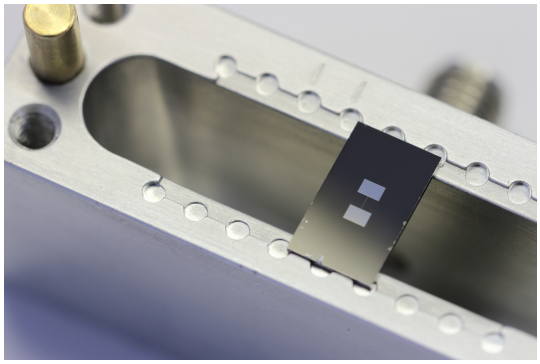

Figure 1: Opened 3D microwave cavity made out of bulk aluminum with a transmon qubit chip placed in it. Only the antenna paddles of the transmon qubit are visible as bright rectangles.

Since the working principle of our 3D quantum memory is strongly based on controlling the coupling of specific modes to the microwave feedlines, we investigate the effect of the geometry of the coupling antenna in a systematic way. Here, a particular goal is to further decrease the external loss rate (increase the quality factor) of the storage mode by a proper design and position of the antenna pins. Whereas the internal quality factor Q_0 is defined by the properties of the used superconducting material, the external quality factor Q_x can be controlled by the position, the protruding length and the diameter of the antenna pin.

As shown in Fig. 2(a), we observe that the accurate positioning of the antenna pin along the x-direction is important to achieve a high external quality factor. The reason lies in the mode profile of the storage mode [cf. inset in Fig. 2(a)], showing a node with vanishingly small electric field. Although an antenna position exactly at the field node is desirable, in reality deviations from this position occur due to a limited fabrication precision.

Regarding the impact of the antenna diameter, we compare two data sets measured with the same setup described in Ref. [1]. The two experiments only differ by different diameters the antenna pins. The data of Fig. 2(b) shows that the decay of a single photon Fock state in the cavity storage mode is reduced by a factor of 2.3 for an antenna diameter of 0.1 mm as compared of 1.26 mm. In contrast, simulations [2] assuming ideal antenna positioning do not predict a significant difference in photon decay of the storage mode for these two antenna diameters. This suggests that the reduced photon decay observed for the slimmer antenna can be mainly attributed to the fact that the slimmer antenna requires a less precise antenna positioning.

[1] The authors acknowledge support from the German Research Foundation through FE 1564/1-1, the doctorate program ExQM of the Elite Network of Bavaria, the IMPRS 'Quantum Science and Technology', the EU Quantum Flagship project 'Quantum Microwaves for Communication and Sensing (QMiCS)', as well as the German Excellence Initiative via the 'Nanosystems Initiative Munich'(NIM) and the 'Munich Center for Quantum Science and Technology (MCQST)'.

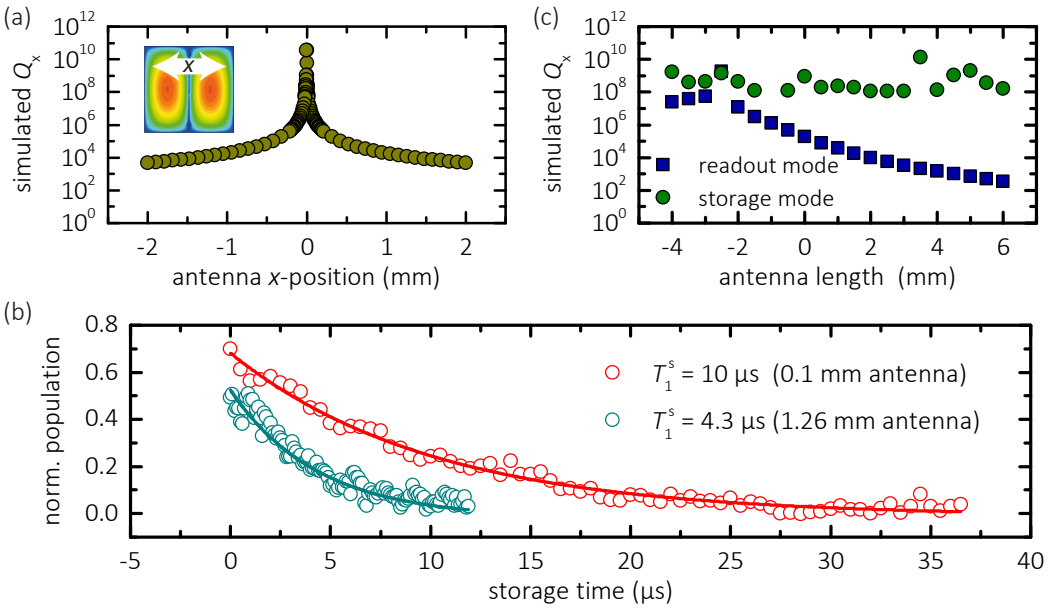

Figure 2: (a) Simulated dependence of the external quality factor on the antenna position. An antenna with a diameter of 1.26 mm and a length of 4.7 mm is assumed. The inset shows the electric field distribution of the storage mode (red: high, blue: low electric field strength). (b) Measured decay (symbols) of a single photon Fock state in the storage mode for two different antenna diameters. The lines show exponential fits to the data to extract the decay times T_1^s. (c) Simulated variation of the external quality factor with the antenna length for the readout and the storage mode. An antenna with a diameter of 0.1 mm and positioned at $x = 0$ is assumed in the simulation.

The length of the antenna determines the coupling to an electric mode in general. However, depending on the electric field strength of the mode at the antenna position, the antenna length has different effects on the coupling. To understand the transition from an undercoupled ($Q_0 > Q_x$) to an overcoupled mode ($Q_0 < Q_x$), we sweep the antenna length in a simulation [2] and monitor Q_x of the relevant modes [cf. Fig. 2 (c)]. In contrast to the constant Q_x of the storage mode in the case of perfect lateral antenna positioning, the quality factor of the readout mode drops over many orders of magnitude with increasing antenna length. This result shows that the coupling to the readout mode can be tuned independently from the coupling to the storage mode. By exploiting this result in future antenna designs, we can realize storage cavities with an even higher ratio between the storage and readout times.

In conclusion, we find that the antenna geometry plays a crucial role in improving 3D quantum memories. From our simulations and experimental findings, we can develop general guidelines for further improving the cavity and antenna design. As an additional step, we plan to change the material of the antenna from copper to a lossless superconducting material, in order to reduce internal losses even further.

References

[1] E. Xie, F. Deppe, M. Renger, D. Repp, P. Eder, M. Fischer, J. Goetz, S. Pogorzalek, K. G. Fedorov, A. Marx, and R. Gross, Appl. Phys. Lett. **112**, 202601 (2018).
[2] CST STUDIO SUITE www.cst.com.

Ultra-Wide Range Photon Number Calibration Using a Nano-Electromechanical and cQED Hybrid Device

P. Schmidt, D. Schwienbacher, M. Pernpeintner, F. Wulschner, F. Deppe, A. Marx, R. Gross, H. Huebl [1]

Cavity opto/electromechanics investigates the interaction of light with a mechanical degree of freedom enabling the readout of its displacement as well as the control of the mechanical state up to the quantum level [1]. Previously we have introduced a nano-electromechanical system consisting of a microwave coplanar waveguide capacitively coupled to a transmon qubit and a nanomechanical string [2]. Here, we focus on calibrating the photon number in the microwave resonator via qubit and nanostring independently, which leads to a determination of the photon number in the low and high occupation regime. Details of our experiments have been published in Ref. [3].

We investigate a hybrid system consisting of a superconducting microwave resonator with an integrated transmon qubit and, spatially separated, a nanostring mechanical oscillator, as sketched in Fig. 1. In our experiments we use transmon spectroscopy techniques, like the measurement of the ac-Stark shift, to determine the photon number in the microwave resonator. This result is compared quantitatively to that obtained from electromechanically induced transparency measurements on the integrated nano-electromechanical system. The microwave measurement setup is sketched in Fig. 1.

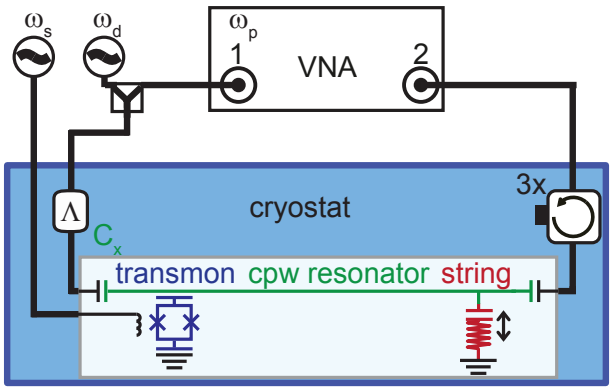

Figure 1: Setup and sample schematics. Several microwave sources provide the qubit spectroscopy tone ω_s and the sideband drive ω_d. A VNA probes the microwave resonator ω_p and allows for an analysis of the transmitted signal. The input signal is attenuated by an unknown amount Λ and couples via C_x to the microwave resonator (green), which itself couples capactively to a transmon qubit (blue) and a nanomechanical string resonator (red). The transmitted signal is screened from thermal noise via circulators and amplified via a cold and a room temperature amplifier (not shown).

The average photon number of the microwave resonator $\bar{n}_r$ is given by [1, 4]

$$\bar{n}_r = \frac{2P_{\mathrm{appl}}}{\hbar\omega_p\left(\kappa^2 + 4\Delta_p^2\right)} \underbrace{\Lambda\kappa_{\mathrm{ext}}}_{\equiv x}. \qquad (1)$$

Here, $\hbar$ is the reduced Planck constant, Δ_p is the detuning between probe tone and resonator frequency, and $\kappa = \kappa_{\mathrm{ext}} + \kappa_{\mathrm{int}}$ is the total loss rate of the resonator. In addition, $\bar{n}_r$ scales linearly with the applied microwave power of frequency ω_p. Note, that for the conversion to the photon number, further knowledge is required about the attenuation of the microwave lines Λ as well as the input coupling rate κ_{ext} of the microwave resonator. As the latter two cannot be distinguished in our experiment, we introduce $x = \Lambda\kappa_{\mathrm{ext}}$ as quantity required for the comparison between the experiments. The quantity x can be quantified from (i) the ac-Stark shift of the transmon qubit referred to as x_{qb} and (ii) from the effective linewidth broadening of the mechanical oscillator due to electromechanical induced absorption (EMIA) for x_{EMIA}.

[1] We acknowledge financial support by the German Excellence Initiative via the 'Nanosystems Initiative Munich'(NIM) and the European Union's Horizon 2020 Research and Innovation Program under Grant Agreement No. 736943.

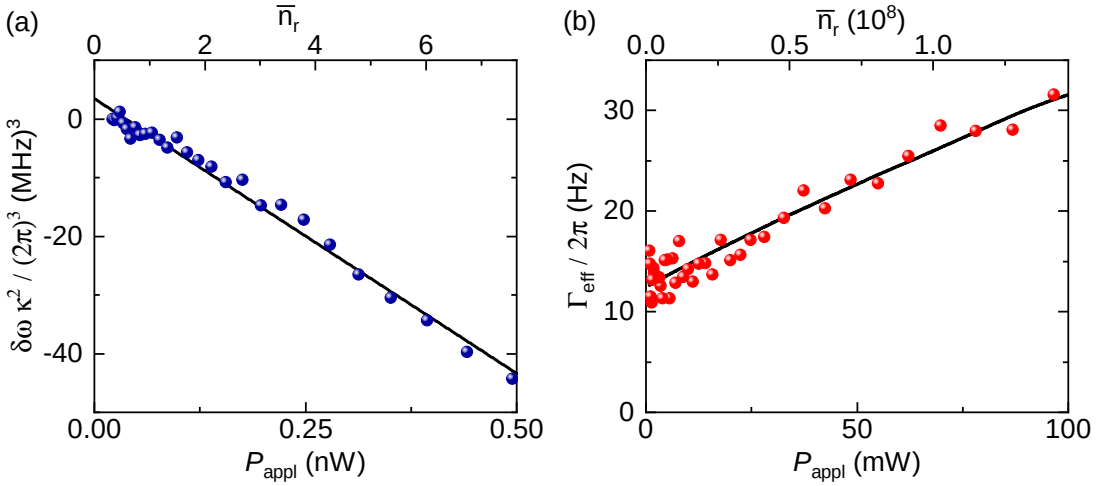

Figure 2: Results on the photon number calibration. Panel a) shows the recorded product of the ac-Stark shift and extracted resonator linewidth $\delta\omega\kappa^2$ (blue dots) over applied probe tone power. As the shift of the transmon qubit per photon is known from precharacterization, we fit the extracted detuning (black line) and find the calibration factor x_{qb}. Panel b) displays the effective linewidth broadening of the nanostring oscillator (red dots), which is linearly modeled (black line) to extract the calibration factor x_{EMIA}.

For the ac-Stark shift calibration, we measure the transition frequency of the transmon qubit at the sweet spot (here, 7.92 GHz). In Fig. 2(a), we plot the product $\delta\omega\kappa^2$ of the shift $\delta\omega$ in the qubit resonance frequency taken with respect to the value at low microwave powers, and the square of the resonator loss rate κ, taking into account for power dependent linewidth variations. From these measurements we can determine the calibration factor $x_{qb} = (4.08 \pm 0.26)\mathrm{s}^{-1}$.

For higher photon numbers $\bar{n}_r$, we measure the nano-electromechanical subsystem using electromechanically induced absorption. Here, we combine a weak probe tone around the microwave resonator frequency and a strong red-sideband drive tone detuned by one mechanical frequency from the microwave resonator ($\Delta_d = -\Omega_m$). In this configuration, the drive tone power P_{appl} sets the photon number. When the probe tone interferes with the anti-Stokes field scattered from the drive tone, we find signatures of the mechanical resonator in the microwave transmission. The extracted linewidth Γ_{eff} and in particular its broadening is shown in Fig. 2(b). The latter can be related to the photon number $\bar{n}_r$. Using this technique we find an electromechanical calibration factor $x_{EMIA} = (5.41 \pm 0.25)\mathrm{s}^{-1}$. This corresponds to a slightly higher calibration value as we have found via the qubit ($x_{qb} = 4.08\,\mathrm{s}^{-1}$).

In summary, we have investigated the photon number calibration of a hybrid device based on a transmon qubit, a microwave resonator and a nanostring oscillator using two complementary techniques and find quantitative agreement despite the fact that the covered photon number range spans from the single photon level to about 10^8. Our experiments represent an important step towards the realization of quantum information storage in a vibrational degree of freedom.

References

[1] M. Aspelmeyer, T. J. Kippenberg, and F. Marquardt, Rev. Mod. Phys. **86**, 1391–1452 (2014).
[2] P. Schmidt *et al.*, Annual report WMI 2016, 55–56 (2016).
[3] P. Schmidt, D. Schwienbacher, M. Pernpeintner, F. Wulschner, F. Deppe, A. Marx, R. Gross, and H. Huebl, Appl. Phys. Lett. **113**, 152601 (2018).
[4] A. A. Clerk, M. H. Devoret, S. M. Girvin, F. Marquardt, and R. J. Schoelkopf, Rev. Mod. Phys. **82**, 1155–1208 (2010).

Materials, Thin Film and Nanotechnology, Experimental Techniques

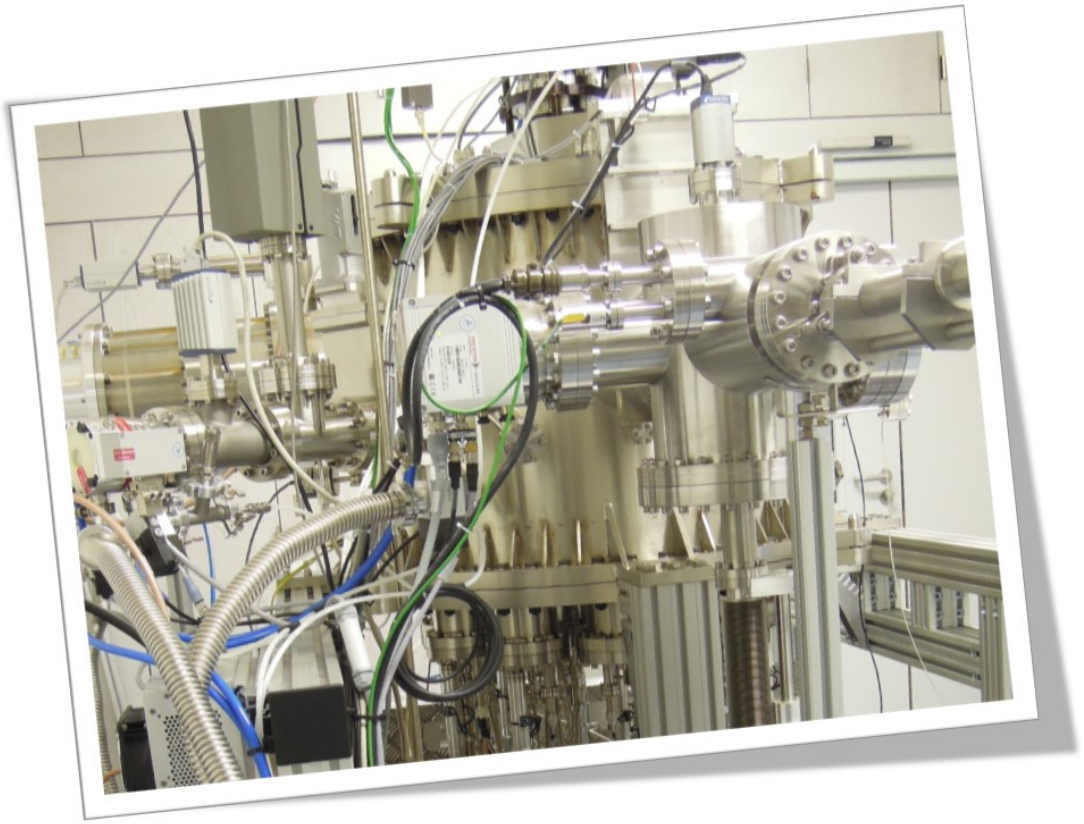

Thin Film Deposition Goes Large Area at the Walther-Meißner-Institut

M. Althammer, R. Gross [1]

The fabrication of high quality materials in form of thin films and heterostructures is one of the key technology areas of expertise of the WMI. To keep up with the recent progress in this field and to adjust to the ever increasing demands in our groups, we have upgraded our thin film deposition machinery over the course of the last years. In 2018, a new UHV sputter deposition system for the fabrication of superconducting thin films on large substrate areas has been successfully installed and started its operation. The system was financed by funds of the Federal Ministry of Education and Research supporting the research network on Quantum Communication. After the project approval in October 2016 and the selection of the supplier via an European Union wide tender, the system was delivered to the WMI by the company Mantis Deposition ltd in November 2018. For the installation of this new equipment, we restructured the installation of existing thin film machinery and renovated the lab space required for the new machine. This also included the installation of a new lifting crane for the heavy top flange of the system. In December 2018, the system started its operation at the WMI after passing the final acceptance tests. The system is running under the acronym «ULTRADISC »: **U**nlimited **L**egendary **T**ool for **R**eliable **A**chievements in the **D**eposition of **I**ntegrated **S**uperconducting **C**omponents.

The main parts of the new sputter deposition system are illustrated in Fig. 2. The system consists of a main deposition chamber and a load lock for introducing the substrates into the ultra-high vacuum main chamber. The load lock is equipped with a motorized storage cassette for up to six substrates, a stab-in heater with automated temperature control for surface cleaning processes and a linear transfer arm for moving samples into and out of the main deposition chamber. An automated gate valve separates the load lock from the main deposition chamber. Specifically designed substrate holders for deposition onto circular and rectangular substrates of various sizes have been shipped with the system.

The main deposition chamber has been designed for flexible and homogeneous deposition on substrates with a diameter of up to 100 mm. For housing such large area substrates, the main chamber has an inner diameter of 800 mm. For mounting the substrates, Mantis designed a new manipulator for this system. On this manipulator the substrate holder is placed onto a quartz plate, which ensures electrical isolation and low thermal losses. The electrical isolation is crucial, since it allows to strike a plasma directly underneath the substrate via applying a DC or RF bias to the substrate holder. A radiative carbide heater is used to homogeneously heat the substrate. In addition, water cooled shielding of this heater prevents heating of other chamber parts. With a heater power of 850 W it is possible to reach temperatures of up to 950 °C on a stainless steel holder over the full 100 mm diameter. For driving the heater a 4.4 kW DC power supply is used, while a thermocouple is used for in-situ temperature monitoring. The manipulator has 3 degrees of freedom to move the substrate in the deposition chamber. A main substrate rotation allows to move the substrate over the different deposition clusters. This is illustrated by the red dashed circle in Fig. 2, which represents the movement of the substrate center for this degree of freedom. In addition, the distance between substrate and sources can be tuned by 100 mm via a motorized z-shift of the manipulator. For homogeneous deposition, the substrate itself can rotate with up to 0.5 Hz. An automated substrate shutter allows to protect the substrate from unintentional deposition. Moreover, a motorized wedge shutter enables the fabrication of controlled thickness variations over the area of the substrate.

[1] Financial support from the Federal Ministry of Education and Research (BMBF) via the research network on 'Quantum Communication' (FKZ: 16KIS0110 4515.1545.4556) is gratefully acknowledged.

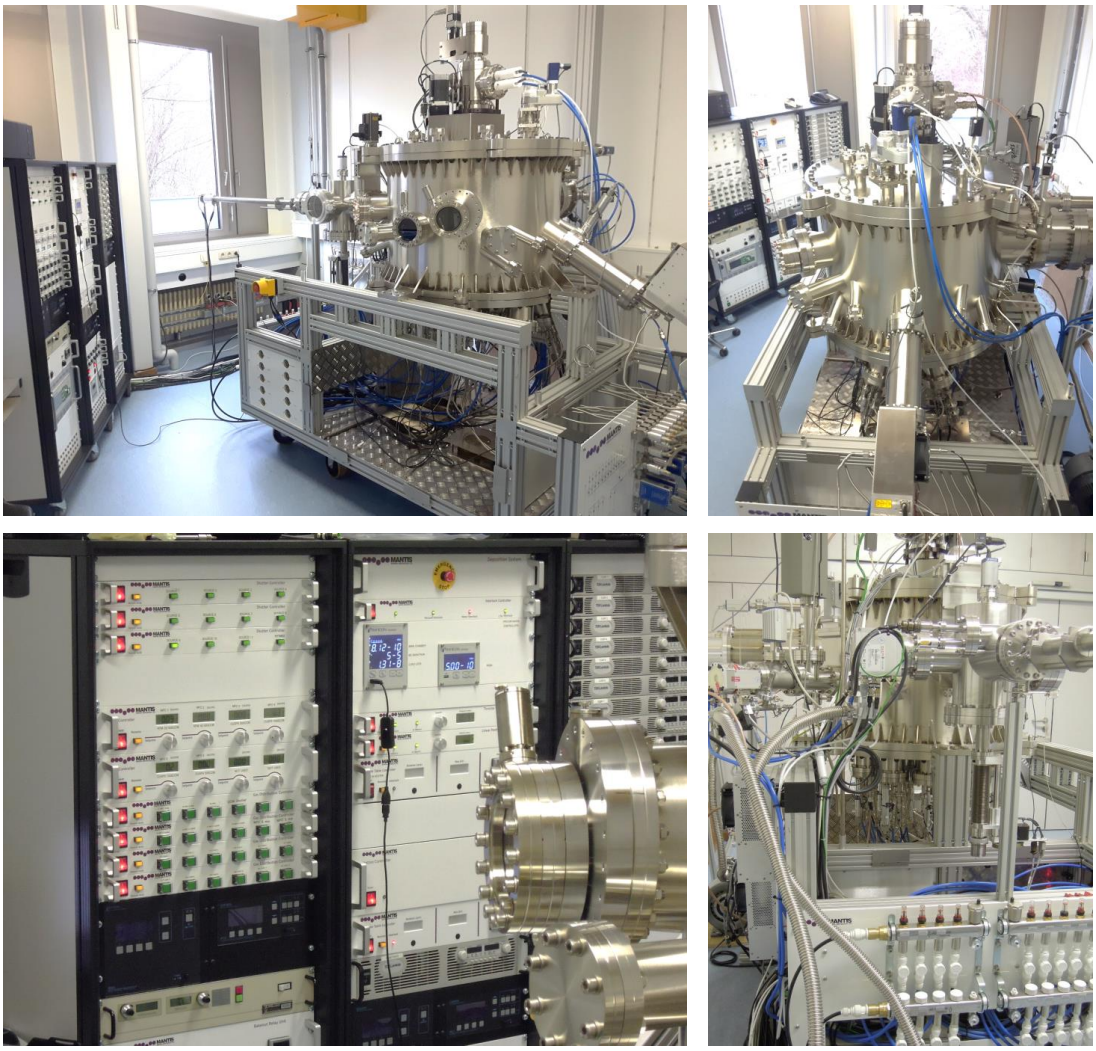

Figure 1: ULTRADISC deposition system after installation and passing final acceptance criteria at the WMI. Three electronics racks contain all the hardware for controlling and powering the deposition system. The main chamber contains the deposition sources in the bottom flange and the substrate manipulator on the top flange.

For in-situ deposition rate measurements, a quartz crystal microbalance is also installed on the manipulator. As it is mounted at the same height as the substrate, external rate calibrations are not necessary in our setup. A unique feature of the manipulator is the special designed sample cradle, which allows to change the distance between the substrate holder and the radiative heater. In this way easy sample loading and unloading on the manipulator is possible, while also maintaining a maximum in the heat transfer between heater and substrate.

Flexibility in materials choice is ensured by a total of 11 magnetron sources installed in the chamber (blue colored parts in Fig. 2). A total of 7 sources can be used for face-to-face deposition on the substrate for high growth rate deposition (several 10 nm/min). In addition, 8 sources can be manually tilted into three separate confocal deposition clusters, which enables simultaneous deposition from up to 3 sources. Automated control of the deposition times is achieved by the motorized shutters attached to each magnetron. The high-purity gas supply is realized via 4 independent mass flow controllers, such that even more complex gas compositions can be automatically controlled and reactive sputtering processes for the deposition of oxide and nitride materials are routinely available in this system. The gas composition can be quantified by the quadrupole mass spectrometer in the attached residual gas analysis (RGA) system (shaded red in Fig. 2). The mass spectrometer provides a high dynamic range over more than two orders of magnitude in partial gas pressures. A differential pumping scheme

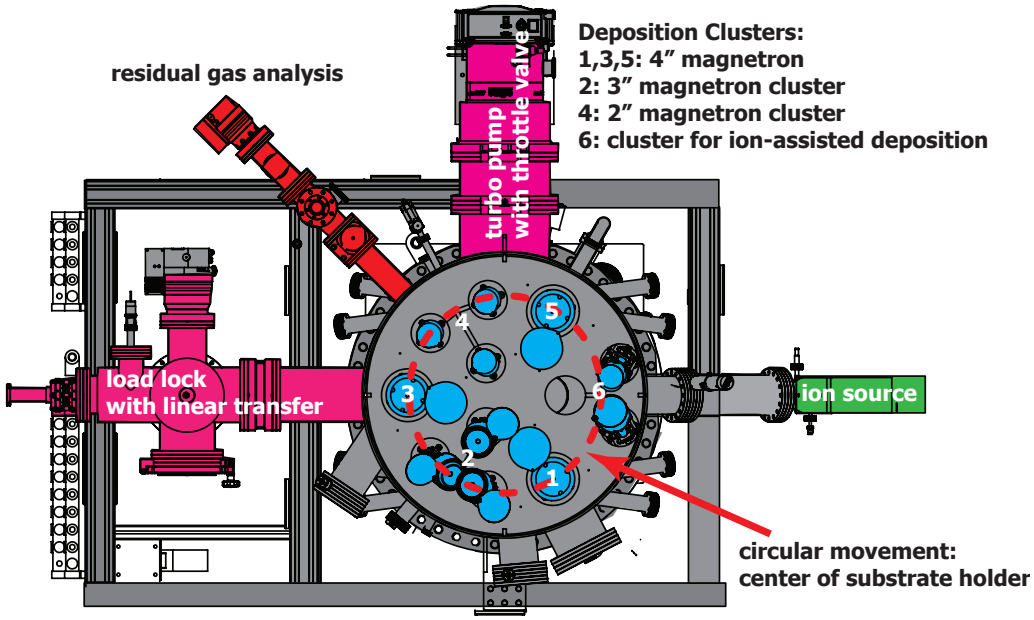

Figure 2: Illustration of the new ULTRADISC deposition tool. The systems consists of a load lock for sample introduction. Inside the main deposition chamber the substrate can be moved over 11 magnetron sputter sources for homogeneous deposition over 100 mm substrate diameter. In addition, the attached residual gas analysis allows for sensitive gas composition analysis. An ion source installed in a confocal sputter configuration enables ion-assisted sputter deposition.

via an additional turbo molecular pump and a regulated leak valve in the RGA system allows for measurements during deposition processes in the main chamber. For more flexibility in reactive sputtering processes and for substrate cleaning purposes the confocal cluster (number 6 and green shading in Fig. 2) is equipped with a RF discharge ion source. The energy of the ions generated in the plasma discharge can be controlled by the applied grid voltage (up to 1.0 kV). Two different grids suitable for nitrogen and oxygen or argon are currently available for the system. Two separate mass flow controllers are used to supply the high purity gases to the ion source.

To strike and maintain the plasma at the magnetron our system is equipped with ten 700 W DC power supplies for simultaneous operation of the sputter sources loaded with metallic targets. In addition, a 700 W RF source with automated matching network is used for operation of sputter sources with insulating materials. Two more 300 W RF supplies with automated matching network are used for the ion source and the substrate bias in the manipulator. For even more control over the deposition process via the power supplies attached to the magnetrons, we also equipped the system with a bipolar pulsed DC supply with a maximum DC power of 1.5 kW. With this power supply pulsed operation with frequencies of up to 100 kHz and current pulses of up to 30 A in bipolar operation are possible. A special pulse train program allows to define custom made patterns for even more advanced plasma control. This new technique provides novel ways of tuning material properties of the fabricated films like the crystallite-size and -distribution, and the atomic composition. It also allows to achieve higher deposition rates in reactive sputtering processes [1].

The main chamber is pumped by a large 1600 l/s turbo molecular pump. A throttle valve between main chamber and turbo molecular pump allows to adjust the pumping speed during deposition processes. In combination with the mass flow controllers attached to the sputter sources, automatic up- or down-stream pressure regulation in a range from 8×10^{-4} mbar to 1×10^{-1} mbar is possible. After the initial bake-out of the main chamber at the WMI, we reached a base pressure of 9×10^{-10} mbar, such that the purity of the deposited materials

is only limited by the target materials itself and the purity of the sputtering gases. The top flange of the main chamber can be either sealed via a copper wire gasket for maximum bake-out temperatures or two differentially pumped Viton rings for low-cost resealing. A custom built crane system allows then to remove the top flange and gain easy access for maintenance of the sputter sources and the substrate manipulator.

The system is fully automated by the supplied computer and software. In this software, manual operation is also possible, but an emphasis is placed on high repeatability of deposition processes by user-written procedures, which can be used to fully automate deposition and surface cleaning processes. The six motorized axes for the substrate manipulator are controlled via a separate stepper motor software, but is also interfaced with the deposition software for full process automatization. For substrate loading and unloading into the main chamber a combination of process automatization and manual operation is currently used, to lower the impact of user errors.

This new thin film deposition system will represent the foundation for further progress in the field of superconducting quantum circuits for optical and microwave applications. On the one hand, superconductors with high critical temperature will lower the impact of fluctuations in the superconducting resonator on quantum measurements and manipulations. On the other hand, different superconducting materials allow to tune the properties of such resonators and engineer for example the kinetic inductance in these systems. A wider choice of materials will also be beneficial to increase the quantum efficiency of single photon detectors for our collaboration partners at the Walter Schottky Institute of TUM [2]. With this new ULTRADISC system now in operation, we are well prepared for the material deposition challenges ahead of us in the next years.

References

[1] A. Anders, Journal of Applied Physics **121**, 171101 (2017).
[2] M. Kaniber, F. Flassig, G. Reithmaier, R. Gross, and J. J. Finley, Applied Physics B **122** (2016).

Direct Laser Writing System PicoMaster 200

F. Deppe, A. Marx, R. Gross [1]

When it comes to structuring thin films with a resolutions down to 1 µm, optical lithography is one of the key methods used by the magnetism group and the superconducting quantum circuits group at the Walther-Meißner-Institute (WMI). Traditionally, a mask aligner (Süss MJB3) was used for this purpose because it allows for fast sample processing and a low entry barrier for typical university group users. However, the lead time associated with the required premanufactured chromium masks severely limits the turn-around time when a new structure design is to be developed. A frequently used alternative is electron beam lithography (EBL), where a deflected electron beam scans the sample area. However, EBL systems are designed to write structures down to a few nanometers and are therefore rather slow. A good compromise are modern direct laser writing systems. They are considerably faster than EBL systems but do not require a physical mask. Furthermore, the vendors of modern laser writers promise even submicron resolution in combination with high writing speeds.

For this reason, supported by the Federal Ministry of Education and Research (BMBF) via the research network Quantum Communication (Q.com), WMI acquired the 4PICO's direct laser writing system *PicoMaster 200* (PM 200) in 2017 and taken into full operation in the course of 2018. In general, the PM 200 accepts substrate sizes between 5 mm × 5 mm and 200 mm × 200 mm via a turnable chuck. For writing the pattern, it allows for three different spot sizes (300 nm/600 nm/900 nm) and a write speed of up to 7.7 mm^2/min. For small substrate sizes, the write speed needs to be reduced so that a 12 mm × 12 mm substrate takes approximately an hour. At WMI, the PM 200 is installed in the clean room (see Fig. 1). One can choose between two compact writing modules equipped with a 405 nm and a 375 nm laser diode, respectively. The user can easily switch between the two modules within minutes since the full optical path is contained in the modules. Both modules feature automatic focus correction for not too heavily varying resist thickness. The writing stage with the substrate holder and the compact optical module is shown in Fig. 2.

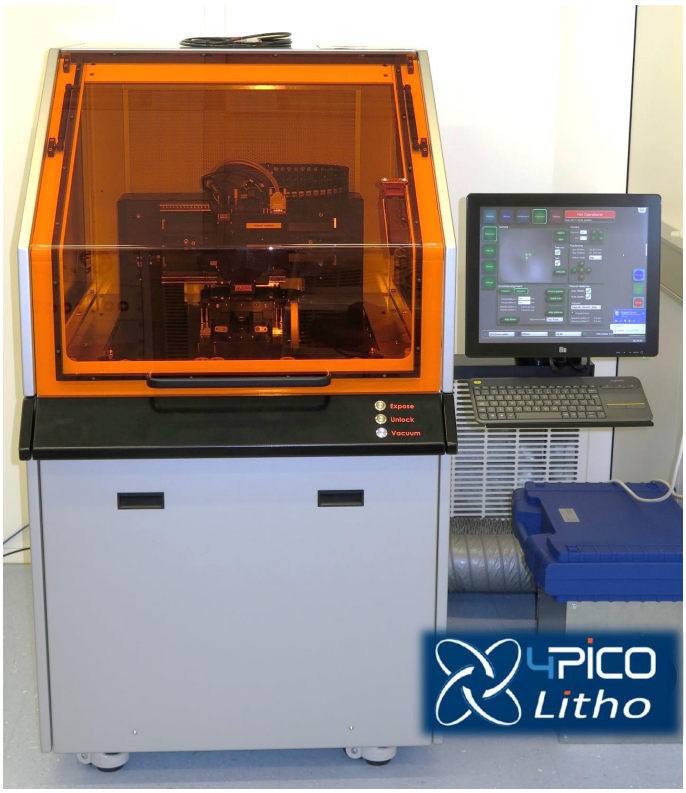

Figure 1: The direct laser writing system *PicoMaster 200* installed in the WMI clean room.

For known process parameters, the writing process is fully automatic. Therefore, the first task has been to adapt the WMI standard optical lithography process, which is based on the resist *AZ5214 E* from *MicroChemicals* to the new machine. In a Bachelor's thesis [1] completed in

[1]Financial support from the Federal Ministry of Education and Research (BMBF) via the research network on 'Quantum Communication' (FKZ: 16KIS0110 4515.1545.4556) is gratefully acknowledged.

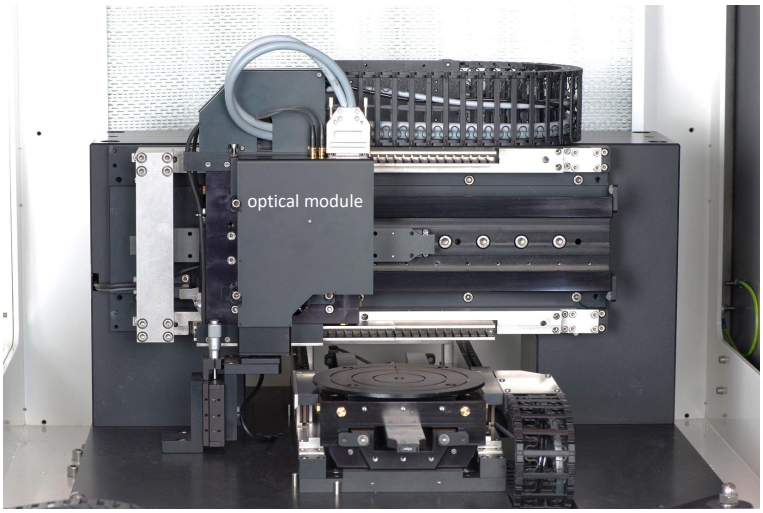

Figure 2: The writing stage of *PicoMaster 200* (PM 200) with the substrate holder and the compact optical module.

2018, structure sizes down to $\simeq$1 µm resolution were successfully patterned and etched out of a 100 nm thin Nb film by reactive ion etching (RIE). The Nb film was sputter deposited on a silicon substrate. This result is already better by a factor 2 to 5 as compared to previous attempts based on the old WMI mask aligner.

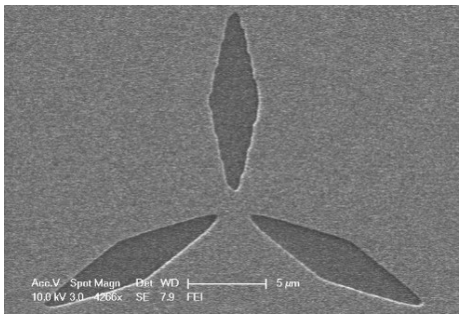

Figure 3: Scanning electron micrograph documenting an optimized optical lithography process with a resolution of $\simeq$1 µm. Light areas are niobium, dark areas correspond to the silicon substrate.

In Fig. 3, a typical result with optimized resist spinning, lithography, and development parameters is shown. Two remarkable features can bee recognized. First, the improved resolution is achieved in the most difficult situation, where small and pointed openings (diamond-shapes) are combined with thin metal bridges. Second, in the shape of the openings, small steps can be noticed. In other words, the resist process is good enough to make the submicron scan lines of the laser writer visible.

In conclusion, the new laser writing system *PicoMaster 200* is set up in the clean room of WMI and the resist process is optimized for typical patterning applications of thin films. As the next steps, the writing and resist process will be adapted to larger wafer sizes and the vector writing mode will be taken into operation.

References

[1] Christoph Scheuer. *Maskenlose optische Lithographie supraleitender Niobfilme*. Bachelor's Thesis, Technische Universität München (2018).

Dry 1K Refrigerator - Vibration-Free for Hours

K. Uhlig

Introduction. In the Annual Report 2017 we explained that our cryogen-free dilution refrigerator (DR) can be run for 15 min without its pulse tube cryocooler (PTC) in operation. This time interval could be used for delicate mK experiments for which the small vibration level generated by the PTC is disturbing. Of course, it would be desirable to extend the off-period of the PTC.

Experimental. In our cryogen-free DR [1], in contrast to standard dry DRs, the dilution refrigeration unit is precooled by a ^{4}He-1K-stage which can be operated in a continuous mode and single-cycle mode (Fig. 1). The necessity for the installation of a separate 1K-circuit came from the requirement for high refrigeration power at $T \sim 1\,\mathrm{K}$. A follow-up model of this DR is used at the WMI for research on superconducting quantum circuits [2]. Moreover, meanwhile a commercial version of a dry DR with 1K-stage has become available at Oxford Instruments [3].

The construction of the 1K-loop follows that of a Joule-Thomson (JT) cooler: the helium flow is precooled by the two stages of a PTC and a counterflow heat exchanger (hx), before it is expanded in a flow restriction. The liquid fraction of the flow is accumulated in a vessel, whereas the gas part is pumped through the counterflow hx and then returned to the inlet of the cooler. The pump in our setup is a standard rotary pump (pumping speed: $33\,\mathrm{m^3\,h^{-1}}$).

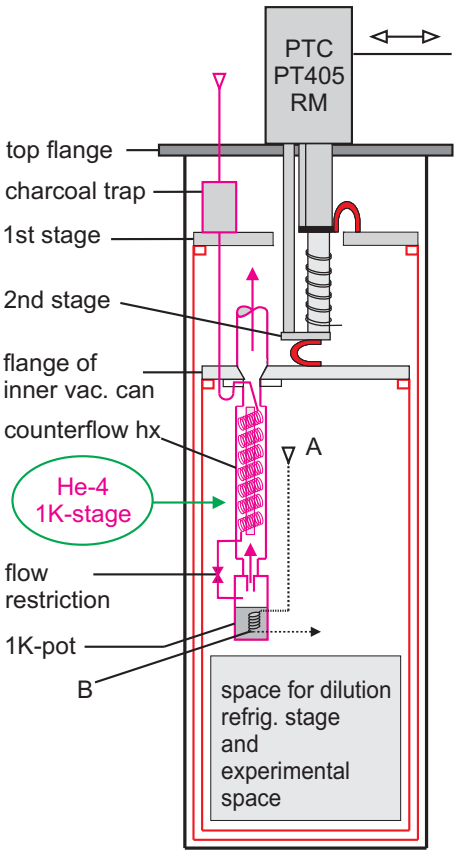

Figure 1: Cross-sectional view of a pulse tube precooled cryostat with 1K-stage and space for a dilution refrigeration stage. A: Inlet of the dilution refrigerator. B: Heat exchanger of the $^{3/4}$He dilution loop.

In order to achieve a long off-period of the PTC, the concept is to fill the pot of the 1K-stage with liquid ^{4}He with the 1K-refrigerator running in continuous mode. The temperature of the liquid helium in the pot is near 1 K. Then, the 1K-stage is switched to single-cycle mode and the PTC is shut off. The liquid ^{4}He in the pot of the 1K-loop serves as a buffer for the DR which is kept in continuous operation, while the two stages of the PTC and the attached radiation shields are slowly warming up. Importantly, the precooling conditions for the DR unit remain unchanged during the off-period of the PTC as the $^{3/4}$He flow of the DR is condensed in a hx in the 1K-pot (labeled as "B" in Fig. 1) which is always at the same temperature of 1 K. As a result, the inlet pressure and the throughput of the DR circuit remain stable and as a consequence the mixing chamber temperature stays constant while the PTC is shut off.

In the experiments reported here, the 1K-stage is run without the DR circuit in operation to study and optimize the 1K-stage and thus the precooling process of the DR. No heat is applied during the off-period of the PTC. Therefore, the helium flow evaporated in the pot is small and mainly given by the heat leak through the tubes of the counterflow hx. For the average helium flow a rate of only $\dot{n}_4 = 10\,\mu\mathrm{mol\,s^{-1}}$ is found which is comparable with the flow rate of a very small DR. A total amount of $1.8\,\mathrm{cm^3}$ of liquid is evaporated during the three-hour shutoff.

In Fig. 2 the course of a PTC shutoff experiment is presented. At the moment "a", the 1K-stage is switched from continuous to single-cycle operation which results in a small temperature drop of the 1K-pot. Then the PTC is turned off and the temperatures of both stages of the PTC started to rise. The off-period of the PTC was three hours (moment "a" to "b"). Whereas the temperature of the 1K-pot remains nearly constant just below 1 K, the 2 stages of the PTC show a pronounced temperature rise in this time span.

The temperature of the first stage increased from 40 K to 130 K and that of the second stage from 3.1 K to 40 K. This strong temperature rise is caused mostly by radiation and the absence of superinsulation on the heat shield of the first stage. On the other hand, it is demonstrated that the temperature of the 1K-stage remains almost undisturbed by the warming of the PTC. In the following, at the moment "b" the PTC is turned on, whereas the 1K-pot is kept in single-cycle mode. After another hour of running, the temperatures of both stages of the PTC are cold enough to switch the 1K-stage from single-cycle to continuous (moment "c"). To do this, a temperature of the 2nd stage of the PTC of $T_{PT2} \approx 8\,\mathrm{K}$ is desirable. The 1st stage should be below about $T_{PT1} \approx 80\,\mathrm{K}$ because a charcoal filter in the inlet line of the 1K-cooler requires this temperature for efficient purification of the helium gas (Fig. 1).

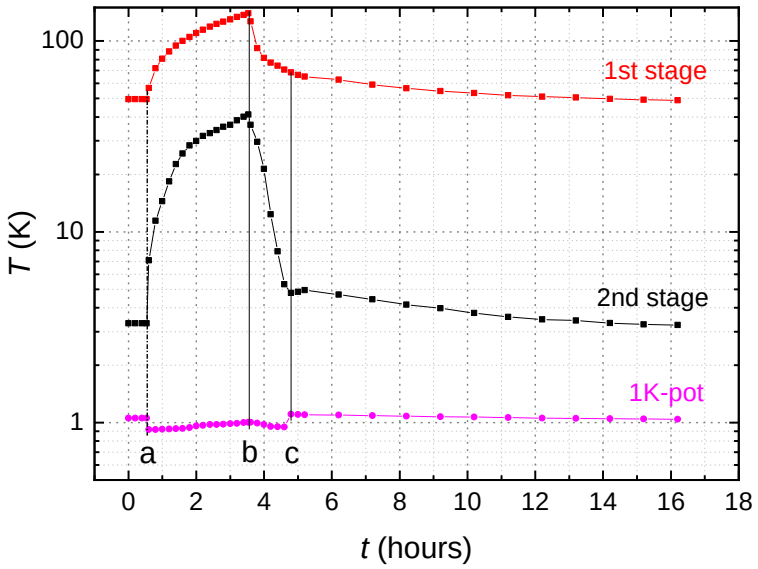

Figure 2: Temperatures of the 1K-pot and of the 2 stages of the PTC as a function of time. For details see text.

Next steps. The are three evident measures for further improvement. First, in order to prolong the holding time of the DR with the PTC off, the radiation shield of the 1st stage has already been equipped with superinsulation. We expect to reduce the radiation-induced heat leak by at least a factor of 2. Second, in the work presented here, the heat load onto the 1K-pot is negligible. If the ^{3}He flow of a DR has to be cooled and condensed, the required cooling power will result in a ^{4}He flow of the 1K-cooler of up to $\dot{n}_4 \approx 1\,\mathrm{mmol\,s^{-1}}$. Therefore, the size of the 1K-pot has to be increased to about $200\,\mathrm{cm}^3$ or higher, depending on the intended off-time of the PTC and the flow rate of the DR. Third, a thermal radiation shield which is thermally anchored at still temperature has to be installed. Its task will be to adsorb the residual exchange gas coming off the vacuum can when it warms up after the PTC is switched off [4]. The residual exchange gas can be the cause for a considerable heat leak and therefore a temperature rise of the mixing chamber of the DR. With these measures an operation period of the DR of well above an hour should be achievable with the PTC of the fridge switched off.

References

[1] K. Uhlig, Cryogenics **66**, 6–12 (2015).
[2] A. Marx, J.Hoess, and K. Uhlig. Dry Dilution Refrigerator for experiments on Quantum Effects in the Microwave Regime. CRYOCOOLERS 18, 481-6; arXiv: 1412.3619 (2014).
[3] Oxford Instruments; https://nanoscience.oxinst.com/products/cryofree-dilution-refrigerators/io.
[4] K. Uhlig, Annual report WMI 2017, 73–74 (2017).

Experimental Facilities

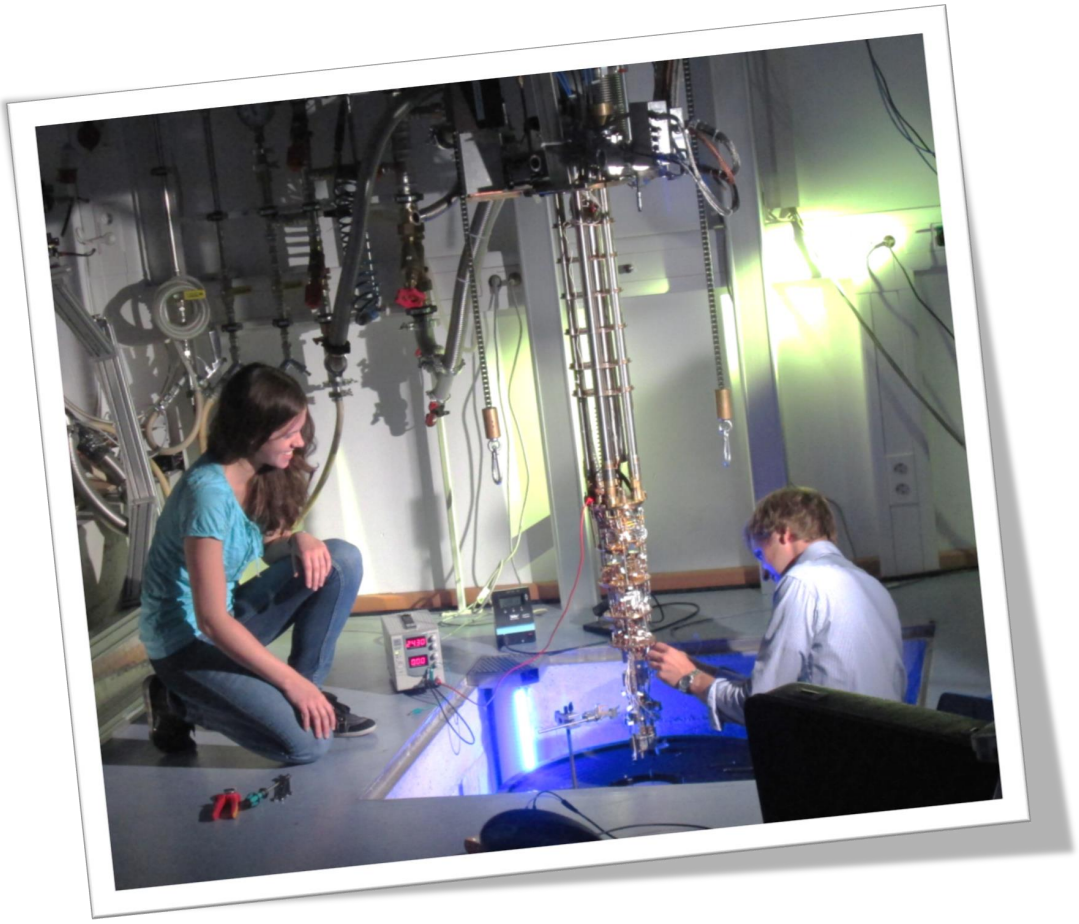

Overview of Key Experimental Facilities and Infrastructure

In the following basic information on the key experimental facilities and components of the technical infrastructure installed at the Walther-Meißner-Institute (WMI) is given.

UHV Laser-MBE

The WMI operates an UHV Laser-Molecular Beam Epitaxy (L-MBE) system for the growth of complex oxide heterostructures. The system has been designed to meet the special requirements of oxide epitaxy. The UHV cluster tool consists of the following main components:

- central transfer chamber;
- load-lock chamber with a heater system for substrate annealing;
- laser deposition chamber with a KrF excimer laser, *in-situ* reflection high energy electron diffraction (RHEED) system, laser substrate heating system, and atomic oxygen/nitrogen source; the RHEED system has been modified to allow for the operation at high oxygen partial pressure up to 0.5 mbar;
- surface characterization chamber with UHV scanning atomic force microscope (Omicron);
- metallization chamber with a four heart electron gun system and a liquid nitrogen cooled sample stage. The sample holder can be tilted for shadow evaporation.

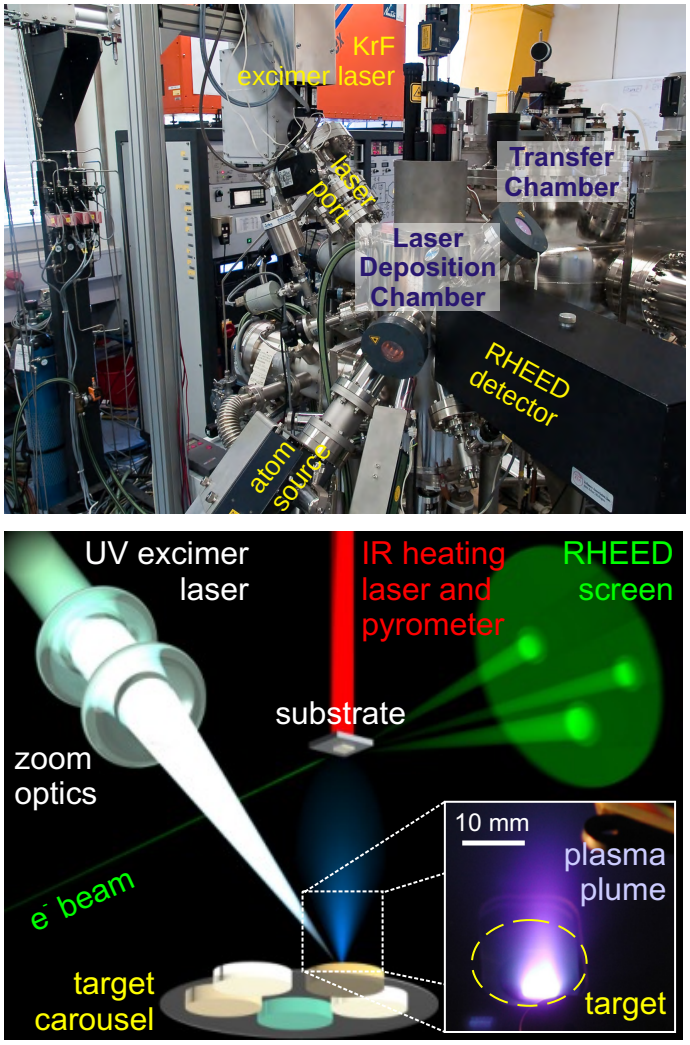

Figure 1: Top: UHV laser-molecular beam epitaxy system. Bottom: principle of the deposition process.

The system is used for the growth of complex oxide heterostructures consisting of superconducting, ferromagnetic, ferroelectric, and semiconducting materials such as high-temperature superconductors, doped manganites, (double) perovskites, magnetite, zinc oxide, rare earth iron garnets, pyrochlore iridates, etc.

The original laser molecular beam epitaxy system (laser-MBE) designed already in 1995/96 has been continuously upgraded and modified until today. In particular, the substrate heating system and the temperature control unit were changed from a resistive radiation heater to an infrared laser heating system (see Fig. 3, left) including a pyrometer for determining the sample temperature. In addition, a source for atomic oxygen and nitrogen has been installed. The main advantage of the new heating system is that only the substrate is heated while the surrounding parts are hardly affected (Fig. 3, right). In this way one can achieve a substantially better vacuum at temperatures well above 1000 °C. The achievable substrate temperature is limited by the melting point and the size of the substrate material (approx. 1410 °C for a 5 mm × 5 mm silicon substrate). The laser heating system has already been successfully used for removing the amorphous silicon oxide layer from the surface of silicon substrates at 1150 °C.

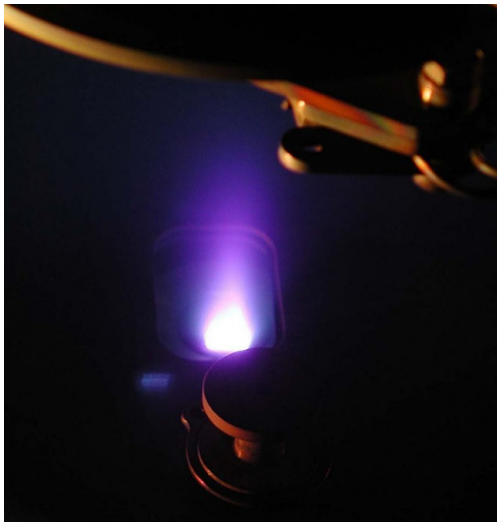

Figure 2: Pulsed Laser Deposition (PLD): When the pulse of the UV laser (KrF excimer laser, 248 nm) hits the target, the target material is ablated and the so-called laser "plume" containing highly excited atoms and molecules is formed.

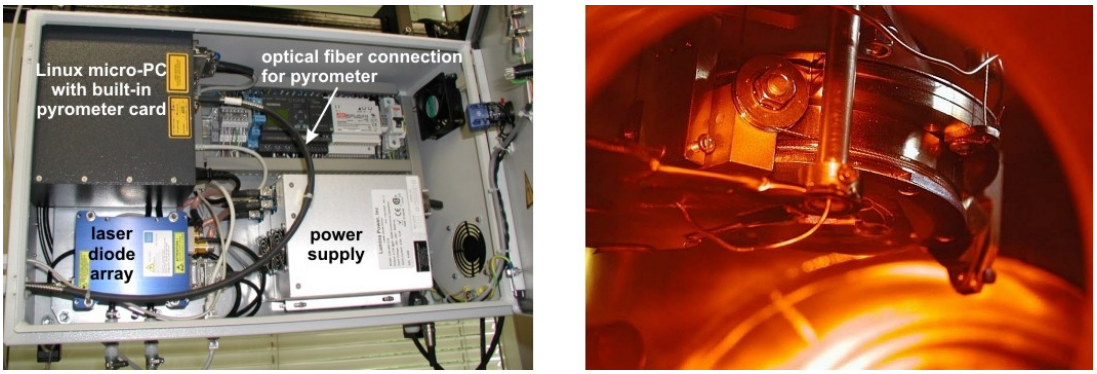

Figure 3: Components of the laser heating system: The substrate is heated using an IR diode laser head that is located in a separate box far away from the deposition chamber (left). The laser light is brought to the substrate (right) via an optical fiber.

We have further developed and installed a home-made telescope zoom optics for the pulsed UV laser light, consisting of in total five lenses on sliding lens holders allowing for a movement over a total distance of 1200 mm. The lens holders are attached to independent stepper motors, each connected to a controller providing an accurate positioning precision. The controllers are driven via a PC, thus allowing for a full automation of the lens system itself. With this telescope zoom optics we are able to change the area of the UV laser spot on the target, resulting in an accessible range of laser fluences from $\rho_L = 0.5\,J/cm^2$ to $5\,J/cm^2$. To maintain a stable laser fluence at the target, we have installed a so-called *intelligent* window (PVD Products) at the laser entrance port combining two unique features. First, it keeps the inner side of the entrance window free of coatings by blocking the ablated plasma plume via a rotatable disc consisting of UV grade fused silica. Second, an insertable mirror positioned in the light path after the disc allows to guide the incoming UV laser pulse through a side window, where its energy is determined by a pyroelectric detector. These measures help to improve the deposition processes by accurately monitoring ρ_L as one of the most critical process parameters.

UHV Sputter Deposition System

The UHV sputter deposition system was set up in 2017 and allows for the fully-automated fabrication of complex multilayers consisting of superconducting and magnetic materials. To avoid cross-contamination of the superconducting and magnetic materials the systems consists of two separate deposition chambers (see Fig. 4). The one deposition chamber is dedicated for superconducting materials (Non-Ferromagnet Chamber: NFC) and the other for the growth of magnetic materials (All Ferromagnet Chamber: AFC). The loadlock chamber is positioned between the two deposition chambers. It serves for inserting substrates and masks into the deposition chambers and enables the in-situ transfer of samples between the two deposition chambers. The system is designed for a face-down substrate orientation with the sputter source residing at the bottom of the deposition chambers. Both deposition chambers achieve a base pressure well below 8×10^{-10} mbar, paving the way for the deposition of high purity materials.

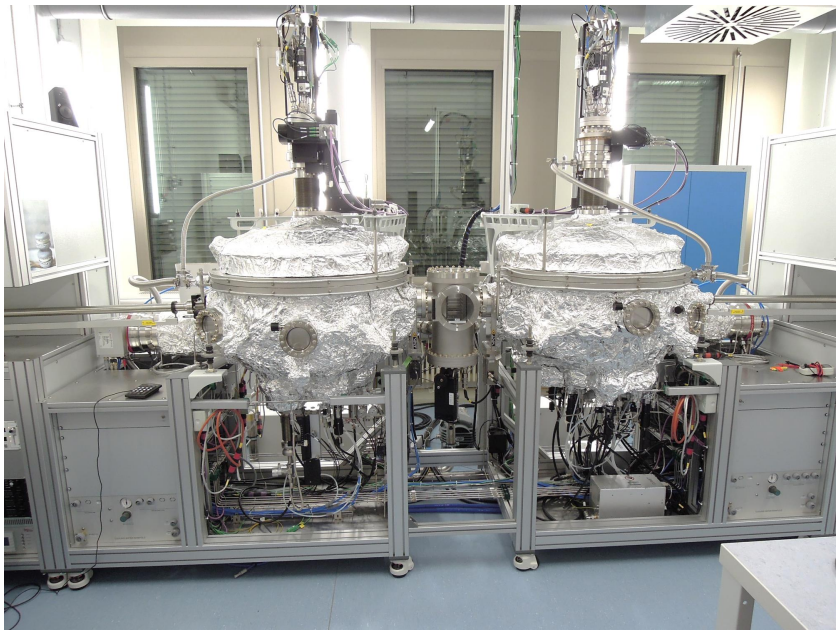

Figure 4: UHV sputter deposition system named «**SUPERBOWLS**». Left chamber is the NFC dedicated to the deposition of superconducting materials, right chamber is the AFC equipped with magnetic materials. Between the two deposition chambers resides the loadlock (LL).

The loadlock chamber is equipped with a substrate and mask storage cassette for up to six substrates. Halogen lamp heaters are installed in the loadlock for thermal precleaning of the substrates. The NFC is currently equipped with two 3 inch magnetrons and one 2 inch magnetron. In the AFC, eight 2 inch tiltable magnetrons are installed. In this chamber the sources can be either oriented into two confocal deposition clusters from 4 sources or 4 sources for face-to-face deposition, providing a large flexibility in the deposition conditions and enabling the fabrication of quaternary alloys from single element targets. All deposition sources are equipped with pneumatically actuated shutters, tilts, and linear translations. This allows for both face-to-face and confocal deposition from all three sources.

Both chambers are equipped with versatile substrate manipulators. They can accommodat substrates with a diameter of up to 2 inch and feature a resistive heater for substrate temperatures up to 800 °C, a motorized substrate shutter for wedge and step-profile deposition, a motorized linear translation for changing the source to substrate position, a main rotation to move the substrate in the chamber to the different deposition positions, a motorized substrate rotation at up to 40 rpm for homogenous deposition, and a quartz crystal microbalance (QCM) for growth rate monitoring. In addition, a Kaufmann source for reactive ion etching is installed in the system for in-situ surface cleaning procedures or even etching processes. Several 1 kW DC power and 600 W RF power supplies are used for the operation of the magnetrons. Mass flow controllers allow to change the composition of the process gas for reactive sputtering processes. More details can be found in the Annual Report 2017.

UHV Electron Beam Evaporation System

The UHV metal MBE system allows for the growth of high quality metallic thin films by electron beam evaporation and molecular beam epitaxy. The system is optimized for the fabrication of superconducting persistent current qubits by aluminum shadow evaporation. It is equipped with an improved substrate holder allowing for multi-angle shadow evaporation. The main components of the system are:

- UHV system with a process chamber with a base pressure below $\sim 1 \times 10^{-8}$ mbar pumped by a 1000 l/s turbo molecular pump with magnetic suspension of the rotor adequate for corrosive gases.
- Load-lock chamber equipped with a magnetic transfer system (push-pull positioner) for sample transfer without breaking the vacuum in the process chamber.
- Downstream pressure control by an adaptive pressure controlled gate valve.
- Electron beam evaporator with six 8 cm^3 crucibles embedded in a linearly movable water cooled rail providing six different materials.
- Film thickness measurement and closed loop evaporation rate control by a quartz crystal microbalance in combination with the evaporation controller.
- Effusion cell for molecular beam epitaxy processes.
- Ion sputtering gun for in-situ sample cleaning
- Manipulator with UHV stepping motors for automated and precise sample tilt and options for rotating and cooling the sample.

A precise and reproducible tilt of the sample is realized by a sample manipulator with process specific degrees of freedom. The downstream pressure control allows for a fast adjustment and precise control of the oxygen partial pressure. This is crucial for a well-defined oxidation process of the Josephson junctions barriers. The entire process can be performed fully automated via a touch screen and is controlled by a LabView program. Up to six effusion cells can be optionally added to the system allowing for further materials. The manipulator allows for further degrees of freedom that can be used to align the sample to the effusion cells, the ion sputtering gun and to measuring equipment such as ellipsometry or RHEED.

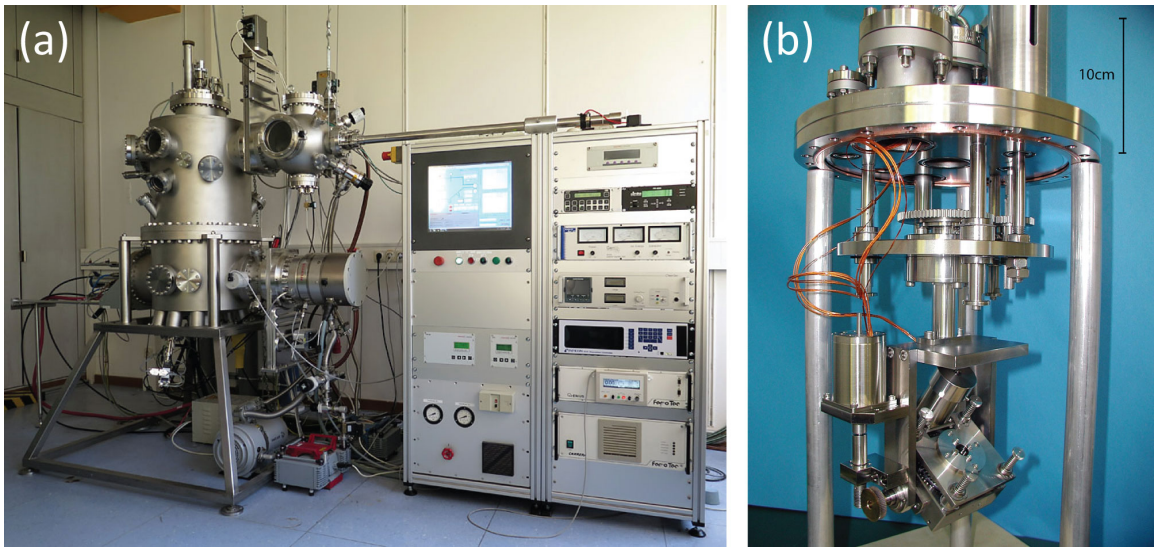

Figure 5: (a) Photograph of the UHV electron beam evaporation system. (b) Manipulator with UHV stepping motors for automated and precise sample tilt and options for rotation.

Single Crystal Growth and Synthesis of Bulk Materials

Transition metal oxides are of great interest due to their various interesting physical properties (e.g. high temperature superconductivity, colossal magnetoresistance, ferroelectricity, nonlinear optical properties etc.) and their high potential for applications. Therefore, the WMI operates a laboratory for the synthesis of bulk materials and single crystals of transition metal oxides. Besides various chamber- and tube furnaces a four-mirror image furnace is used for the crystal growth of various oxide systems. With this furnace crystals of many different compounds of the high temperature superconductors and various other transition metal oxides have been grown as single crystals using the traveling solvent floating zone technique. The furnace consists basically of 4 elliptical mirrors with a common focus on the sample rod and with halogen lamps in their other focus. By irradiation of the focused light the sample rod is locally heated and eventually molten. The molten zone can be moved up and down along the entire sample rod under simultaneous rotation. Due to the anisotropic growth velocity a preferential growth of those grains with the fastest growth velocity along the pulling direction is obtained and the formerly polycrystalline rod is transformed into a single crystal. Single crystal growth can be performed with this furnace at maximum temperatures up to 2200 °C in the pressure range from 10^{-5} mbar up to 10 bar and in oxidizing, reducing as well as inert atmosphere.

Figure 6: The four-mirror image furnace installed at the crystal laboratory of the WMI. Crystals can be grown by the floating zone and traveling solvent floating zone techniques at temperatures up to 2200 °C and pressures up to 10 bar.

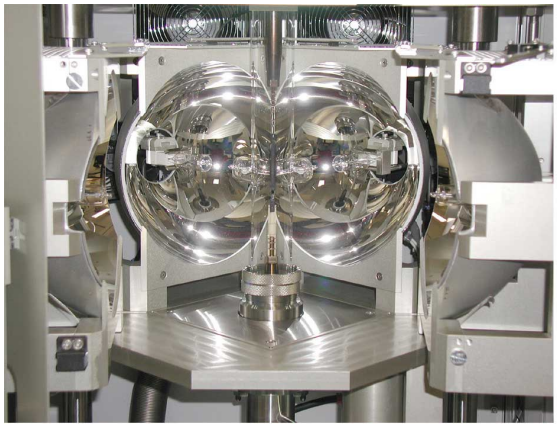

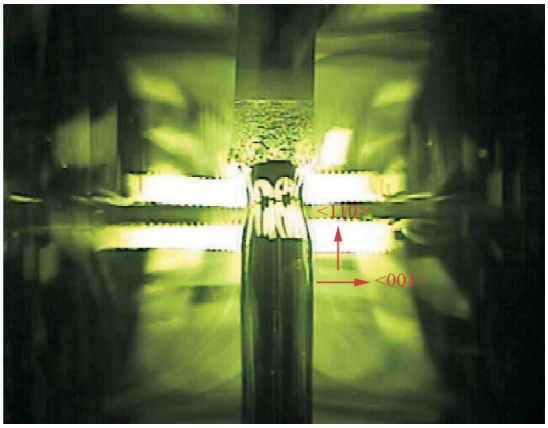

Figure 7: Left: Central part of the image furnace with four elliptical mirrors. In the center one can see the quartz tube with a polycrystalline rod. Right: View on the molten zone of $Pr_{2-x}Ce_xCuO_4$ (melting point: 1280 °C) obtained by a CCD camera.

The X-ray diffraction systems

For X-ray analysis the WMI operates two X-ray diffractometers (Bruker D8 Advance and D8 Discover). The two-circle system is used for powder diffraction. In this system the samples can be heated in oxygen atmosphere up to 1600 °C. It is equipped with a Göbel mirror and an area detector to save measuring time. The second system is a high resolution four-circle diffractometer that can be used for reciprocal space mappings. It is equipped with a Göbel mirror and an asymmetric two-fold Ge monochromator and allows for the texture analysis of thin film heterostructures, superlattices and single crystalline materials. In both systems measurements can be carried out fully computer controlled.

Beside these two Bruker X-ray systems a Laue camera for single crystal analysis and a Debye-Scherrer camera are available.

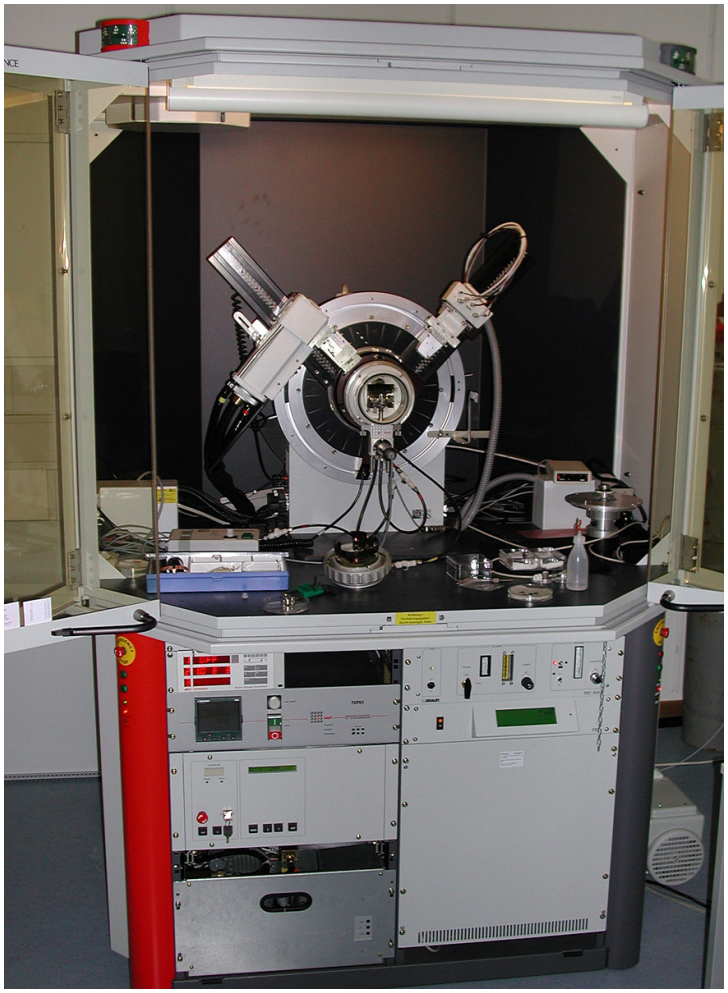

Figure 8: The two-circle X-ray diffractometer Bruker D8 Advance.

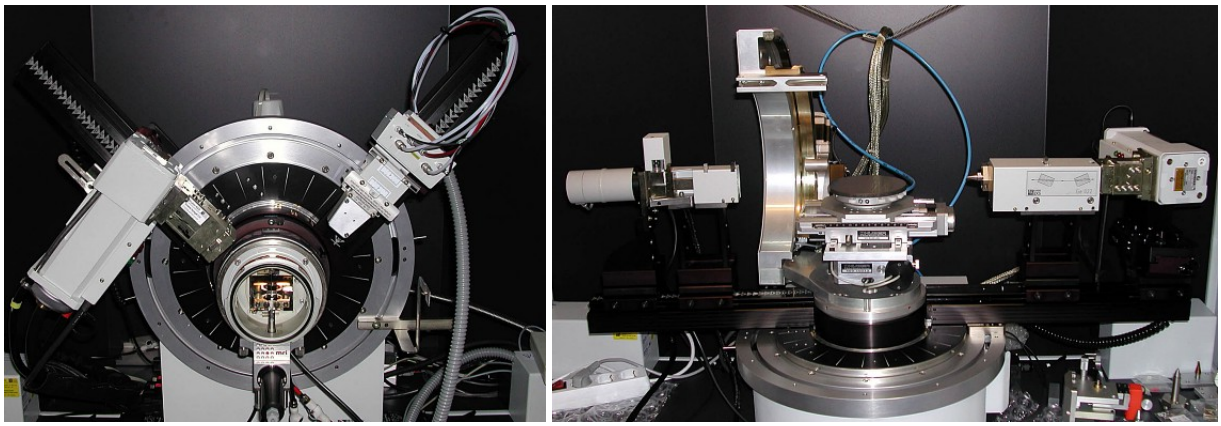

Figure 9: Left: High temperature sample holder of the D8 Advance system. Right: Four-circle high resolution X-ray diffractometer Bruker D8 Discover.

Figure 10: Quantum Design SQUID magnetometer.

The SQUID magnetometer

For the analysis of the magnetic properties of materials, a Quantum Design SQUID magnetometer system (Fig. 10) is operated at the WMI. The SQUID magnetometer allows for measurements in the temperature regime from 1.8 to 400 K and provides excellent sensitivity particularly in the low field regime. Due to the excellent sensitivity of the system, thin film samples with a very small sample volume can be analyzed. The SQUID magnetometer is equipped with a superconducting solenoid allowing for a maximum field of 7 T. At present, the magnetometer is used for the characterization of magnetic and superconducting materials (both in bulk and thin film form). Examples are the cuprate high temperature superconductors, the doped manganites, magnetite, the double perovskites, magnetic semiconductors, or multiferroics.

The High Field Laboratory

Transport and thermodynamic properties of samples are often studied as a function of the applied magnetic field. For such measurements several superconducting magnets are available at the WMI. Two of them (8/10 and 15/17 Tesla magnet system) are located in the high magnetic field laboratory in the basement of the WMI. The magnet systems are installed below the floor level to facilitate the access to the top flange and the change of the sample sticks. The magnet systems are decoupled from the building to avoid noise due to mechanical vibrations. A variety of sample holders can be mounted allowing for e.g. sample rotation during the measurement. For standard sample holders the accessible temperature regime is $1.5\,\mathrm{K} < T < 300\,\mathrm{K}$. However, also ^{3}He/^{4}He dilution refrigerator inserts ($T > 20\,\mathrm{mK}$) or high temperature units ($T < 700\,\mathrm{K}$) can be mounted. All measurements are fully computer controlled (by the use of the LabView software tool) allowing for remote control and almost continuous measurements.

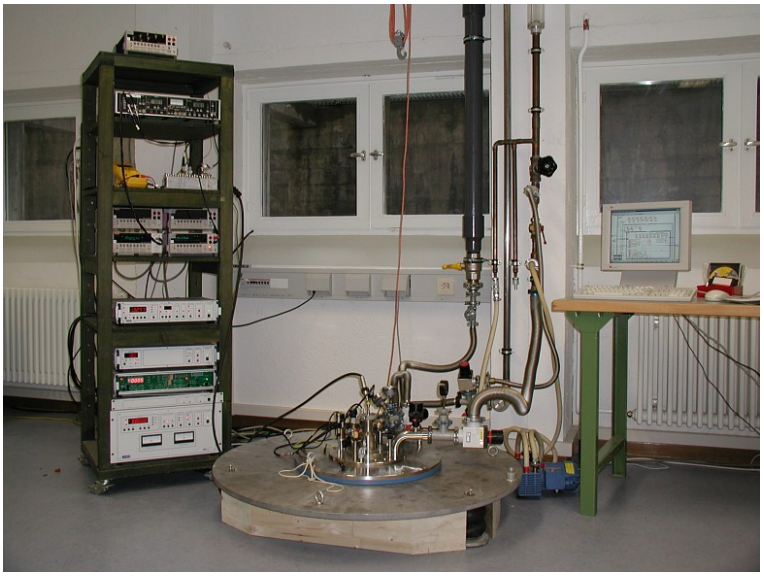

Figure 11: High field laboratory with Oxford 17 T magnet system.

Since 2012, a 3D vector magnet with variable temperature insert, allowing for 2.5 T in-plane and 6 T out-of-plane magnetic fields is available for thermal and electrical transport experiments. This system has been named "Chaos" cryostat (acronym for "Cold, Hot And Other Secret experiments"). It consists of a ^{4}He flow cryostat with a liquid nitrogen shield and in-

cludes a vertically oriented 6 T solenoid combined with two horizontally oriented split coil pairs. The magnet system can be operated in two ways:

- in a single axis mode: up to 6(2.5) T are provided in the vertical (horizontal) direction.
- in a arbitrary axis mode: the flux density vector can be oriented in arbitrary directions and the magnitude of the flux density is limited to 2.5 T.

The magnetic field is controlled by a Mercury IPS superconducting magnet power supply master/slave system. It provides output currents of up to 120 A in bipolar operation for each magnet axis. The control of the system is feasible either directly via touch-screen or remote using a LabView based software.

Figure 12: The 3D vector magnet with control electronics in the "CHAOS" Laboratory.

The Chaos cryostat has a IN100 variable temperature insert (VTI), enabling an operation for temperature setpoints between 1.5 K and 300 K. The temperature control of the sample space inside the VTI can be achieved via an automatic needle valve drive for helium flow control and/or an automatic heater system. The temperature of the VTI is read via a Cernox sensor fitted to the heat exchanger. A remote control of the system is realized by a LabView based software. It provides control of the VTI (heater, needle valve, temperature setpoint) and the IPS (control of the magnetic field setpoints and energizing rates for the three vector components of the field) as well as the display of the actual He and liquid nitrogen levels.

A further 3D vector magnet allowing for 1 T in-plane and 6 T out-of-plane magnetic fields is installed in the WMI Quantum Laboratories as part of a cryogen-free dilution system.

The Clean Room Facility

For the fabrication of nanostructures and quantum circuits including superconducting, spintronic and nanomechanical devices, the WMI operates a class 1000 clean room facility with an area of about 50 m^2. The clean room is subdivided into two parts for optical lithography and electron beam lithography, respectively. The clean room is equipped with the standard tools for optical lithography such as resist coaters, hot plates, wet benches, a Karl Süss MJB3 mask aligner, a direct laser writing system *PicoMaster 200* from 4 PICO, and an optical projection lithography system. The technical infrastructure for the clean room is located in the basement of the WMI directly below the clean room area.

Figure 13: Top: Part of the clean room facility with optical lithography equipment and clean room benches. Bottom: Resist coater and hot plates.

The clean room also is equipped with a reactive ion etching system, Plasmalab 80 Plus with ICP plasma source (Oxford Instruments Plasma Technology).

Electron Beam Lithography

A 100 kV Electron Beam Lithography System nB5 fabricated by NanoBeam Ltd., UK, is installed in the second part of the clean room facility. The nB5 is a round-beam step-and-repeat system oriented towards high-end R&D applications at universities and research institutes. It is designed for nanopatterning and mix-and-match lithography. The innovative design of the electron optics and automation system enhances its throughput and reliability. It is an ideal tool for nano-device research and production. The electron beam lithography is used for the fabrication of nanostructures in metallic and oxide systems required for the study of quantum effects in mesoscopic samples.

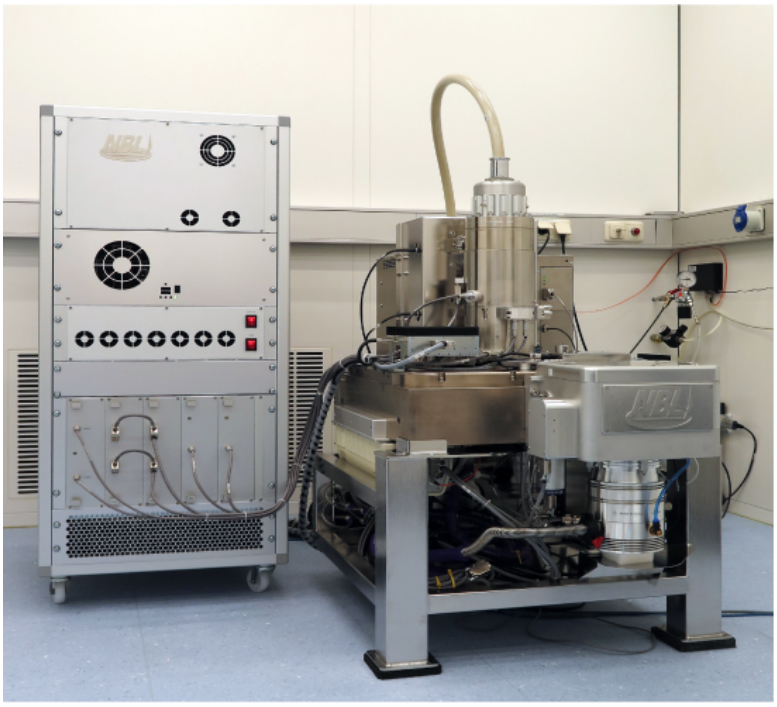

Figure 14: 100 kV Electron Beam Lithography System nB5 of NanoBeam Ltd., UK, inside the WMI cleanroom facility.

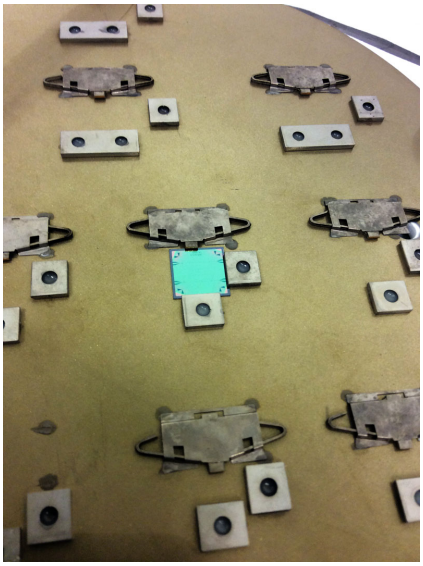

Figure 15: Chuck of the nB5 e-beam lithography system with a mounted $12 \times 12\,\mathrm{mm}^2$ silicon wafer.

The nB5 Electron Beam Lithography System employs low Coulomb-effect electron optics and sophisticated column designs to reduce beam size. The shorter optical column eliminates column bending and reduces system vibration. The modern electronics has low noise and low thermal effects. The perfectly integrated machine structure greatly improves system settling time and total stage move time. The advanced vibration tracking design enables the nB5 system to write on the fly. All these features combined with the fast deflection speed and high data processing rate make the nB5 the highest throughput system available today. Moreover, the nB5 requires undemanding cleanroom conditions, in particular regarding temperature stability, stray field magnitude, and floor vibration level.

The nB5 system is equipped with a thermal field emitter (TFE), an electrostatic lens and magnetic condenser lens, a conjugate beam blanking at $< 5\,\mathrm{ns}$ slew rate and a dual beam deflection. The latter is used to achieve ultra-high deflection speed for beam writing (clock rate: 55 MHz). The total deflection coverage is combined with the mainfield and the subfield and controlled by two independent deflection sub-systems (field size: $1000\,\mu\mathrm{m}$, address resolution: 1 nm). The characteristic performance parameters of the electron optics of the nB5 system are: (i) beam voltage range: 20 kV to 100 kV, (ii) minimum beam current: 0.1 nA, (iii) maximum beam current: 100 nA, (iv) theoretical beam size: 2.3 nm at 100 kV, (v) guaranteed writing beam size: $< 5\,\mathrm{nm}$ at 2 nA, (vi) beam current drift: $< 0.5\%$/hour at 5 nA, (vii) beam position drift: $< 50\,\mathrm{nm}$/hour for 3 nA beam current, including blanking, deflection and stage move.

The XY-stage allows for a traversal distance of 200 mm with a total stage move time of only 150 ms for 1 mm stage movement and a position measurement resolution of 0.3 nm using laser interferometry. The maximum substrate sizes are $2 - 8$ in for round substrates, $2 - 5$ for square glass masks up to 3 mm thickness. Finally, the nB5 system has airlock operation with automatic loading robotics with a loading cassette for 6 chucks with a maximum diameter of 8 inch.

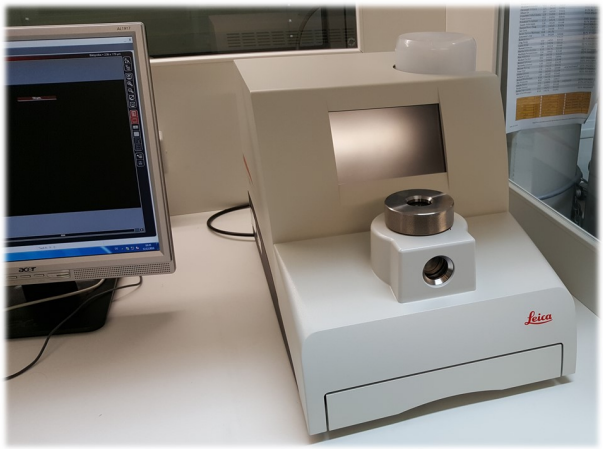

Figure 16: The fully automated Critical Point Dryer Leica EM CPD 300.

Automated Critical Point Dryer Leica EM CPD 300

The fabrication of nanomechanical systems requires the removal of solvent used for wet chemical processing by a critical point dryer. At WMI, we use the Critical Point Dryer Leica EM CPD 300, which allows the fully automated drying of biological specimens such as pollen, tissue, plants, insects etc., as well as NEMS (Nano Electro Mechanical Systems).

To ensure a low CO_2 consumption and a very short process time a new filler concept is used in the Leica EM CPD 300. Special attention has been put on safety issues by implementing software controlled cut-off functions and integrating a waste separator.

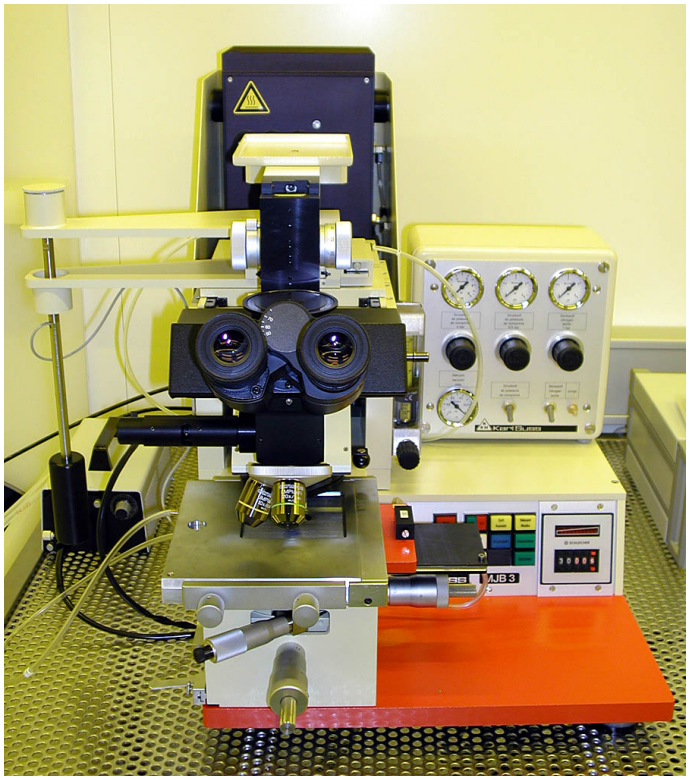

Figure 17: Top: Süss MJB 3 maskaligner for optical lithography. Bottom: Direct laser writing systems *PicoMaster 200*.

Optical Lithography

For optical lithography, a Karl Süss MJB 3 maskaligner or a direct laser writing system are used. The maskaligner operates in the 1 : 1 soft or hard contact mode and uses chromium metal masks.

The direct laser writing system *PicoMaster 200* (PM 200) of the company 4PICO accepts substrate sizes between 5 mm × 5 mm and 200 mm × 200 mm via a turnable chuck. For writing the pattern, it allows for three different spot sizes (300 nm/600 nm/900 nm) and a write speed of up to 7.7 mm^2/min. One can choose between two compact writing modules equipped with a 405 nm and a 375 nm laser diode, respectively. The user can easily switch between the two modules within minutes since the full optical path is contained in the modules. Both modules feature automatic focus correction for not too heavily varying resist thickness. More details can be found in the report on page 73.

Low and Ultra-Low Temperature Facilities

At the WMI, we have constructed the first dilution refrigerator with pulse tube pre-cooling for ultra-low temperature experiments. This type of refrigerator works without cryo-liquids, and thus is a lot more practical, more economical and more reliable than cryostats with liquid helium pre-cooling. These days, all major cryo-engineering companies are offering commercial versions of this Millikelvin cooler, and these so-called "dry" refrigerators outsell conventional refrigerators by a wide margin. The general construction concept of most manufacturers is unchanged from our original prototype, where the refrigerator consists of three basic components. The first cooling stage is a commercial pulse tube cryocooler which reaches a base temperature of 2.5 K. The second stage is a Joule-Thomson stage, and the last stage is a dilution refrigeration stage, where the lowest temperature of the cryostat is about 0.01 K (Fig. 18).

Figure 18: The "dry" dilution refrigerator of the WMI.

Figure 19: Low-temperature unit of a WMI dilution refrigerator ready to go into a cryostat.

Figure 20: Two mixing chamber mounting plates with silver sponges. Those are needed to overcome the thermal resistance (Kapitza resistance) between the liquid ^{3,4}He and the mounting plate of the mixing chamber. To fabricate the mounting of the sponge (square pins embedded in the sponge) a spark erosion technique has been employed.

In many low temperature applications high refrigeration capacities are required. Our design allows for a high circulation rate of ^{3}He which in the end determines the cooling power of a dilution refrigerator. Presently our "dry" fridge reaches a refrigeration capacity of 700 µW at a temperature of the mixing chamber of 0.1 K, seven times the cooling power of the WMI nuclear demagnetization cryostat. Goals of our present work are a further increase of cooling power and a lower base temperature of the dry dilution refrigerator. A smaller version of our cryogen-free fridge has become commercially available later on by *VeriCold Technologies, Ismaning*) which was taken over by *Oxford Instruments* in 2007. It had a refrigeration capacity of 250 µW at a mixing chamber temperature of 0.1 K (Fig. 19).

The WMI also develops and fabricates dilution refrigerator inserts for temperatures down to

about 20 mK. The inserts fit into all cryogenic systems (e.g. superconducting magnets) having a two inch bore. They allow fast sample change and rapid cool down cycles of less than five hours. The dilution refrigerator inserts are engineered and fabricated in-house and are also provided to other low temperature laboratories for ultra-low temperature experiments.

Millikelvin Temperatures in Combination with 3D Vector Magnetic-Fields

Figure 21: The dilution refrigerator with the 3D vector magnet located in the Quantum Laboratories.

In one room of the WMI Quantum Laboratories a cryogen-free dilution refrigerator is installed. This system is equipped with a 3D vector magnet allowing for 1 T in-plane and 6 T out-of-plane magnetic fields. Additional microwave coaxial lines allow for the microwave spectroscopy up to 18 GHz under these experimental conditions.

Scientifically, several directions in the field of fundamental light-matter interaction are envisaged:

(i) Circuit quantum electrodynamics (circuit QED), where superconducting qubits form hybrids with microwave resonators. These experiments are time consuming, because quantum effects arise in the limit of low excitation numbers. Hereby, challenging requirements are imposed on the detection systems allowing to detect microwave signals in the attowatt regime.

(ii) Storage of quantum states. One possibility is the transfer of the quantum information contained in photons to long-lived spin states. Additionally, exchange coupled systems or ferromagetic systems come into focus, because the effective coupling strength scales with the square-root of the number of spins contributing. In general, we study the light-matter interaction with long-lived spin systems and integrate them into superconducting quantum circuits.

(iii) Spin systems. Here, our studies are not limited to paramagnetic spin systems, but also involve exchange coupled (ferro- or ferri-) magnetic systems. Hereby, magnetization damping can be investigated as a function of temperature, frequency and magnetic field direction.

(iv) Circuit electro-mechanical hybrid systems consisting of a nano-mechanical element coupled to a superconducting microwave resonator. In this context, sideband cooling of the mechanical system into its ground state and pulsed spectroscopy of hybrid system are performed and will be extended.

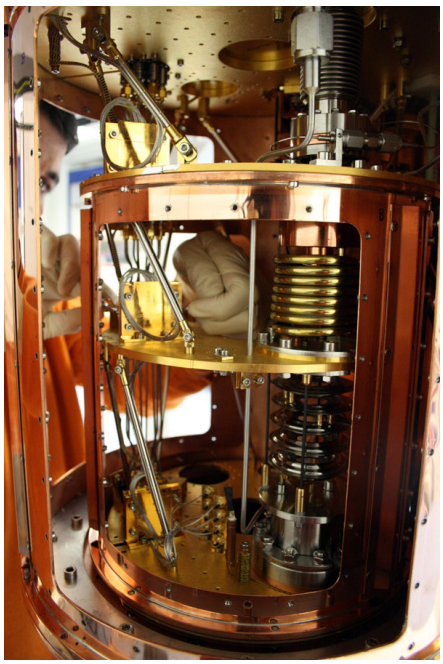

Figure 22: Inside of the dilution system. The windows of the 4 K and the still shield are removed providing access to the low temperature stages.

WMI Millikelvin Facilities for Experiments with Superconducting Quantum Circuits

The research on superconducting quantum circuits at WMI focuses mainly on systems sensitive to externally applied flux (flux qubits), circuit QED systems where flux qubits are coupled to transmission line resonators, squeezing physics in flux driven Josephson parametric amplifiers, and propagating quantum microwaves (e.g., quantum state reconstruction methods). In order to further develop our activities on quantum effects in the microwave regime, additional cryogenic capacities at millikelvin temperatures have been established. In addition to sufficient cooling power, the specifications for these cryostats are mainly dictated by the dimensions (typically a few centimeters in each direction) of bulky microwave components such as circulators or microwave switches.

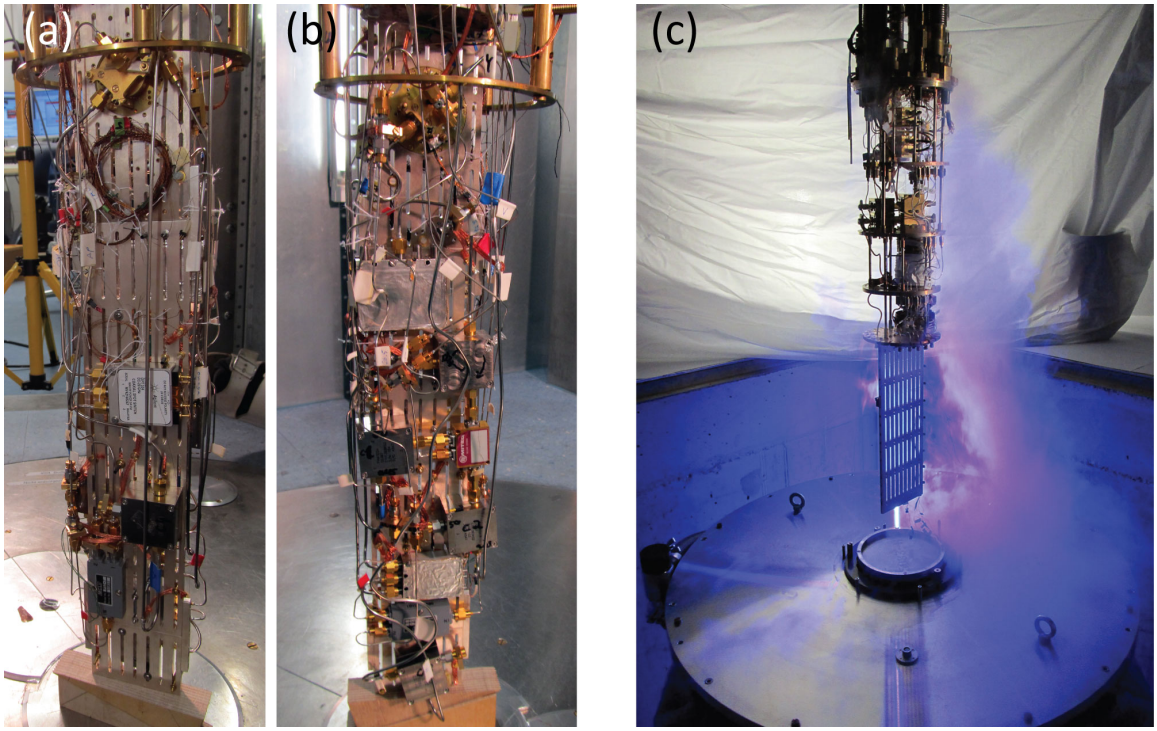

Figure 23: Liquid-helium precooled dilution refrigerators for experiments with superconducting quantum circuits. (a), (b) Back and front sides of the sample stage of the K12-refrigerator equipped with four circuit QED experiments. The height of the silver rod is 50 cm. (c) Sample stage and dewar of the dilution refrigerator in the quantum laboratory K04.

Two liquid-helium precooled dilution refrigerators are available for experiments with superconducting quantum circuits. The dilution refrigerator in laboratory K12 provides a sample space with a cylindrical volume with 11 cm diameter 55 cm height. The refrigerator is equipped with four microwave amplifiers at the 4 K-stage, seven broadband input lines and 80 twisted pair DC lines. This allows for mounting four experiments simultaneously to avoid idle times by interleaved measurements (see Fig. 23(a) and (b)). The base temperature of this refrigerator is 20 mK.

A new liquid-helium precooled dilution refrigerator for experiments with superconducting quantum circuits has been set up in the quantum laboratory K04. To provide enough space at the sample stage we have installed a Cryogenic Ltd. stainless steel dewar with a ^{4}He volume of 89 l. The time between two refills exceeds nine days. The cryostat is equipped with 16 coaxial measurement lines suitable for microwave frequencies down to the mixing chamber stage and low-noise cryogenic high electron mobility transistor (HEMT) amplifiers. Presently up to four samples can be mounted simultaneously to the sample stage. By expanding the number of input lines in the near future a more complex experiment can be set up. The cooling power of

the mixing chamber at 100 mK was determined to about 140 µW.

A new cryogen-free dilution refrigerator with a pulse tube refrigerator (PTR) for precooling and with a large sample stage has been set up in room K21 of the WMI Quantum Laboratories using the longstanding experience in dry dilution refrigerators at WMI. This refrigerator features large diameters (tens of centimeters) of all temperature stages providing sufficient space for advanced quantum experiments. The main components of the refrigerator are the PTR, a 1 K-stage and a dilution unit. The two stages of the PTR cool the incoming ^{4}He and the ^{3}He/^{4}He mixture as well as one radiation shield at each stage. To provide sufficiently high cooling power near 1 K to cool microwave components and cables, this refrigerator has been equipped with a 1 K-stage operating in a closed cycle. A refrigeration capacity of the 1 K-stage of up to 100 mW could be reached. The dilution refrigerator is precooled by a dedicated ^{4}He circuit. The minimum base temperature of the refrigerator is below 11 mK. The cooling power at 100 mK was determined to about 300 µW at the maximum ^{3}He flow rate.

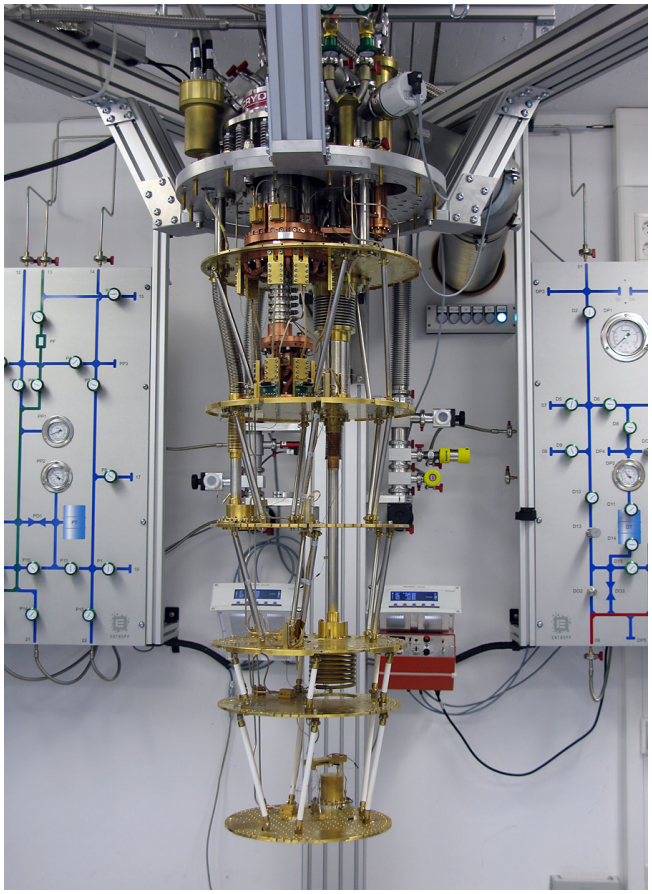

Figure 24: Dry dilution refrigerator with a large sample space.

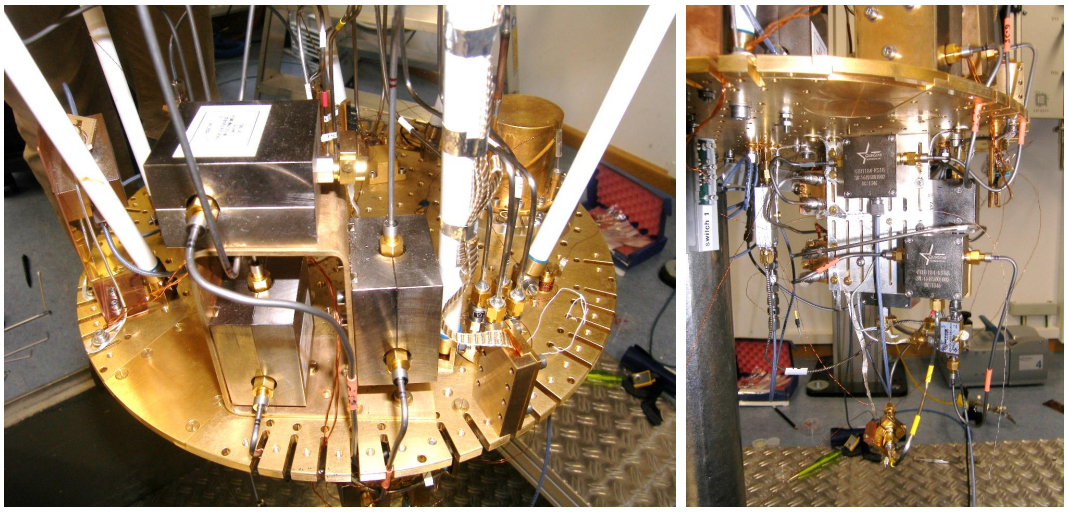

Figure 25: Low temperature platform of K21 dilution refrigerator with experimental setup for circuit QED experiments.

Statistics

Publications

1. **Festkörperphysik** (3. erweiterte Auflage)
   R. Gross, A. Marx
   Walter de Gruyter GmbH, Berlin (2018), ISBN 978-3-11-055822-7 (gebunden), ISBN 978-3-11-055918-7 (eBook).

2. **Festkörperphysik: Aufgaben und Lösungen (2. Auflage)**
   R. Gross, A. Marx, D. Einzel, S. Geprägs
   Walther de Gruyter GmbH, Berlin/Boston (2018), ISBN 978-3-11-056611-6 (gebunden), ISBN 978-3-11-056635-2 (eBook).

3. **Spin Hall effect**
   M. Althammer
   In: Topology in Magnetism, Zang J., Cros V., Hoffmann A. (eds). Springer Series in Solid-State Sciences, vol 192, pp. 209–237, Springer, Cham (Print ISBN: 978-3-319-97333-3).

4. **Spin-Torque Excitation of Perpendicular Standing Spin Waves in Coupled YIG/Co Heterostructures**
   Stefan Klingler, Vivek Amin, Stephan Geprägs, Kathrin Ganzhorn, Hannes Maier-Flaig, Matthias Althammer, Hans Huebl, Rudolf Gross, Robert D. McMichael, Mark D. Stiles, Sebastian T.B. Goennenwein, Mathias Weiler
   Phys. Rev. Lett. **120**, 127201 (2018).

5. **Lock-in thermography measurements of the spin Peltier effect in a compensated ferrimagnet and its comparison to the spin Seebeck effect**
   Ahmet Yagmur, Ryo Iguchi, Stephan Gepraegs, Andreas Erb, Shunsuke Daimon, Eiji Saitoh, Rudolf Gross, Ken-ichi Uchida
   Journal of Physics D: Applied Physics **51**, 194002 (2018).

6. **Finite-time quantum entanglement in propagating squeezed microwaves**
   Kirill G. Fedorov, S. Pogorzalek, U. Las Heras, M. Sanz, P. Yard, P. Eder, M. Fischer, J. Goetz, E. Xie, K. Inomata, Y. Nakamura, R. Di Candia, E. Solano, A. Marx, F. Deppe, R. Gross
   Scientific Reports **8**, 6416 (2018).

7. **Compact 3D quantum memory**
   Edwar Xie, Frank Deppe, Michael Renger, Daniel Repp, Peter Eder, Michael Fischer, Jan Goetz, Stefan Pogorzalek, Kirill G. Fedorov, Achim Marx, Rudolf Gross
   Appl. Phys. Lett. **112**, 202601 (2018).

8. **Pure spin currents in magnetically ordered insulator/normal metal heterostructures**
   Matthias Althammer
   J. Phys. D: Appl. Phys. **51**, 313001 (2018).

9. **Parity-engineered light-matter interaction**
   Jan Goetz, Frank Deppe, Kirill G. Fedorov, Peter Eder, Michael Fischer, Stefan Pogorzalek, Edwar Xie, Achim Marx, Rudolf Gross
   Phys. Rev. Lett. **121**, 060503 (2018).

10. **Derivative divide, a method for the analysis of broadband ferromagnetic resonance in the frequency domain** Hannes Maier-Flaig, Sebastian T. B. Goennenwein, Ryo Ohshima, Masashi Shiraishi, Rudolf Gross, Hans Huebl, Mathias Weiler
    Review of Scientific Instruments **89**, 076101 (2018).

11. **Spin Hall magnetoresistance in antiferromagnet/heavy-metal heterostructures**
    Johanna Fischer, Olena Gomonay, Richard Schlitz, Kathrin Ganzhorn, Nynke Vlietstra, Matthias Althammer, Hans Huebl, Matthias Opel, Rudolf Gross, Sebastian T.B. Goennenwein, S. Geprägs
    Phys. Rev. B **97**, 014417 (2018).

12. **Solid-state magnetic traps and lattices**
    J. Knörzer, M. J. A. Schuetz, G. Giedke, H. Huebl, M. Weiler, M. D. Lukin, and J. I. Cirac

Phys. Rev. B **97**, 235451 (2018).

13. **Inductive detection of fieldlike and dampinglike ac inverse spin-orbit torques in ferromagnet/normal-metal bilayers**
A. J. Berger, E. R. J. Edwards, H. T. Nembach, A. D. Karenowska, M. Weiler, and T. J. Silva
Phys. Rev. B **97**, 094407 (2018).

14. **Phonon anomalies in FeS**
A. Baum, A. Milosavljevic, N. Lazarevic, M. M. Radonjic, B. Nikolic, M. Mitschek, Z. Inanloo Maranloo, M. Šcepanovic, M. Grujuic-Brojcin, N. Stojilovic, M. Opel, Aifeng Wang, C. Petrovic, Z.V. Popovic, R. Hackl
Phys. Rev. B **97**, 054306 (2018).

15. **Magnetotransport evidence for irreversible spin reorientation in the collinear antiferromagnetic state of underdoped $Nd_{2-x}Ce_xCuO_4$**
A. Dorantes, A. Alshemi, Z. Huang, A. Erb, T. Helm, M. V. Kartsovnik
Phys. Rev. B **97**, 054430 (2018).

16. **Magnetic excitations and amplitude fluctuations in insulating cuprates**
N. Chelwani, A. Baum, T. Böhm, M. Opel, F. Venturini, L. Tassini, A. Erb, H. Berger, L. Forró, and R. Hackl
Phys. Rev. B **97**, 024407 (2018).

17. **Spin Hall magnetoresistance in the non-collinear ferrimagnet GdIG close to the compensation temperature**
Bo-Wen Dong, Joel Cramer, Kathrin Ganzhorn, H. Y. Yuan, Er-Jia Guo, Sebastian T. B. Goennenwein, and Mathias Kläui
Journal of Physics - Condensed Matter **30**, 035802 (2018).

18. **Quantum probe of an on-chip broadband interferometer for quantum microwave photonics**
P. Eder, T. Ramos, J. Goetz, M. Fischer, S. Pogorzalek, J. Puertas Martínez, E.P. Menzel, F. Loacker, E. Xie, J.J. Garcia-Ripoll, K.G. Fedorov, A. Marx, F. Deppe, R. Gross
Supercond. Sci. Technol. **31**, 115002 (2018).

19. **Frequency control and coherent excitation transfer in a nanostring resonator network**
Matthias Pernpeintner, Philip Schmidt, Daniel Schwienbacher, Rudolf Gross, Hans Huebl
Phys. Rev. Appl. **10**, 034007 (2018).

20. **Ultrawide-range photon number calibration using a hybrid system combining nanoelectromechanics and superconducting circuit quantum electrodynamics**
Philip Schmidt, Daniel Schwienbacher, Matthias Pernpeintner, Friedrich Wulschner, Frank Deppe, Achim Marx, Rudolf Gross, and Hans Huebl
Appl. Phys. Lett. **113**, 152601 (2018).

21. **Shubnikov–de Haas oscillations in the magnetoresistance of layered conductors in proximity to the topological Lifshitz transition**
V. G. Peschansky, M. V. Kartsovnik, S. Fust
Low Temperature Physics **44**, 791 (2018).

22. **Measurements and atomistic theory of electron g-factor anisotropy for phosphorus donors in strained silicon**
Mohammad Usman, Hans Huebl, Andre R. Stegner, C. D. Hill, Martin S. Brandt, and Lloyd C. L. Hollenberg
Phys. Rev. B **98**, 035432 (2018).

23. **Indication of subdominant d-wave interaction in superconducting $CaKFe_4As_4$**
D. Jost, J.-R. Scholz, U. Zweck, W. R. Meier, A. E. Böhmer, P. C. Canfield, N. Lazarevic and R. Hackl
Phys. Rev. B **98**, 020504 (2018).

24. **Determination of spin Hall effect and spin diffusion length of Pt from self-consistent fitting**

of damping enhancement and inverse spin-orbit torque measurements
A. J. Berger, E. R. J. Edwards, H. T. Nembach, O. Karis, M. Weiler, and T. J. Silva
Phys. Rev. B **98**, 024402 (2018).

25. **Bulk charge ordering in the CuO_2 plane of the cuprate superconductor $YBa_2Cu_3O_{6.9}$ by high pressure NMR**
Steven Reichardt, Michael Jurkutat, Robin Gühne, Jonas Kohlrautz, Andreas Erb, Jürgen Haase
Condens. Matter **3**(3), 23 (2018).

26. **Microscopic origin of Cooper pairing in the iron-based superconductor $Ba_{1-x}K_xFe_2As_2$**
T. Böhm, F. Kretzschmar, A. Baum, M. Rehm, D. Jost, R. Hosseinian Ahangharnejhad, R. Thomale, C. Platt, T. A. Maier, W. Hanke, B. Moritz, T. P. Devereaux, D. J. Scalapino, S. Maiti, P. J. Hirschfeld, P. Adelmann, T. Wolf, Hai-Hu Wen, R. Hackl
NPJ Quantum Materials **3**, 48 (2018).

27. **Magnetic nanoparticle-containing soft-hard diblock copolymer films with high order**
Senlin Xia, Lin Song, Volker Körstgens, Matthias Opel, Matthias Schwartzkopf, Stephan V. Roth, Peter Müller-Buschbaum
Nanoscale **10**, 11930 (2018).

28. **Printed Thin Magnetic Films Based on Diblock Copolymer and Magnetic Nanoparticles**
Senlin Xia, Ezzeldin Metwalli, Matthias Opel, Paul A. Staniec, Eva M. Herzig, Peter Müller-Buschbaum
ACS Appl. Mater. Interfaces 10, 2982-2991 (2018).

29. **Challenges in Open-air Microwave Quantum Communication and Sensing**
Mikel Sanz, Kirill G. Fedorov, Frank Deppe, Enrique Solano
IEEE Conference on Antenna Measurements Applications (CAMA), Västerås, 2018, pp. 1-4.

30. **Non-local magnon transport in the compensated ferrimagnet GdIG**
Kathrin Ganzhorn, Tobias Wimmer, Joseph Barker, Gerrit E. W. Bauer, Zhiyong Qiu, Eiji Saitoh, Nynke Vlietstra, Stephan Geprägs, Rudolf Gross, Hans Huebl, Sebastian T.B. Goennenwein
arXiv:1705.02871, submitted for publication (2017).

31. **Perpendicular magnetic anisotropy in insulating ferrimagnetic gadolinium iron garnet thin films**
H. Maier-Flaig, S. Geprägs, Z. Qiu, E. Saitoh, R. Gross, M. Weiler, H. Huebl, S. T. B. Goennenwein
arXiv:1706.08488, submitted for publication (2017).

32. **Characterizing spin transport: detection of spin accumulation via magnetic stray field**
Matthias Pernpeintner, Akashdeep Kamra, Sebastian T.B. Goennenwein, Hans Huebl
arXiv 1709.01820, submitted for publication (2017).

33. **Frustrated spin order and stripe fluctuations in FeSe**
A. Baum, H. N. Ruiz, N. Lazarevic, Yao Wang, T. Böhm, R. Hosseinian Ahangharnejhad, P. Adelmann, T. Wolf, Z. V. Popovic, B. Moritz, T. P. Devereaux, and R. Hackl
arXiv 1709.08998, submitted for publication (2017).

34. **Magnetically Ordered Insulators for Advanced Spintronics**
Matthias Althammer, Sebastian T.B. Goennenwein, Rudolf Gross
arXiv:1712.08517, submitted for publication (2017).

35. **Echo trains in pulsed electron spin resonance of a strongly coupled spin ensemble**
Stefan Weichselbaumer, Christoph W. Zollitsch, Martin S. Brandt, Rudolf Gross, Hans Huebl
arXiv:1809.10116, submitted for publication (2018).

36. **Limits on Dark Matter Effective Field Theory Parameters with CRESST-II**
G. Angloher, P. Bauer, A. Bento, E. Bertoldo, C. Bucci, L. Canonica, A. D'Addabbo, X. Defay, S. Di Lorenzo, A. Erb, F. v. Feilitzsch, N. Ferreiro Iachellini, P. Gorla, D. Hauff, J. Jochum, M. Kiefer, H. Kluck, H. Kraus, A. Langenkämper, M. Mancuso, V. Mokina, E. Mondragon, V. Morgalyuk, A. Münster, M. Olmi, C. Pagliarone, F. Petricca, W. Potzel, F. Pröbst, F. Reindl, J. Rothe, K. Schäffner,

J. Schieck, V. Schipperges, S. Schönert, M. Stahlberg, L. Stodolsky, C. Strandhagen, R. Strauss, C. Türkoglu, I. Usherov, M. Willers, M. Wüstrich, V. Zema, R. Catena
arXiv:1809.037536, submitted for publication (2018).

37. **Quantitative modeling of superconducting planar resonators with improved field homogeneity for electron spin resonance**
Stefan Weichselbaumer, Petio Natzkin, Christoph W. Zollitsch, Mathias Weiler, Rudolf Gross, Hans Huebl
arXiv:1811.02971, submitted for publication (2018).

38. **Current direction anisotropy of the spin Hall magnetoresistance in nickel ferrite thin films with bulk-like magnetic properties**
Matthias Althammer, Amit Vikam Singh, Tobias Wimmer, Zbigniew Galazka, Hans Huebl, Matthias Opel, Rudolf Gross, Arunava Gupta
arXiv:1811.04696, submitted for publication (2018).

39. **Fermi surface properties of the bifunctional organic metal κ-(BETS)$_2$Mn[N(CN)$_2$]$_3$ near the metal - insulator transition**
V.N. Zverev, W. Biberacher, S. Oberbauer, I. Sheikin, P. Alemany, E. Canadell, and M.V. Kartsovnik
arXiv:1811.10265 (2018).

40. **Spin transport in a charge current induced magnon Bose-Einstein condensate at room temperature**
Tobias Wimmer, Matthias Althammer, Lukas Liensberger, Nynke Vlietstra, Stephan Geprägs, Mathias Weiler, Rudolf Gross, Hans Huebl
arXiv:1812.01334, submitted for publication (2018).

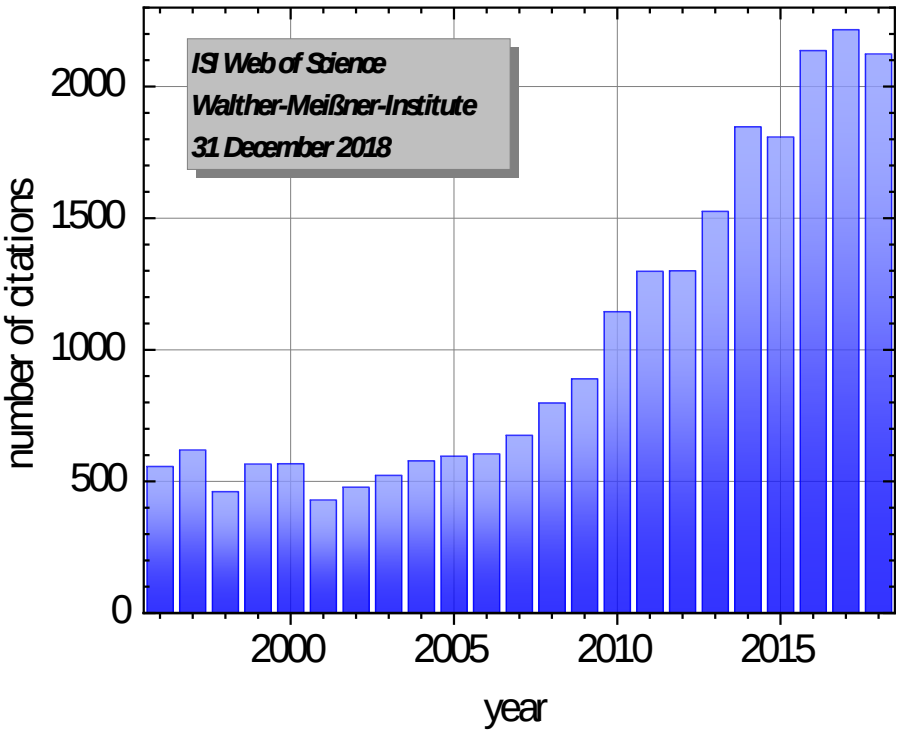

The total number of citations per year of papers published by members of WMI since 1996. This number is continuously increasing and has about quadrupled within the last fifteen years. Presently it is exceeding 2 100.

Books

Festkörperphysik (3. überarbeitete und erweiterte Auflage)

The first and second edition of the solid state physics textbook «***Festkörperphysik***» by Rudolf Gross and Achim Marx appeared in 2012 and 2014. The textbook as well as the related book with exercises and solutions are well received by university teachers and highly esteemed by the students (see e.g. review by Prof. Daniel Hägele in Physik Journal **12** (2013) Nr. 10, p. 60). Since the second edition was going to be out of print in 2017, a third expanded edition has been prepared during 2017 and has become available in January 2018 from De Gruyter Oldenbourg (ISBN 978-3-11-055822-7). It is now also available as an ebook (ISBN 978-3-11-055918-7).

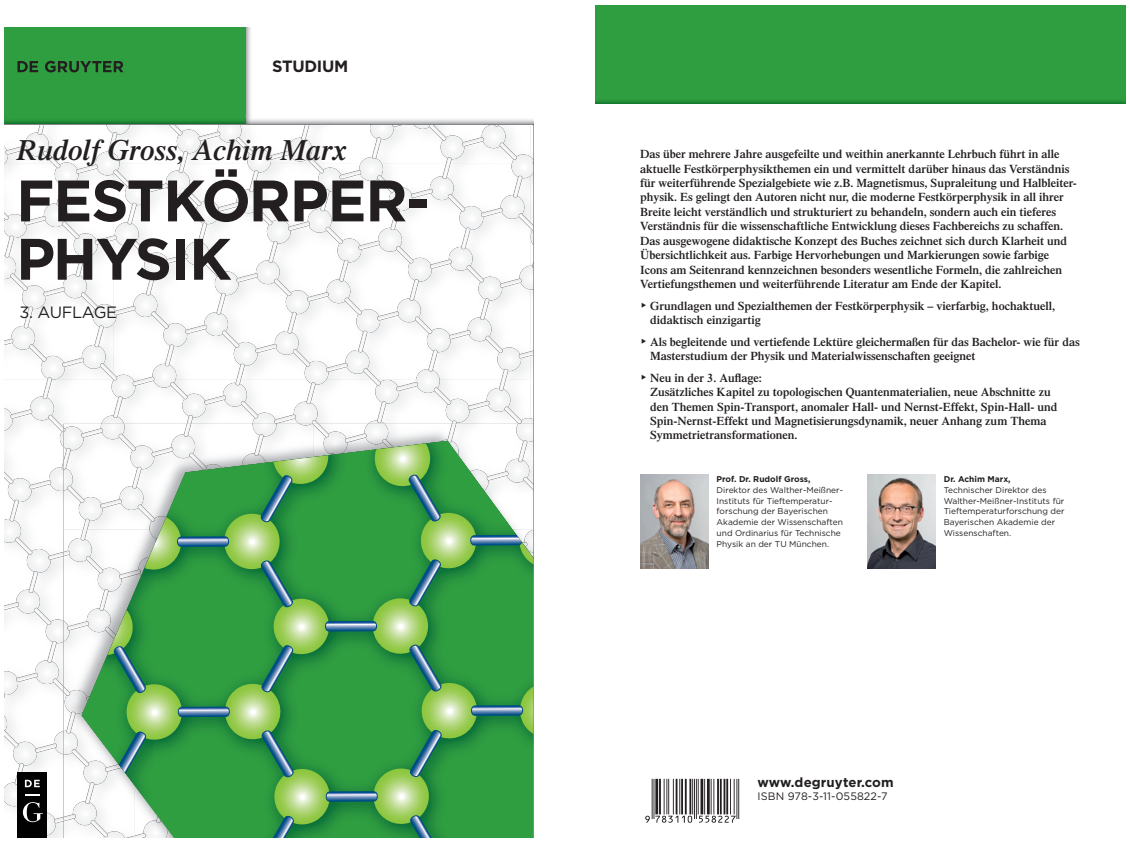

Since quantum matter and the concept of topology became important topics in solid state physics over the past years, the third edition of the textbook has been expanded by a new chapter on topological quantum matter. Furthermore, the chapter on transport phenomena has been revised and now includes the key aspects of the novel transport phenomena resulting from spin-orbit coupling such as the Spin Hall effect, as well as a discussion of the anomalous transport effects (e.g. anomalous Hall and Nernst effect) in materials with finite magnetization. It also gives an introduction to the plethora of the novel spin-thermo-electric transport phenomena such as the spin Hall, spin Seebeck, spin Nernst and spin Ettingshausen effect. These effects naturally arise when one is expanding the well-known thermo-electric coupling by the spin degree of freedom to arrive at the spin-thermo-electric coupling. Since these transport phenomena have been studied intensively over the past years – e.g. within the DFG Priority Program 1538 on Spin Caloritronics – it was now time to provide an introductory overview to students. Very recently, one of the fundamental spin-thermo-electric transport effects – the spin Nernst effect – has been measured for the first time at WMI within the PhD thesis of Sibylle Meyer (see *Observation of the spin Nernst effect*, Sibylle Meyer , *et al.*, Nature

Materials **16**, 977–981 (2017)).

Festkörperphysik. Aufgaben und Lösungen (2. überarbeitete und erweiterte Auflage)

In December 2013, the supplementary book entitled «***Festkörperphysik. Aufgaben und Lösungen***» by Rudolf Gross, Achim Marx and Dietrich Einzel has been published by the Oldenbourg Wissenschaftsverlag München. The book contains more than 100 problems listed at the end of the chapters of the related solid state physics textbook «***Festköperphysik***» together with detailed model solutions. The exercises & solutions book is ideal for preparing for examinations and for learning on one's own. It is used and recommended by many colleagues teaching solid state physics.

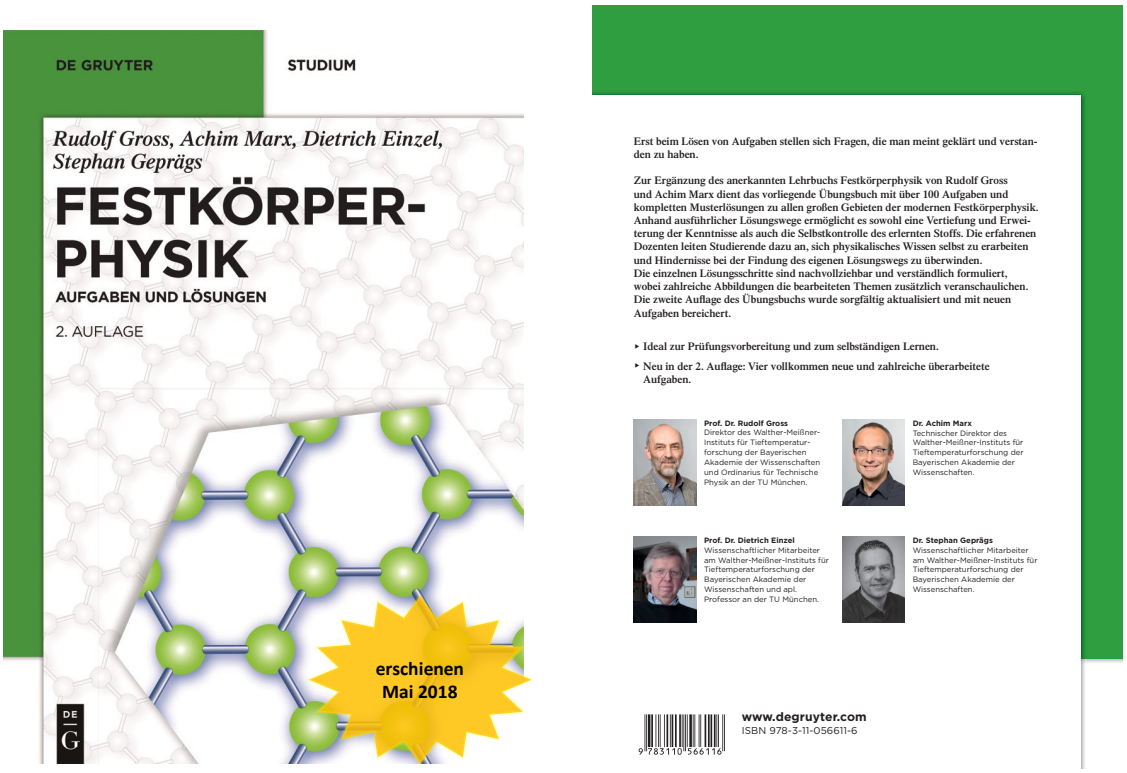

Since also this book was going to be out of print, a second revised edition has been prepared recently by Rudolf Gross, Achim Marx, Dietrich Einzel and Stephan Geprägs with several new exercises and solutions. This book has become available in May 2018 from De Gruyter Oldenbourg (ISBN 978-3-11-056613-0). It is also available as an ebook (ISBN 978-3-11-056613-0).

Bachelor, Master, Doctoral, and Habilitation Theses

A. Completed and Ongoing Habilitation Theses

The promotion of highly qualified young scholars is a key concern of WMI. The fostering of young scholars goes hand in hand with equipping them to stand on their own in fields that are very competitive on both the national and international scales. At present, three postdoctoral researcher – Mathias Weiler, Matthias Althammer and Kirill Fedorov – are passing through the habilitation procedure of the Technical University of Munich. The habilitation serves as the formal assessment tool ascertaining whether or not a candidate is suitable, from an academic and a pedagogical point of view, to be a professor in a particular field at the university level.

1. Dr. Mathias Weiler

Mathias Weiler started the habilitation process at TUM in June 2015. The research topic of his habilitation project is *Spin-Orbit Interactions in Magnetic Thin Film Systems*. On 2nd November 2017 he successfully passed the intermediate evaluation of his habilitation process. He was presenting a talk entitled *"Spin-Orbit Dynamics"* within the Solid State Physics Colloquium of TUM, summarizing his recent scientific achievements. The *Fachmentorat* consisting of Rudolf Gross (TU Munich), Christian Pfleiderer (TU Munich) and Christian Back (University of Regensburg) was pleased to see that many of the goals fixed in the target agreement of 2015 were overfulfilled. Therefore, the *Fachmentorat* recommended to finish the habilitation process within the coming two years. Meanwhile, Mathias Weiler has completed the first draft of his habilitation thesis which he is going to submit early in 2019.

Mathias Weiler joined WMI in December 2014 after a two-year postdoctoral stay at the National Institute of Standards and Technology, Boulder, Colorado, USA, where he worked on spin current transport. His stay abroad was supported by a DAAD fellowship. Besides his successful research work, he took over the lectures on *Magnetism* (winter semester 2015/2016 and 2017/2018) and *Spin Electronics* (summer semester 2016), and contributed to several WMI seminars. His lectures attracted a large number of students and received very good marks from the students.

2. Dr. Matthias Althammer

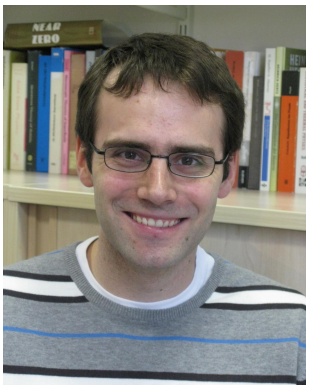

Matthias Althammer joined WMI in December 2013 after a postdoctoral stay (10/2012 – 11/2013) at the Center for Materials for Information Technology, University of Alabama, Tuscaloosa, USA, where he worked on oxide based spintronics. From 05/2014 to 02/2015 he was on leave from WMI to acquire experience in industry as an Engineering Consultant at Esprit Engineering GmbH, Munich.

Matthias Althammer was accepted as a *"Habilitand"* by the Faculty of Physics of TU Munich in January 2016. In his case, Rudolf Gross (TU Munich), Martin Brandt (TU Munich) and Arunava Gupta (MINT Center, University of Alabama) form the *Fachmentorat*. The research topic of his habilitation project is the *"Experimental Study of Spin-dependent Transport Phenomena"*. As part of the midterm evaluation, Matthias Althammer gave a talk entitled *"Pure spin currents in magnetically ordered insulators"* within the Colloquium on Solid-State Physics on

14th June 2018. The talk has been evaluated very positively by the present faculty members. The *Fachmentorat* appreciated that most of goals fixed in 2016 have been perfectly achieved. The target agreement has been extended for the second two-year phase of the habilitation procedure.

3. Dr. Kirill Fedorov

Kirill Fedorov studied physics in Russia (Institute for Physics of Microstructures, Russian Academy of Sciences, Nizhny Novgorod), where he received his master degree in 2008. He then joined the group of Prof. Alexey Ustinov at the Karlsruhe Institute of Technology as a PhD student. He finished his PhD thesis entitled *Fluxon readout for superconducting flux qubits* in 2013 and then joined Walther-Meißner-Institute as a postdoctoral researcher in December 2013. His key research topic is the realization of seminal quantum experiments based on propagating quantum microwaves.

Kirill Fedorov was accepted as a *"Habilitand"* by the Faculty of Physics of TU Munich in September 2016. In his case, Rudolf Gross (TU Munich), Jonathan Finley (TU Munich/Walther Schottky Institute) and Enrique Solano (Universidad del País Vasco and Ikerbasque Foundation, Bilbao, Spain) form the *Fachmentorat*. The official midterm evaluation of his habilitation process will take place on 18th January 2019, when Kirill Fedorov will give a talk within the Colloquium on Solid-State Physics of the Faculty of Physics.

B. Completed and Ongoing Ph.D. Theses

Completed Ph.D. Theses:

1. **Crystal Growth and Characterization of the Magnetic Properties of the Electron Underdoped Superconductor $Nd_{2-x}Ce_xCuO_4$**
   Alma G. Dorantes Palacios, Technical University of Munich, June 2018.
2. **Scanning Microscopy and Momentum-Resolved Raman Scattering in Semiconductors and Oxides**
   Nitin Chelwani, Technical University of Munich, August 2018.
3. **Spin Transport in Insulating Ferrimagnets**
   Kathrin Marlène Ganzhorn, Technical University of Munich, Oktober 2018.
4. **Interrelation of Lattice, Charge, and Spin Degrees of Freedom in Iron Based Systems**
   Andreas Christoph Baum, Technical University of Munich, November 2018.
5. **Magnetic Resonance of Ferrimagnetic Insulators**
   Hannes Benjamin Maier-Flaig, Technical University of Munich, Dezember 2018.

Four of the Ph.D. students of the Walther-Meißner-Institute finishing their Ph.D. theses in 2018.

Ongoing Ph.D. Theses:

6. **Quantum Information Processing with Propagating Quantum Microwaves**
   Peter Eder, Technical University of Munich, since November 2012.
7. **Circuit Quantum Electrodynamics with Three-dimensional Cavities**

Edwar Xie, Technical University of Munich, since December 2013.

8. **Chains of Nonlinear and Tunable Superconducting Resonators**
   Michael Fischer, Technical University of Munich, since January 2015.
9. **Magnetization Dynamics in Coupled Photon/Phonon-Magnon Systems**
   Stefan Klingler, Technical University of Munich, since February 2015.
10. **Nanomechanical Quantum Systems**
    Philip Schmidt, Technical University of Munich, since October 2015.
11. **Magnetic Resonance at Millikelvin Temperatures**
    Stefan Weichselbaumer, Technical University of Munich, since December 2015.
12. **Untersuchung des Wärmetransports in porösen Pulvermedien zur Entwicklung einer ökonomischen Hochtemperatur-Vakuumsuperisolation auf Perlitbasis für Anwendungen in Wärmespeichern bis zu 700°C**
    Matthias Johannes Demharter, Technical University of Munich, since February 2016.
13. **Quantum Gates with Continuous Variable Microwaves**
    Stefan Pogorzalek, Technical University of Munich, since March 2016.
14. **ReBCO-Schichten auf ISD biaxial texturierten Substraten für supraleitende Bandleiterder 2. Generation**
    Oleksiy Troshyn, Technical University of Munich, since August 2016.
15. **Momentum and Spatially Resolved Raman Experiments in Correlated Systems**
    Daniel Jost, Technical University of Munich, since October 2016.
16. **Spin Currents in Magnetic Heterostructures**
    Tobias Wimmer, Technical University of Munich, since January 2017.
17. **Direct and Inverse Spin-Orbit Torques**
    Lukas Liensberger, Technical University of Munich, since January 2018.
18. **Spatially and Momentum Resolved Raman Studies of Unconventional Superconductors**
    Gabriele Rager, Technical University of Munich, since March 2018.
19. **Evaluierung und Neuentwicklung durch Nutzung von Supraleitern in einer zirkularen Anordnung zur quasi verlustfreien kontaktlosen Energieübertragung für sehr hohe Leistungen**
    Christoph Utschick, Technical University of Munich, since June 2018.
20. **Spin Dynamics of Hybrid Skyrmion-Magnon Solitons**
    Luis Flacke, Technical University of Munich, since September 2018.
21. **Quantum Simulation with Superconducting Quantum Circuits**
    Qi-ming Chen, Technical University of Munich, since October 2018.
22. **Quantum Microwave Communication**
    Michael Renger, Technical University of Munich, since November 2018.

C. Completed and Ongoing Bachelor and Master Theses

Completed Master Theses:

1. **Prediction of a Potential Power Duration for High Voltage Batteries in Electromobility**
   Markus Full, Master Thesis, Technical University of Munich, January 2018.
2. **Anisotropie- und Resonanzverhalten des Ag-Phonons in $BaFe_2As_2$**
   Florian Löffler, Master Thesis, Technical University of Munich, April 2018.
3. **Remote State Preparation of Propagating Quantum Microwaves**
   Seyed Behdad Ghaffari, Master Thesis, Technical University of Munich, March 2018.
4. **Electronic and magnetic excitations in underdoped $YBa_2Cu_3O_{6+x}$**
   Ulricke Zweck, Master Thesis, Technical University of Munich, April 2018.
5. **Inductively Coupled Nano-Electromechanics in Flux Tunable Superconducting Resonators**
   Christoph Utschick, Master Thesis, Technical University of Munich, April 2018.
6. **Spin Pumping and Spin Wave Damping in Co25Fe75 Thin Film Heterostructures**
   Luis Flacke, Master Thesis, Technical University of Munich, May 2018.
7. **Laser Ablation Loading and Single-Ion Addressing of Strontium in a Linear Paul Trap**
   Andreas Pöschl, Master Thesis, Technical University of Munich, June 2018.
8. **Untersuchung des magnetoelastischen Verhaltens von strukturierten xMR-Winkelsensoren auf Waferebene**
   Moritz Keller, Master Thesis, Technical University of Munich, June 2018.
9. **Multi-SQUID Josephson Parametric Amplifiers**
   Daniel Arweiler, Master Thesis, Technical University of Munich, June 2018.
10. **Analysis of Pure Spin Current Transport in Yttrium Iron Garnet | Normal Metal Heterostructures**
    Birte Cöster, Master Thesis, Technical University of Munich, July 2018.
11. **2-Input-2-Output Quantum Feedback Amplification and Coherent PID Feedback Control**
    Yuki Nojiri, Master Thesis, Technical University of Munich, July 2018.
12. **Validierung der Normalkraftmessung für elektrische Kontakte für Prüfungen in Labor und Fertigung**
    Stefanie Blob, Master Thesis, Technical University of Munich, July 2018.
13. **Design and Realisation of Superconducting Quantum Circuits for Nano-Electromechanical Experiments**
    Lisa Rosenzweig, Master Thesis, Technical University of Munich, August 2018.
14. **A Transport Laser with Shape and Amplitude Control for Ultracold Strontium Atoms**
    Fabian Finger, Master Thesis, Technical University of Munich, October 2018.
15. **Quantum Process Tomography of a 3D Quantum Memory**
    Michael Uwe Renger, Master Thesis, Technical University of Munich, October 2018.
16. **Design and Characterization of an UV Laser-System for Rydberg Experiments with Potassium**
    Anne-Sophie Walter, Master Thesis, Technical University of Munich, November 2018.
17. **Quantum Correlations in Remote State Preparation**
    Minxing Xu, Master Thesis, Technical University of Munich, November 2018.
18. **Coupling Strings, String Networks and Magnon-Phonon Interaction**
    Thomas Luschmann, Master Thesis, Technical University of Munich, November 2018.

Completed Bachelor Theses:

19. **Spinwellenpropagation in Kobalt-Eisen-Dünnschichtfilmen**
David Rogerson, Technical University of Munich (2018).
20. **Maskenlose optische Lithographie supraleitender Niobfilme**
Christoph Scheuer, Technical University of Munich (2018).
21. **Quantifizierung von Vibrationen in Laborumgebungen**
Korbinian Rubenbauer, Technical University of Munich (2018).
22. **Hochwertige supraleitende Dünnfilme für fortgeschrittene Spinelektronik**
Michael Reichert, Technical University of Munich (2018).
23. **Investigation and Analysis of Anomalies in the Build-up of Roll Rates of Sounding Rockets**
Clara Schäfer, Technical University of Munich (2018)

Ongoing Master Theses:

24. **An Exploration of Quantum Magnetic Materials**
Ludwig Holleis, Master Thesis, Technical University of Munich, since April 2018.
25. **Coherent coupling between superconducting quantum circuits and ferrimagnetic magnons**
Mohammad T. Amawi, Master Thesis, Technical University of Munich, since April 2018.
26. **Superconductor/Ferromagnet Heterostructures for Superconducting Spintronics**
Manuel Müller, Master Thesis, Technical University of Munich, since October 2018.
27. **Development of fast feedback for quantum information processing protocols**
Robert Neagu, Master Thesis, Technical University of Munich, since October 2018.
28. **Magnetic Fast Wafer Level Reliability (fWLR)**
Thai Phi Long Pham, Master Thesis, Technical University of Munich, since October 2018.
29. **Untersuchung von Fluktuationen und Spin Anregungen in magnetisch entzwillingtem Eu122**
Leander Peis, Master Thesis, Technical University of Munich, since November 2018.
30. **Magneto-Acoustic Torques**
Adrian Gomez, Master Thesis, Technical University of Munich, since November 2018.
31. **Fabrication and Characterization of Broadband Josephson Parametric Amplifiers**
Daniel Singh, Master Thesis, Technical University of Munich, since December 2018.
32. **Spin Seebeck Effect as a Probe of Magnon Properties**
Maxim Dietlein, Master Thesis, Technical University of Munich, since December 2018.
33. **Optimal control of a 3D quantum memory**
Stephan Trattnig, Master Thesis, Technical University of Munich, from February 2019.

Ongoing Bachelor Theses:

34. **Implementierung adiabatischer Pulse in supraleitenden Resonatoren für Elektronenspinresonanz**
Daniela Lutz, Technical University of Munich (2018)
35. **Quantensimulation mit supraleitenden Schaltkreisen**
Stefanie Grotowski, Technical University of Munich (2018)

Research Projects

A large number of our research projects are benefiting from the collaboration with external groups in coordinated research projects, as well as from individual collaborations, exchange programs and visitors. Most collaborations are based on joint projects, which are funded by different research organizations (see list below). A considerable number of collaborations also exists with universities, other research institutions and industry without direct financial support.

A. German Research Foundation: Excellence Strategy

Cluster of Excellence «*Munich Center for Quantum Science and Technology*» *(MCQST)*

The new Cluster of Excellence has been granted in September 2018 and will start in January 2019. Together with Immanuel Bloch of LMU Munich and Ignacio Cirac of Max Planck Institute of Quantum Optics, Rudolf Gross of Walther-Meißner-Institute is one of the three spokespersons of MCQST.

Cluster of Excellence «*Nanosystems Initiative Munich*» *(NIM)*

1. Research Area I: *Quantum Nanophysics*
   F. Deppe, R. Gross, H. Huebl, A. Marx
2. Research Area II: *Hybrid Nanosystems*
   R. Gross, H. Huebl

B. German Research Foundation: Collaborative Research Centers

Transregional Collaborative Research Center TRR 80: ***«From Electronic Correlations to Functionality»***

1. Project A2: *Spatially and Momentum Resolved Raman Studies of Correlated Systems*
   R. Hackl

C. German Research Foundation: Priority Programs

1. Spin Dynamics of Hybrid Skyrmion-Magnon Solitons
   within the DFG Priority Program 2137 *Skyrmionics: Topological Spin Phenomena in Real-Space for Applications*
   M. Weiler, R. Gross (Az. WE 5386/5-1)
2. Pulsed Electron Paramagnetic Resonance at Millikelvin Temperatures
   within the DFG Priority Program 1601 *New frontiers in sensitivity for EPR spectroscopy: from biological cells to nano materials*
   H. Huebl (Az. HU 1896/2-1)

D. German Research Foundation: Research Projects

1. Project: *Fluctuations and Novel Phases in Systems with Spin, Charge and Orbital Correlations*
   R. Hackl (Az. HA 2071/12-1)
2. Project: *Pure Spin Currents in Oxide-Based Epitaxial Heterostructures*
   M. Althammer, R. Gross (Az. AL 211012-1)

3. Project: *Direct and Inverse Spin-Orbit Torques*
   M. Weiler (Az. WE 5386/14-1)
4. Project: *Correlated Quantum Microwaves: Continuous-Variables for Remote State Preparation and Quantum Illumination*
   K.G. Fedorov (Az. FE 1564/1-1)

E. European Union

1. EU Collaborative Project (call identifier H2020-FETFLAG-2018-2020), project title *Quantum Microwave Communcation and Sensing – QMiCS*
   F. Deppe, K. Fedorov, A. Marx, R. Gross, Grant Agreement No. 820505
   project coordination: Walther-Meißner-Institute, partners: several European Universities, research facilities and companies.
2. EU Collaborative Project (call identifier H2020-FETOPEN-1-2016-2017), project title *Magnetomechanical Platforms for Quantum Experiments and Quantum Enabled Sensing Technologies – MaQSens*
   H. Huebl, R. Gross, Grant Agreement No. 736943
   partners: several European Universities and research facilities.

F. Free State of Bavaria

1. International PhD Programme of Excellence *Exploring Quantum Matter (ExQM)* within the Elite Network of Bavaria, Project No. K-NW-2013-231
   R. Gross, A. Marx, F. Deppe, K. Fedorov
   Partners: jointly with 12 quantum physics research groups at the TU Munich, the LMU Munich, and the Max Planck Institute of Quantum Optics.

G. Max Planck Society

1. International Max Plank Research School for *Quantum Science and Technology (IMPRS-QST)*, Spokesperson: Prof. Dr. J. Ignacio Cirac
   R. Gross, A. Marx, F. Deppe, K. Fedorov
   with several partners from the Max Planck Institute of Quantum Optics, the Ludwig-Maximilians-Universität Munich and the Technical University of Munich.

H. Bavaria California Technology Center (BaCaTeC)

1. Project: *Bypassing thew Analytic Continuation: A New Approach to the Analysis of Spectroscopic Data* (No. 21 [2016-2])
   R. Hackl,
   partners: Profs. Thomas Devereaux, Steve Kivelson, and Sri Raghu (Stanford University)

I. German Academic Exchange Service

1. Project-based Personnel Exchange Programme (PPP) with Serbia, project 57449106: *Fluctuations, Magnetic Frustration, and Sub-Dominant Pairing in Fe-Based Compounds*, collaboration with the Institute of Physics, University of Belgrade (Dr. Z. V. Popovic)
   R. Hackl

2. Project-based Personnel Exchange Programme (PPP) with Serbia, project 57335339: *Spin and Charge Instabilities in Sulfur-substituted FeSe*, collaboration with the Institute of Physics, University of Belgrade (Dr. Z.V. Popovic).
   R. Hackl
3. Project-based Personnel Exchange Programme (PPP) with India, project 57085749: *Spin Current Generation and Detection Using FMI/NM Hybrids*, collaboration with the IIT Madras, Chennai (Prof. Dr. M. S. Ramachandra Rao).
   R. Gross

J. Scientific Instrumentation

1. Maskless lithography UV Direct Laser Writer, SPS PicoMaster 200 UV
   BMBF project Q.com, FKZ: 16KIS0110 4515.1545.4556
2. UHV Sputtering System for Superconducting Materials
   BMBF project Q.com, FKZ: 16KIS0110 4515.1545.4556

Conferences, Workshops, Public Engagement

The Walther-Meißner-Institute has organized/co-organized several conferences, workshops and symposia in 2018. It also was participating in several public outreach events aiming at making science accessible to the public.

A. NIM Conference «The Future of Nanoscience» (04 – 06 September 2018, Evangelische Akademie Tutzing, Germany)

The NIM conference *«The Future of Nanoscience»* was co-organized by Rudolf Gross. It was intended to review the scientific progress achieved within the twelve-year funding period of the Cluster of Excellence NIM and, most importantly, to look into the future of nanosciences and to define important future research topics. To this end, internationally leading scientists of all research areas of NIM have been invited as speakers.

In a technology transfer session, the conference provided a forum for spin-off companies emerging out of NIM. The session included presentations of Federico Bürsgens (GNA Biosolutions GmbH), Stefan Duhr (NanoTemper Technologies GmbH), Niels Fertig (Nanion Technologies GmbH), Dirk Haft (attocube systems AG), and Roman Zantl (ibidi GmbH).

In an evening panel discussion entitled "Quo Vadis Nanoscience" we invited the well-known opinion leaders Christian Kehrt (TU Braunschweig), Harald Lesch (LMU Munich), Robert Schlögl (MPI CEC Mühlheim), and Petra Schwille (MPI Biochemistry Munich) to provide their view of quantum science and technology to the public. The discussion was presented by Jörg P. Kotthaus (LMU Munich) and Gerhard Abstreiter (TUM).

B. Annual Workshop of the Section «Intermetallic and Oxide Systems with Spin and Charge Degrees of Freedom» of the DGKK (11 – 12 October 2018, Research Campus Garching, Germany)

The Annual Workshop of the *Deutsche Gesellschaft für Kristallzüchtung und Kristallwachstum (DGKK)* was organized by Andreas Erb, who presently is spokesperson of its section «Intermetallic and Oxide Systems with Spin and Charge Degrees of Freedom». Due to the ongoing building activities at WMI and the large number of participants, the workshop has to be shifted from the WMI building to the IGSSE building (the so-called Villa

Kunterbunt) close to the Faculty of Mechanical Engineering on the Research Campus Garching.

C. Course 3 of the Ferienakademie: «Physics and Electronics in Everyday Life» (23 September – 05 October 2018, Sarntal, Italy)

As in the previous years, WMI co-organized the course on *«Physics and Electronics in Everyday Life»* of the ***Ferienakademie***. The Ferienakademie is jointly organized by the Technical University of Munich, the University of Erlangen-Nuremberg, and the University of Stuttgart to motivate and foster highly talented students. It takes place annually at Sarntal in the Italian Alps. The course was hold by Rudolf Gross (WMI) together with Gert Denninger (University of Stuttgart), and Vojislav Krstic (University of Erlangen-Nuremberg) as visiting lecturer.

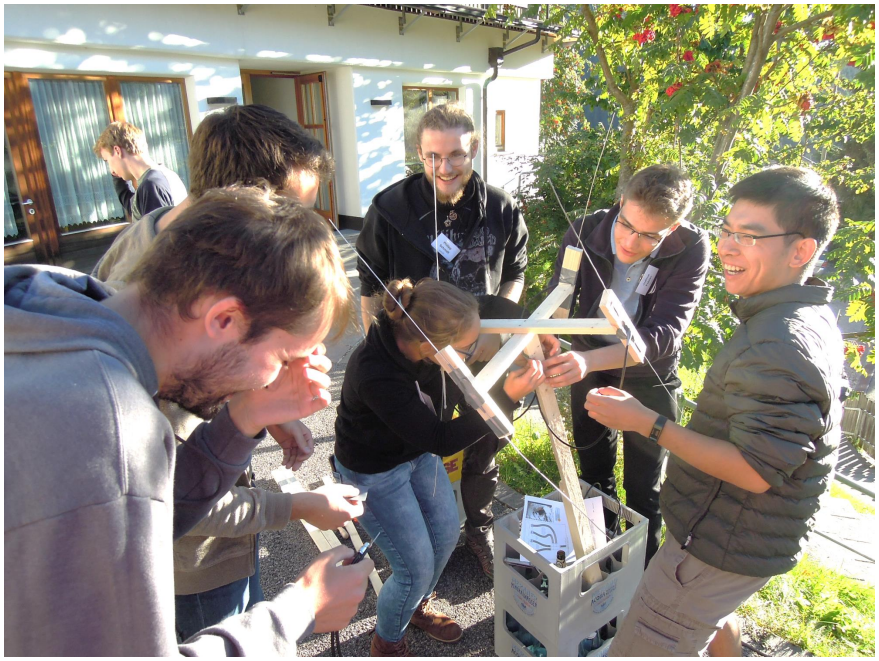

Some of the students of course 3 working hard on the construction of the antenna used for receiving data from a weather satellite.

Within the course 3 on *«Physics and Electronics in Everyday Life»* of the Ferienakademie the students prepare presentations on physical phenomena and problems which play an important role in our everyday-life, but usually are poorly understood. Besides the seminar talks there are intensive discussions with the professors and members of other courses. A particular emphasis of course 3 of Ferienakademie is put on hands-on experiments. They aim at providing students an in-depth insight into physical phenomena by performing experiments by themselves. WMI contributes with a variety of experiments on superconductivity,

magnetism and low temperature properties of solids. In 2018, the students were building an antenna for receiving the data of a weather satellite. After tedious construction work, they were proud of generating a weather chart with the data received by the homemade antenna.

A relaxing and inspiring atmosphere is provided by a varied supporting program (mountain hiking, excursions to Bozen, table tennis and chess tournament, Törgelen, etc.). Moreover, within the Ferienakademie the students have the opportunity to meet leaders from industry, politics and science. In 2018, an evening talk was presented by the president of the University of Erlangen-Nuremberg, Prof. Dr. Joachim Hornegger, who gave interesting insights into the development strategy of his university.

D. Kickoff Meeting of the EU Quantum Flagship Project «QuMiCS» (22 – 23 November 2018, WMI, Garching, Germany)

The WMI (Frank Deppe, Kirill Fedorov, Rudolf Gross, Achim Marx) organized the kickoff meeting of the EU Quantum Flagship project ***«Quantum Microwave Communication and Sensing» (QMiCS)***, which started in October 2018 (see report on page 31 – 32). Scientists from the partner institutions Aalto University (Finland), École Normale Supérieure de Lyon (France), Instituto de Telecomunicações (Portugal), Universidad del País Vasco/Euskal Herriko Unibertsitatea Bilbao (Spain), and the VTT Technical Research Centre of Finland Ltd. (Finland) as well as team leaders of the industry partners Oxford Instruments Nanotechnology Ltd. (United Kingdom) and TTI Norte S.L. (Spain) were attending the meeting and enjoying the hospitality of WMI.

E. Day of Open House 2018 (13 October 2018, Research Campus Garching, Germany)

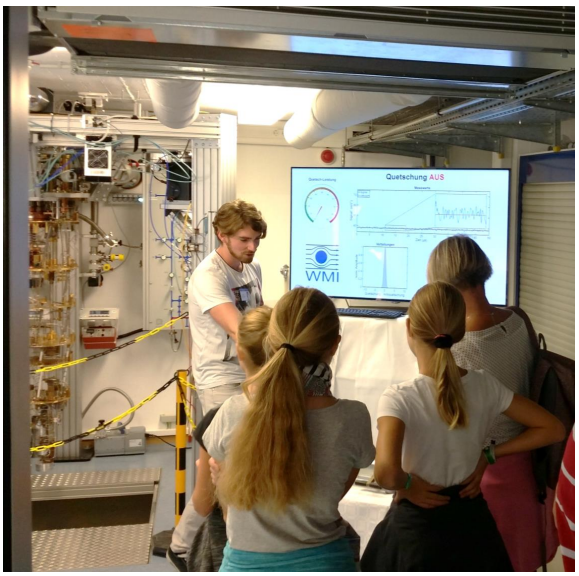

The Walther-Meißner-Institute contributed to the ***Open House Event 2018*** (Tag der offenen Tür) on the Research Campus Garching by an attractive program for everybody interested in science. In talks and demonstration experiments, an insight into current research projects in the fields of superconductivity, low temperature research, as well as quantum and nanotechnology was given. In addition, the WMI facilities for thin film technology could be visited to get an

impression of state-of-the-art materials technology. In one of the low temperature laboratories the visitors could get insight into the experimental study of superconducting qubits and quantum circuits. WMI also offered hourly talks in the WMI seminar room on the topics *«On the Way to Quantum Computers»* (Rudolf Gross) and *«Superconductivity and Superfluidity»* (Dietrich Einzel) which were completely overcrowded. In addition, Rudolf Gross gave a presentation on *«Quantum Science, Technology and Engineering at the Technical University of Munich»* within a series of talks at the Institute of Advanced Study of TUM presenting the new Clusters of Excellence.

Particularly fascinating for visitors are demonstration experiments on low temperature phenomena. Therefore, WMI has made a considerable effort to set up high quality demonstration experiments on the Meißner effect in superconductors (superconducting levitation) and the fountain effect in superfluid ^{4}He. For kids and pupils the superconducting racetrack of WMI and the large number of fascinating hands-on experiments with liquid nitrogen are always highly attractive. They can experience that low temperature physics is a lot of fun.

Cooperations

Other collaborations without direct project funding involve:

- Stanford University, Stanford, USA (T.P. Devereaux, I. Fisher, B. Moritz, H.N. Ruiz, S.A. Kivelson)
- Universidad del País Vasco and Ikerbasque Foundation, Bilbao, Spain (E. Solano, M. Sanz, L. Lamata)
- Instituto de Física Fundamental, CSIC, Madrid, Spain (J.J. Garcia-Ripoll)
- Instituto de Ciencia de Materials de Barcelona, CSIC, Spain (E. Canadell)
- Osaka Prefecture University, Osaka, Japan (H. Fujiwara)
- Central Research Institute of the Electric Power Industry, Tokyo, Japan (Dr. S. Ono, Dr. Y. Ando)
- Green Innovation Research Laboratories, NEC Corporation, Japan (Y. Nakamura, J.S. Tsai, K. Inomata, T. Yamamoto)
- University of Tohoku, Sendai, Japan (G.E.W. Bauer, E. Saitoh, J. Barker)
- Japan Science and Technology Agency, Sendai, Japan (H. Adachi, S. Maekawa)
- University of Tokyo, Tokyo, Japan (Y. Nakamura)
- European Synchrotron Radiation Facility (ESRF), Grenoble (H. Müller, F. Wilhelm, K. Ollefs, A. Rogalev)
- Lund University, Lund, Sweden (D. Mannix)
- Materials Science Research Centre, IIT Madras, India (M.S. Ramachandra Rao, J. Mukherjee)
- ETH-Zurich, Switzerland (A. Wallraff, L. Degiorgi, R. Monnier, Dr. M. Lavagnini)
- University of Geneva, Geneva, Switzerland (I. Maggio-Aprile)
- Chalmers University of Technology Gothenburg, Sweden (P. Delsing, G. Wendin)
- University of Alabama, MINT Center, Tuscaloosa, USA (A. Gupta)
- Helsinki University of Technology, Materials Physics Laboratory, Finland (T. Heikkilä)
- Delft University of Technology, Kavli Institute of NanoScience, Delft, The Netherlands (T.M. Klapwijk, G.E.W. Bauer)
- B. Verkin Institute for Low Temperature Research and Engineering, Kharkov, Ukraine (V.G. Peschansky)
- Landau Institute for Theoretical Physics, Chernogolovka, Russia (P. Grigoriev)
- University of Oxford, Clarendon Laboratory, England (A. Karenowska)
- Institute of Solid State Physics, Chernogolovka, Russia (V. Zverev)
- Russian Academy of Sciences, Chernogolovka, Russia (N. Kushch, E. Yagubskii)
- High Magnetic Field Laboratory, Dresden (E. Kampert, J. Wosnitza, T. Helm)
- High-Magnetic-Field Laboratory, Grenoble, France (I. Sheikin, D. LeBoeuf)
- High Magnetic Field Laboratory, Toulouse, France (C. Proust, D. Vignolles)
- National High Magnetic Field Laboratory, Tallahassee, USA (J. Brooks)
- University of British Columbia, Vancouver, Canada (D. Bonn, A. Damascelli)
- Université de Toulouse, Laboratoire de Physique Théorique, Toulouse, France (R. Ramazashvili)
- Lawrence Berkeley National Laboratory, Berkeley, USA (A. F. Kemper)
- University of Belgrade, Belgrade, Serbia (Z. Popovic, N. Lazarevic, D. U. Ralevic, R.

Gajic)

- University of Aveiro, Portugal (N. A. Sobolev)
- Macquarie University, MQ Research Centre for Quantum Science and Technology, Australia (J. Twamley)
- Hungarian Academy of Sciences, Research Institute for Solid State Physics and Optics, Budapest, Hungary (K. Kamaras, I. Tüttö)
- University of Rome "La Sapienza", Rome, Italy (S. Caprara, C. Di Castro, M. Grilli)
- Budapest University of Technology and Economics, Budapest, Hungary (A. Virosztek, G. Mihály)
- Universidad de Zaragoza, Departamento de Fisica de la Materia Condensada, Spain (L. Morellon, J.M. de Teresa, D. Zueco)
- EPFL Lausanne, Switzerland (T. Kippenberg, H. Ronnov)
- University of New South Wales, Sydney, Australia (M. Simmons, A. Morello, J. Pla)
- McMaster University, Hamilton, Canada (J.P. Carbotte)
- Technical University of Graz, Austria (E. Schachinger)
- University of Vienna, Austria (M. Aspelmeyer)
- Johannes-Kepler University of Linz, Institute for Semiconductor and Solid State Physics, Austria (A. Ney)
- National Institute of Standards and Technology, Boulder, USA (H. Nembach, J. Shaw, T.J. Silva, E. Edwards)
- University of Florida, Gainesville, Florida, USA (P.J. Hirschfeld, S. Maiti)
- University of California, Santa Barbara, USA (D.J. Scalapino)
- University of Manitoba, Winnipeg, Canada (C.-M. Hu)
- Kyoto University, Japan (M. Shiraishi)
- Heriot Watt University, Edinburgh, Scotland (M. Hartmann)
- Universidad Nacional de Colombia, Colombia (O. Moran)
- University of Birmingham, UK (E.M. Forgan)
- University of Groningen, The Netherlands (T. Palstra, M. Mostovoy, A. Aqeel)
- IFW Dresden, Germany (B. Büchner, J. Fink, S.V. Borisenko, M. Knupfer, A. Thomas)
- Max-Planck-Institut für Festkörperforschung, Stuttgart (B. Keimer, L. Boeri)
- University of Tübingen, Germany (R. Kleiner, D. Kölle)
- University of Würzburg, Germany (W. Hanke, F. Assaad, C. Honerkamp, M. Potthoff)
- University of Augsburg, Germany (P. Hänggi, A. Wixforth, A. Kampf, A. Loidl, J. Deisenhofer, V. Tsurkan)
- University of Hamburg, Germany (G. Meier, W. Wurth)
- University of Leipzig, Germany (J. Haase)
- University of Ulm, Abt. Halbleiterphysik, Germany (W. Limmer, M. Abdi)
- RWTH Aachen, Germany (G. Güntherodt, B. Beschoten)
- Ernst-Moritz-Arndt Universität Greifswald, Germany (M. Münzenberg)
- Martin-Luther-Universität Halle, Germany (G. Woltersdorf)
- Universität Bielefeld, Germany (G. Reiss, T. Kuschel M. Meinert)
- Free University of Berlin, Berlin, Germany (R. Di Candia)
- Technical University of Munich, Physics Department, Germany (Ch. Back, P. Böni, Ch. Pfleiderer, M. Poot, F.C. Simmel, P. Müller-Buschbaum)

- Technical University of Munich, Walter Schottky Institute, Germany (M. Stutzmann, J. Finley, M. Brandt, A. Holleitner, U. Wurstbauer)
- Technical University of Munich, Electrical Engineering (M. Becherer)
- LMU Munich, Physics Department, Germany (J. von Delft, E. Frey, J. Rädler, S. Ludwig)
- LMU Munich, Chemistry Department, Germany (H. Ebert, D. Ködderitzsch)
- University of Konstanz (A. Leitenstorfer, E. Weig, J. Demsar, A. Pashkin)
- Jülich Centre for Neutron Science JCNS, Garching, Germany (S. Pütter)
- Goethe University, Frankfurt, Germany (S. Winter, M. Lang)
- Technical University of Braunschweig, Germany (D. Menzel, S. Süllow)
- Technical University of Dresden, Germany (S.T.B. Gönnenwein)
- Fritz Haber Institut Berlin, Germany (T. Seifert, T. Kampfrath)
- Technical University of Dortmund, Germany (M. Müller)
- Johannes-Gutenberg University, Mainz, Germany (C. Cramer, M. Kläui, O. Gomomay)
- Universität Potsdam, Potsdam, Germany (A.v. Reppert, M. Bargheer)
- Saarland University, Saarbrücken (F.K. Wilhelm-Mauch)
- Innovent Technologieentwicklung Jena, Germany (C. Dubs, O. Surzhenko)
- BMW Group, Munich, Germany (J. Schnagl, W. Stadlbauer, G. Steinhoff)
- Attocube, Munich, Germany (K. Karrai, D. Andres, E. Hoffmann)
- THEVA Dünnschichttechnik, Ismaning, Germany (W. Prusseit)

Stays abroad

Extended visits of members of the Walther-Meißner-Institute at foreign research laboratories:

1. **Hans Hübl**
   Centre for Quantum Computing and Communication Technology, University of New South Wales, Sydney, Australia
   08. 11. - 21. 11. 2018
2. **Stephan Geprägs**
   Institut Laue-Langevin, Grenoble, France
   20. 06. - 27. 06. 2018
3. **Mark Kartsovnik**
   Institute of Solid State Physics, Russian Academy of Sciences, Chernogolovka, Russia
   15. 08. - 31. 08. 2018
4. **Mark Kartsovnik**
   High Magnetic Field Laboratory, Grenoble, France
   29. 03. - 15. 04. 2018
5. **Rudolf Hackl**
   Institute of Physics, University of Belgrade, Serbia
   29. 05. - 04. 06. 2018, 06. 11. - 10. 11. 2018
6. **Rudolf Hackl**
   Stanford Institute of Materials and Energy Sciences (SIMES), Stanford Linear Accelerator Center (SLAC), Stanford, USA
   01. 03. - 04. 03. 2018, 18. 03. - 26. 03. 2018
7. **Rudolf Hackl**
   University of Florida, Gainesville, Florida, USA
   12. 03. - 17. 03. 2018

Conference Talks and Seminar Lectures

Matthias Althammer

1. **Magnetic insulators for dissipationless spintronics**
   Invited Talk, TO-BE Spring Meeting, Sant Feliu de Guixols, Spain
   14. 03. 2018

Frank Deppe

1. **Quantum communication with propagating microwaves**
   Invited Talk, DPG Spring Meeting, Berlin, Germany
   16. 03. 2018
2. **Measurements using squeezed microwaves**
   Invited Talk, Cryocourse 2018, Aalto University, Aalto, Finland
   26. 09. 2018

Andreas Erb

1. **Single crystal production of various oxide materials for basic research and applications**
   Invited Talk, 7^{th} French-German Workshop on Oxide, Dielectric and Laser Crystals 2018, Forschungsinstitut für mineralische und metallische Werkstoffe Edelsteine/Edelmetalle, Idar-Oberstein, Germany
   13. 09. 2018

Kirill Fedorov

1. **Remote state preparation with squeezed microwaves**
   Spring Meeting of the American Physical Society (APS), Los Angeles, USA
   06. 03. 2018

Stephan Geprägs

1. **Static Magnetic Proximity Effects and Spin Hall Magnetoresistance in Pt/$Y_3Fe_5O_{12}$**
   German Conference for Research with Synchrotron Radiation, Neutrons and Ion Beams at Large Facilities, Munich, Germany,
   16. - 19. 09. 2018
2. **Spin Hall Magnetoresistance in Heavy Metal/Magnetic Insulator Heterostructures**
   Workshop on Oxide Electronics, Les Diablerets, Swiss
   01. - 03. 10. 2018

Rudolf Gross

1. **Quantum Memories, Remote State Preparation and Selection Rules in Superconducting Quantum Circuits**
   Invited Talk, International Conference on Frontiers of Circuit QED and Optomechanics (FCQO 18)
   12 – 14 February 2018, Klosterneuburg, Austria.
2. **Superconducting Quantum Circuits**
   Invited Tutorial Lecture, Joint Meeting of the DPG and EPS Condensed Matter Divisions
   11 – 16 March 2018, Berlin, Germany.
3. **Quantum Microwave Communication with Superconducting Quantum Circuits**
   Invited Talk, Superconducting Quantum Technologies Conference
   29 July – 03 August 2018, Moscow, Russia.
4. **Quantum Computing with Superconducting Circuits**
   Invited Tutorial Lecture, DPG Physics School on Quantum Technologies
   05 – 10 August 2018, Bad Honnef, Germany.
5. **Highlights and Achievements in Quantum Nanophysics**
   NIM Conference on "The Future of Nanoscience"
   04 – 06 September 2018, Evangelische Akademie Tutzing, Germany.

6. **Auf dem Weg zum Quantencomputer**
   Public Lecture, Day of Open House at the Technical University of Munich
   13 October 2018, Garching Research Campus, Germany.
7. **Das Münchener Zentrum für Quanten-Wissenschaft und -Technologie: Heiße Forschung bei tiefen Temperaturen**
   Public Lecture, Day of Open House at the Technical University of Munich
   13 October 2018, Institute for Advanced Study, Garching Research Campus, Germany.
8. **Quantum Science, Technology and Engineering at the Technical University of Munich**
   Official Function "150 Jahre Physik an der TUM"
   08 November 2018, Institute of Advanced Study, Garching, Germany.
9. **Superconducting Quantum Technology: From Hot Dreams to Cool Reality**
   Physics Colloquium of the FAU Erlangen-Nuremberg
   28 November 2018, Erlangen, Germany.

Rudolf Hackl

1. **Spin Order and Fluctuations in FeSe**
   Spring Meeting of the American Physical Society (APS), Los Angeles, USA
   04. - 09. 03. 2018
2. **Magnetism, Nematicity and Fluctuations in FeSe**
   Invited Talk, 26th International Conference on Raman Spectroscopy, Jeju, Korea
   26. - 31. 08. 2018
3. **Fingerprints of Cooper Pairing in Iron-Based Superconductors**
   Invited Talk, 12th International Conference on Materials and Mechanisms of Superconductors, Beijing, China
   19. - 24. 08. 2018
4. **Fingerprints of Cooper Pairing in Iron-Based Superconductors**
   Seminar Talk, University of Florida, Gainesville, USA
   12. 03. 2018

Hans Hübl

1. **Controlling the collective coupling in spin-photon hybrids**
   Seminar Talk, University of Oxford, UK
   25. 01. 2018
2. **Hybrid Quantum Systems**
   Seminar Talk, Symposium Experimentalphysik, Universität Ulm, Germany
   11. 04. - 12. 04. 2018
3. **Magnons boosting spin-photon interaction**
   Seminar Talk, Austrian Academy of Science, Innsbruck, Austria
   30. 10. 2018
4. **Controlling the Collective Coupling in Spin-Photon Hybrids**
   Invited Talk, 658th WE-Heraeus Seminar, Bad Honnef, Germany
   07. 01. - 10. 01. 2018
5. **Stressing Spins and Tuning Strings**
   Invited Talk, International Conference Spin Mechanics 5, Chamonix, France
   11. 02. - 15. 02. 2018
6. **Defects in silicon - Old story or new horizons?**
   Spring Meeting of the American Physical Society (APS), Los Angeles, USA
   05. 03. - 09. 03. 2018
7. **Spin-Photon Hybrids**
   Invited Talk, SPICE Workshop on Cavity Spintronics, Mainz, Germany
   15. 05. 2018
8. **Progress Report on MaqSens**
   Invited Talk, Workshop on Quantum Engineering of Levitated Systems, Benasque, Spain
   16. 09. - 20. 09. 2018
9. **Spin Dynamics in Strongly Coupled Spin-Photon Hybrids**
   Silicon Quantum Electronics Workshop, University of New South Wales, Sydney, Australia

13. 11. - 15. 11. 2018

Daniel Jost

1. **Evolution of Pairing Interactions in Fe-Based Superconductors**
   Spring Meeting of the American Physical Society (APS), Los Angeles, USA
   04. 03. - 09. 03. 2018

Achim Marx

1. **Scalable 3D quantum memory**
   Spring Meeting of the American Physical Society (APS), Los Angeles, USA
   05. 03. 2018

Matthias Opel

1. **Spin Hall Magnetoresistance (SMR) in Antiferromagnetic NiO**
   DPG Spring Meeting, Berlin Germany
   16. 03. 2018
2. **Tiefe Temperaturen, Supraleitung und Spin-Elektronik**
   Invited Talk, MINT-Berufsinformationstag im Rahmen der "Humboldt Academy of Science and Engineering", Humboldt-Gymnasium Vaterstetten, Germany
   23. 03. 2018
3. **Spin Hall magnetoresistance (SMR) in antiferromagnetic NiO/Pt bilayers**
   Joint European Magnetic Symposia (JEMS 2018), Mainz, Germany
   06. 09. 2018

Nynke Vlietstra

1. **Impact of the magnetic sublattice configuration on the Spin-Hall Magnetoresistance**
   Spring Meeting of the American Physical Society (APS), Los Angeles, USA
   05. - 09. 03. 2018

Mathias Weiler

1. **Spin dynamics in a chiral magnonic crystal**
   Invited Talk, 658th WE-Heraeus Seminar, Bad Honnef, Germany
   09. 01. 2018
2. **Spin-torque excitation of spin waves at the YIG/Co interface**
   Invited Talk, Workshop on Nanomagnetics, Kaiserslautern, Germany
   20. 02. 2018
3. **Spin-torque excitation of spin waves at the YIG/Co interface**
   Invited Talk, IEEE International Conference on Microwave Magnetics, Exeter, U.K.
   25. 06. 2018
4. **Nanoscale spin waves in magnetic bilayers and chiral magnets**
   Invited Talk, Spin, waves and interactions, Greifswald, Germany
   29. 08. 2018
5. **Nanoscale spin waves in magnetic bilayers and chiral magnets**
   Seminar Talk, University of Regensburg, Germany
   10. 07. 2018
6. **Nanoscale spin waves in magnetic bilayers and chiral magnets**
   Invited Talk, University of Groningen, The Netherlands
   12. 09. 2018

Membership in Advisory Boards, Committees, etc.

1. **Frank Deppe** is Associate Member of the Cluster of Excellence *Nanosystems Initiative Munich (NIM)*.
2. **Frank Deppe** is Coordinator of the European Quantum Technology Flagship Project *Quantum Microwaves for Communication and Sensing (QMiCS)*.
3. **Andreas Erb** is spokesmen of the "Arbeitskreis Intermetallische und oxydische Systeme mit Spin- und Ladungskorrelationen" of the *Deutsche Gesellschaft für Kristallzüchtung und Kristallwachstum (DGKK)*.
4. **Rudolf Gross** is member of the Scientific Advisory Board of the Bayerisches Geoinstitut, Bayreuth, Germany.
5. **Rudolf Gross** is member of the Scientific Advisory Board of the Institut de Ciència de Materials de Barcelona, Spain.
6. **Rudolf Gross** is member of the committee for the allocation of Alexander von Humboldt Foundation Research Awards.
7. **Rudolf Gross** is member of the "Forum Technologie" of the Bavarian Academy of Sciences and Humanities.
8. **Rudolf Gross** is member of the Appointment and Tenure Board of the Technical University of Munich.
9. **Rudolf Gross** is member of the Executive Board of the Cluster of Excellence *Nanosystems Initiative Munich (NIM)* and coordinator of the Research Area 1 on *Quantum Nanosystems*.
10. **Rudolf Gross** is spokesperson of the Cluster of Excellence *Munich Center for Quantum Science and Technology (MCQST)*.
11. **Rudolf Gross** is member of the *Munich Quantum Center (MQC)*.
12. **Rudolf Gross** is course leader at the Ferienakademie of the Universities Munich (TU), Stuttgart and Erlangen-Nürnberg since 2005.
13. **Rudolf Hackl** is member of the evaluation board of the neutron source Heinz Maier-Leibnitz (FRM II).
14. **Hans Hübl** is member and Principal Investigator of the Cluster of Excellence *Nanosystems Initiative Munich (NIM)*.
15. **Hans Hübl** is member and Principal Investigator of the Cluster of Excellence *Munich Center for Quantum Science and Technology (MCQST)*.
16. **Mark Kartsovnik** is member of the Selection Committee of EMFL (European Magnetic Field Laboratories).
17. **Mark Kartsovnik** is member of the International Advisory Committee of the 13^{th} International Symposium on Crystalline Organic Metals Superconductors and Ferromagnets (ISCOM 2019).
18. **Matthias Opel** is one of the four elected members of the Speaker Council for the scientists of the Bavarian Academy of Sciences and Humanities.
19. **Mathias Weiler** is member of the Editorial Review Board of IEEE Magnetics Letters.

Teaching

Lectures, Courses and other Teaching Activities

Several members of the Walther-Meißner-Institute give lectures and seminars at the Technical University of Munich.

Matthias Althammer

WS 2017/2018	• Seminar: Spin Caloritronics and Spin Pumping (with H. Hübl, M. Weiler) • Seminar: Advances in Solid-State Physics (with R. Gross, H. Hübl, A. Marx, M. Opel, M. Weiler) • Seminar: Current Topics in Magneto and Spin Electronics (with H. Hübl, M. S. Brandt, M. Weiler)
SS 2018	• Seminar: Spin Caloritronics and Spin Pumbing (with H. Hübl, M. Weiler) • Seminar: Current Topics in Magneto and Spin Electronics (with M. Brandt, H. Hübl, M. Weiler) • Seminar: Advances in Solid-State Physics (with R. Gross, H. Hübl, A. Marx, M. Opel, M. Weiler)
WS 2018/2019	• Magnetismus (Magnetism) • Übungen zu Magnetismus (Magnetism, Problem Sessions) • Seminar: Spin Currents and Skyrmionics (with H. Huebl, M. Weiler) • Seminar: Advances in Solid-State Physics (with R. Gross, H. Hübl, A. Marx, M. Opel) • Seminar: Current Topics in Magneto and Spin Electronics (with H. Hübl, M. S. Brandt, M. Weiler)

Frank Deppe

WS 2017/2018	• Seminar: Superconducting Quantum Circuits (with R. Gross, A. Marx, K. Fedorov)
SS 2018	• Seminar: Superconducting Quantum Circuits (with R. Gross, A. Marx, K. Fedorov)
WS 2018/2019	• Seminar: Superconducting Quantum Circuits (with R. Gross, A. Marx, K. Fedorov)

Dietrich Einzel

WS 2017/2018	• Mathematische Methoden der Physik I (Mathematical Methods of Physics I) • Übungen zu Mathematische Methoden der Physik I (Mathematical Methods of Physics I, Problem Sessions)
SS 2018	• Mathematische Methoden der Physik II (Mathematical Methods of Physics II) • Übungen zu Mathematische Methoden der Physik II (Mathematical Methods of Physics II, Problem Sessions)
WS 2018/2019	• Mathematische Methoden der Physik I (Mathematical Methods of Physics I) • Übungen zu Mathematische Methoden der Physik I (Mathematical Methods of Physics I, Problem Sessions)

Kirill Fedorov

WS 2017/2018	• Seminar: Superconducting Quantum Circuits (with F. Deppe, R. Gross, A. Marx)

SS 2018
- Angewandte Supraleitung: Josephson Effekte, supraleitende Elektronik und supraleitende Quantenschaltkreise (Applied Superconductivity: Josephson Effects, Superconducting Electronics and Superconducting Quantum Circuits, with R. Gross)
- Seminar: Superconducting Quantum Circuits (with F. Deppe, R. Gross, A. Marx)

WS 2018/2019
- Seminar: Superconducting Quantum Circuits (with F. Deppe, R. Gross, A. Marx)

Rudolf Gross

WS 2017/2018
- Physik der Kondensierten Materie I (Condensed Matter Physics I)
- Übungen zu Physik der Kondensierten Materie I (Condensed Matter Physics I, Problem Sessions, with S. Geprägs)
- WMI Seminar on Modern Topics of Low Temperature Solid-State Physics (with R. Hackl, H. Hübl, A. Marx, M. Opel)
- Seminar: Advances in Solid-State Physics (with H. Hübl, A. Marx, M. Opel)
- Seminar: Superconducting Quantum Circuits (with F. Deppe, K. Fedorov, A. Marx)
- Festkörperkolloquium (Colloquium on Solid-State Physics, with D. Einzel)

SS 2018
- Physik der Kondensierten Materie II (Condensed Matter Physics II)
- Übungen zu Physik der Kondensierten Materie II (Condensed Matter Physics II, Problem Sessions, with S. Geprägs)
- Seminar: Advances in Solid-State Physics (with H. Hübl, A. Marx, M. Opel)
- WMI Seminar on Modern Topics of Low Temperature Solid-State Physics (with R. Hackl, H. Hübl, A. Marx, M. Opel)
- Seminar: Superconducting Quantum Circuits (with F. Deppe, K. Fedorov, A. Marx)
- Festkörperkolloquium (Colloquium on Solid-State Physics, with D. Einzel)
- Ferienakademie: Course 3 “Physics and Electronics in Everyday Life”

WS 2018/2019
- Physik der Kondensierten Materie I (Condensed Matter Physics I)
- Übungen zu Physik der Kondensierten Materie I (Condensed Matter Physics I, Problem Sessions, with S. Geprägs)
- WMI Seminar on Modern Topics of Low Temperature Solid-State Physics (with R. Hackl, H. Hübl, A. Marx, M. Opel)
- Seminar: Advances in Solid-State Physics (with H. Hübl, A. Marx, M. Opel)
- Seminar: Superconducting Quantum Circuits (with F. Deppe, K. Fedorov, A. Marx)
- Festkörperkolloquium (Colloquium on Solid-State Physics, with D. Einzel)

Rudi Hackl

WS 2017/2018
- Supraleitung und Tieftemperaturphysik I (Superconductivity and Low Temperature Physics I)
- Übungen zu Supraleitung und Tieftemperaturphysik I (Superconductivity and Low Temperature Physics I, Problem Sessions)
- WMI Seminar on Current Topics of Low Temperature Solid-State Physics (with R. Gross, H. Hübl, A. Marx, M. Opel)

SS 2018
- Supraleitung und Tieftemperaturphysik II (Superconductivity and Low Temperature Physics II)

- Übungen zu Supraleitung und Tieftemperaturphysik II (Superconductivity and Low Temperature Physics II, Problem Sessions)
- WMI Seminar on Current Topics of Low Temperature Solid-State Physics (with R. Gross, H. Hübl, A. Marx, M. Opel)
- Seminar: Advances in Solid-State Physics (with R. Gross, H. Hübl, A. Marx, M. Opel)

WS 2018/2019

- Seminar: Advances in Solid-State Physics (with R. Gross, H. Hübl, A. Marx, M. Opel)
- WMI Seminar on Current Topics of Low Temperature Solid-State Physics (with R. Gross, H. Hübl, A. Marx, M. Opel)

Hans Hübl

WS 2017/2018

- Seminar: Spin Caloritronics and Spin Pumping (with M. Althammer, M. Weiler)
- Seminar: Advances in Solid-State Physics (with R. Gross, A. Marx, M. Opel)
- WMI Seminar on Current Topics of Low Temperature Solid State Physics (with R. Gross, R. Hackl, A. Marx, M. Opel)
- Seminar: Current Topics in Magneto and Spin Electronics (with M. S. Brandt, M. Althammer, M. Weiler, S. Geprägs)

SS 2018

- Seminar: Spin Caloritronics and Spin Pumping (with M. Althammer, M. Weiler)
- Seminar: Advances in Solid-State Physics (with R. Gross, A. Marx, M. Opel)
- WMI Seminar on Current Topics of Low Temperature Solid State Physics (with R. Gross, R. Hackl, A. Marx, M. Opel)
- Seminar: Current Topics in Magneto and Spin Electronics (with M. S. Brandt, M. Althammer, M. Weiler, S. Geprägs)

WS 2018/2019

- Supraleitung und Tieftemperaturphysik I (Superconductivity and Low Temperature Physics I)
- Übungen zu Supraleitung und Tieftemperaturphysik I (Superconductivity and Low Temperature Physics I, Problem Sessions)
- Seminar: Spin Currents and Skyrmionics (with M. Althammer, M. Weiler, M. Opel, S. Geprägs)
- Seminar: Advances in Solid-State Physics (with R. Gross, A. Marx, M. Opel)
- WMI Seminar on Current Topics of Low Temperature Solid State Physics (with R. Gross, R. Hackl, A. Marx, M. Opel)
- Seminar: Current Topics in Magneto and Spin Electronics (with M. S. Brandt, M. Althammer, M. Weiler, S. Geprägs)

Mathias Weiler

WS 2017/2018

- Magnetismus (Magnetism)
- Übungen zu Magnetismus (Magnetism, Problem Sessions)
- Seminar: Spin Caloritronics and Spin Pumping (with M. Althammer, H. Hübl)
- Seminar: Current Topics in Magneto and Spin Electronics (with M. Althammer, H. Hübl, M. S. Brandt)

SS 2018

- Spin Elektronik (Spin Electronics)
- Übungen zu Spin Elektronik (Spin Electronics, Problem Sessions)

- Seminar: Spin Caloritronics and Spin Pumping (with M. Althammer, H. Huebl)
- Seminar: Current Topics in Magneto and Spin Electronics (with M. Althammer, H. Hübl, M. S. Brandt)

WS 2018/2019

- Seminar: Spin Currents and Skyrmionics (with M. Althammer, H. Hübl)
- Seminar: Current Topics in Magneto and Spin Electronics (with M. Althammer, H. Hübl, M. S. Brandt)

Seminars and Colloquia

A. Walther-Meißner-Seminar on Modern Topics in Low Temperature Physics WS 2017/2018, SS 2018 and WS 2018/2019

WS 2017/2018:

1. **Quenching the Stripes: Ultrafast Dynamics of Emergent Electronic and Vibrational Order**
   Dr. Robert Kaindl, E.O. Lawrence Berkeley National Laboratory, Berkeley, USA
   18. 10. 2017
2. **Growth of $GdBa_2Cu_3O_{7-\delta}$ Films on Hastelloy Metal Substrates**
   Oleksiy Troshyn, Theva Dünnschichttechnik GmbH, Ismaning, Germany
   20. 10. 2017
3. **Heat Transport in Insulating Powder Materials**
   Matthias Demharter, Bayerisches Zentrum für Angewandte Energieforschung, Garching, Germany
   10. 11. 2017
4. **A Transmon Quantum Annealer: Decomposing Many-Body Ising Constraints Into Pair Interactions**
   Dr. Martin Leib, Universität Innsbruck, Innsbruck, Austria
   14. 12. 2017
5. **Applications and Readout of Metallic Magnetic Calorimeters**
   Priv.-Doz. Dr. Sebastian Kempf, Universität Heidelberg, Heidelberg, Germany
   19. 01. 2018
6. **Superconducting Circuit Lattices with Nonlinear Couplers**
   Prof. Dr. Michael Hartmann, Heriot-Watt University, Edinburgh, United Kingdom
   26. 01. 2018
7. **Deterministic Quantum State Transfer and Generation of Remote Entanglement using Microwave Photons**
   Prof. Dr. Andreas Wallraff, ETH Zurich, Zurich, Switzerland
   16. 02. 2018
8. **Suppressing Quasiparticle-Noise of the Environment in Superconducting Qubits**
   Amin Hosseinkhani, Forschungszentrum Jülich, Jülich, Germany
   09. 03. 2018

SS 2018:

9. **Experimental determination of the magnon spin diffusion length by the local and nonlocal spin Seebeck effects**
   Dr. Timo Kuschel, Universität Bielefeld, Bielefeld, Germany
   20.04.2018
10. **Dynamical signatures of topologically ordered phases**
    Prof. Dr. Frank Pollmann, Technische Universität, München, Germany
    02. 05. 2018
11. **Generation and Distribution of Nonclassical Microwave States**
    Prof. Dr. Christopher Wilson, University of Waterloo, Ontario, Canada
    09. 05. 2018
12. **Control of Quantum Devices: Merging Pulse Calibration and System Characterization using Optimal Control**
    Dr. Shai Machnes, Universität des Saarlandes, Saarbrücken, Germany
    18. 05. 2018
13. **Superconducting Qubits for Analog Quantum Simulation**
    Prof. Dr. Gerhard Kirchmair, Institut für Quantenoptik und Quanteninformation, Innsbruck, Austria
    30. 05. 2018

14. **A new approach to design ceramics with a giant magnetoelectric response**
Prof. Dr. Rajeev Ranjan, Indian Institute of Science, Bangalore, India
22. 06. 2018
15. **Magnetization Dynamics in Nanostructures and Thin Films**
Dr. Hans Nembach, National Institute of Standards and Technology, Boulder, USA
06. 07. 2018
16. **Kostenanalyse und Fahrerassistenzsysteme innerhalb der BMW Group**
Dr. Thomas Niemczyk, BMW Group München, Germany
13. 07. 2018
17. **Spin pumping and proximity effect in ferrimagnet-(super)conductor hybrids**
Dr. Akashdeep Kamra, Norwegian University of Science and Technology, Trondheim, Norway
20. 07. 2018
18. **2-Input-2-Output Quantum Feedback Amplification and Coherent PID Feedback Control**
Yuki Nojiri, Keio University, Yokohama, Japan
08. 08. 2018
19. **Wiener meets Schrödinger**
Qi-Ming Chen, Princeton University, NJ, USA
14. 08. 2018
20. **Heat Control Techniques for Superconducting Microwave Circuits**
Matti Partanen, Aalto University, Aalto, Finland
28. 08. 2018

WS 2018/2019:

21. **Charakterisierung von DC-SQUIDs aus granularem Aluminium**
Felix Friedrich, Karlsruher Institut für Technologie, Karlsruhe, Germany
13. 11. 2018
22. **Tip enhanced near-field optical spectroscopy**
Dr. Kai Braun, Institut für Physikalische und Theoretische Chemie, Tübingen, Germany
07. 12. 2018
23. **Possible proximity effect in a nanoscale-size superconductor semiconductor ring devices**
Dr. Michael Stuiber, University of Melbourne, Australia
14. 12. 2018

B. Topical Seminar on Advances in Solid State Physics WS 2017/2018, SS 2018 and WS 2018/2019

WS 2017/2018:

1. **Preliminary discussion and assignment of topics**
R. Gross, Walther-Meißner-Institute
17. 10. 2017 and 24. 10. 2017
2. **Demonstration of an ac Josephson junction laser**
Lucas Hollender, Technical University of Munich
05. 12. 2017

SS 2018:

3. **Preliminary discussion and assignment of topics**
R. Gross, Walther-Meißner-Institute
10. 04. 2018 and 17. 04. 2018
4. **Quantum correlations from a room-temperature optomechanical cavity**
Christopher Waas, Technical University of Munich
08. 05. 2018

5. **Towards phase-coherent caloritronics in superconducting circuits**
   Leander Peis, Technical University of Munich
   15. 05. 2018
6. **Spin Transfer due to Quantum Magnetization Fluctuations**
   Manuel Müller, Technical University of Munich
   29. 05. 2018
7. **Do Quantum Spin Liquids Exist**
   Joop Adema, Technical University of Munich
   05. 06. 2018
8. **Real-space imaging of non-collinear antiferromagnetic order with a single-spin magnetometer**
   Maxim Dietlein, Technical University of Munich
   12. 06. 2018
9. **Shubnikov-de Haas quantum oscillations reveal a reconstructed Fermi surface near optimal doping in a thin film of the cuprate superconductor Pr1.86Ce0.14CuO4+?**
   Raffael Ferdigg, Technical University of Munich
   12. 06. 2018
10. **Unidirectional spin Hall magnetoresistance in ferromagnet/normal metal bilayers**
    Laura Wagner, Technical University of Munich
    19. 06. 2018
11. **Unconventional superconductivity in magic-angle graphene superlattices**
    Pablo Cova, Technical University of Munich
    19. 06. 2018
12. **Interface-driven topological Hall effect in SrRuO3-SrIrO3**
    Mark Kamper, Technical University of Munich
    26. 06. 2018
13. **Thermal Conductance of a Single-Electron Transistor**
    Natalie Galfe, Technical University of Munich
    26. 06. 2018
14. **Collapse of Ferromagnetism and Fermi Surface Instability near Reentrant Superconductivity of URhGe**
    Ludwig Holleis, Technical University of Munich
    03. 07. 2018
15. **Insulating Nanomagnets Driven by Spin Torque**
    Christoph Scheuer, Technical University of Munich
    03. 07. 2018

WS 2018/2019:

16. **Preliminary discussion and assignment of topics**
    R. Gross, Walther-Meißner-Institute
    16. 10. 2018 and 23. 10. 2018
17. **Superconductivity at 215 K in lanthanum hydride at high pressure**
    Raffael Ferdigg, Technical University of Munich
    11. 12. 2018
18. **Tunable long-distance spin transport in a crystalline antiferromagnetic iron oxide**
    Thomas Narr, Technical University of Munich
    18. 12. 2018

C. Topical Seminar: Spin Caloritronics and Spin Pumping WS 2017/2018 and SS 2018

WS 2017/2018:

1. **Preliminary discussion and assignment of topics**
   Mathias Weiler, Matthias Althammer, Stephan Geprägs, Hans Hübl, Walther-Meißner-Institute

19. 10. 2017 and 26. 10. 2017

2. **Kittens on the rise**
   Natalie Segercrantz, Walther-Meißner-Institute
   16. 11. 2017
3. **Magnetoelasticity in Nanostrings**
   Daniel Schwienbacher, Walther-Meißner-Institute
   23. 11. 2017
4. **TBA**
   Lisa Rosenzweig, Walther-Meißner-Institute
   30. 11. 2017
5. **Magnon-Phonon Coupling in Nanostructures**
   Thomas Luschmann, Walther-Meißner-Institute
   11. 01. 2018
6. **TBA**
   Luis Flacke, Walther-Meißner-Institute
   25. 01. 2018
7. **Non-local Magnetoresistance**
   Birte Cöster, Walther-Meißner-Institute
   01. 02. 2018
8. **Magnon-Phonon Coupling in Nanostructures**
   Thomas Luschmann, Walther-Meißner-Institute
   01. 02. 2018

SS 2018:

9. **Preliminary discussion and assignment of topics**
   Mathias Weiler, Matthias Althammer, Stephan Geprägs, Hans Hübl, Walther-Meißner-Institute
   12. 04. 2018 and 19. 04. 2018
10. **Magnetization dynamics in CSO**
    Lukas Liensberger, Walther-Meißner-Institute
    24. 05. 2018
11. **Quantifying vibrations in cryogenics environments**
    Korbinian Rubenbauer, Walther-Meißner-Institute
    07. 06. 2018
12. **Superconducting properties of NbN thin films**
    Michael Reichert, Walther-Meißner-Institute
    07. 06. 2018
13. **Excitation transfer in coupled nanostrings**
    Thomas Luschmann, Walther-Meißner-Institute
    14. 06. 2018
14. **Spin current transport in insulating magnets**
    Tobias Wimmer, Walther-Meißner-Institute
    28. 06. 2018
15. **Tailoring superconducting resonators for magnetic resonance**
    Stefan Weichselbaumer, Walther-Meißner-Institute
    05. 07. 2018
16. **Efficient microwaves antennas for spin dynamics**
    David Rogerson, Walther-Meißner-Institute
    05. 07. 2018
17. **Observing magnetization in nanostructures**
    Nynke Vlietstra, Walther-Meißner-Institute
    12. 07. 2018

C. Topical Seminar: Spin Currents and Skyrmionics WS 2018/2019

WS 2018/2019:

1. **Preliminary discussion and assignment of topics**
   Mathias Weiler, Matthias Althammer, Stephan Geprägs, Hans Hübl, Walther-Meißner-Institute
   18. 10. 2018 and 25. 10. 2018
2. **Ultra-enhanced spin transport in YIG**
   Tobias Wimmer, Walther-Meißner-Institute
   22. 11. 2018
3. **Controlling the magnon transport in YIG**
   Nynke Vlietstra, Walther-Meißner-Institute
   06. 12. 2018
4. **Low damping in a metallic ferromagnet**
   Luis Flacke, Walther-Meißner-Institute
   13. 12. 2018
5. **Mode hybridization in GdIG**
   Lukas Liensberger, Walther-Meißner-Institute
   10. 01. 2019
6. **Magnon-Photon coupling in a superconducting resonator**
   Mohammad Amawi, Walther-Meißner-Institute
   17. 01. 2019
7. **Spin pumping in superconductor/ferromagnet hybrids**
   Manuel Müller, Walther-Meißner-Institute
   24. 01. 2019
8. **NbN superconducting resonators**
   Andreas Faltermeier, Walther-Meißner-Institute
   31. 01. 2019

D. Topical Seminar on Superconducting Quantum Circuits WS 2017/2018, SS 2018 and WS 2018/2019

WS 2017/2018:

1. **Preliminary discussion and assignment of topics**
   F. Deppe, A. Marx, R. Gross, Walther-Meißner-Institute
   17. 10. 2017 and 24. 10. 2017
2. **Approaching ultrastrong coupling in transmon circuit QED using a high impedance resonator**
   Philip Schmidt, Walther-Meißner-Institute
   19. 12. 2017
3. **Strain Coupling of a Mechanical Resonator to a Single Quantum Emitter in Diamond**
   Daniel Schwienbacher, Walther-Meißner-Institute
   16. 01. 2018
4. **Converting Quasiclassical States into Arbitrary Fock State Superpositions in a Superconducting Circuit**
   Edwar Xie, Walther-Meißner-Institute
   23. 01. 2018
5. **Observation of a Dissipative Phase Transition in a One-Dimensional Circuit QED Lattice**
   Michael Fischer, Walther-Meißner-Institute
   30. 02. 2018
6. **Coherent Rabi dynamics of a superradiant spin ensemble in a microwave cavity**
   Stefan Weichselbaumer, Walther-Meißner-Institute
   06. 02. 2018
7. **Intracity Quantum Communication via Thermal Microwave Networks**

Stefan Pogorzalek, Walther-Meißner-Institute
13. 02. 2018

SS 2018:

8. **Preliminary discussion and assignment of topics**
F. Deppe, A. Marx, R. Gross, Walther-Meißner-Institute
10. 04. 2018 and 17. 04. 2018
9. **Effect of Higher-Order Nonlinearities on Amplification and Squeezing in Josephson Parametric Amplifiers**
Stefan Pogorzalek, Walther-Meißner-Institute
08. 05. 2018
10. **Dissipative quantum reservoir for microwave light using mechanical resonators**
Philip Schmidt, Walther-Meißner-Institute
29. 05. 2018
11. **Quantum acoustics with superconducting qubits**
Robert Neagu, Technical University of Munich
12. 06. 2018
12. **Mechanical on-chip microwave circulator**
Daniel Schwienbacher, Walther-Meißner-Institute
26. 06. 2018
13. **Implementing a universal gate set on a logical qubit encoded in an oscillator**
Iman Afroozeh Borojeni, Technical University of Munich
03. 07. 2018
14. **Long-range spin wave mediated control of defect qubits in nanodiamonds**
Stefan Weichselbaumer, Walther-Meißner-Institute
17. 07. 2018

WS 2018/2019:

15. **Preliminary discussion and assignment of topics**
F. Deppe, A. Marx, R. Gross, Walther-Meißner-Institute
16. 10. 2018 and 23. 10. 2018
16. **Superradiant emission of color centers in diamond**
Stefan Weichselbaumer, Walther-Meißner-Institute
13. 11. 2018
17. **Programmable interference between two microwave quantum memories**
Edwar Xie, Walther-Meißner-Institute
27. 11. 2018
18. **Control of two-non-linear resonators**
Stefanie Grotowski, Walther-Meißner-Institute
04. 12. 2018
19. **Universal Stabilization of a Parametrically Coupled Qubit**
Saibin Zhou, Technical University of Munich
11. 12. 2018
20. **Deterministic quantum state transfer and remote**
Yu Zhu, Technical University of Munich
18. 12. 2018
21. **Strong Coupling Cavity QED with Gate-Defined Double Quantum Dots Enabled by a High Impedance Resonator**
Patrick Schnierle, Technical University of Munich
15. 01. 2019
22. **Cavity quantum acoustic device in the multimode strong coupling regime**
Philip Schmidt, Walther-Meißner-Institute
22. 01. 2019

23. **Stroboscopic Qubit Measurements with Squeezed Illumination**
Stefan Pogorzalek, Walther-Meißner-Institute
29. 01. 2019

E. Solid State Colloquium

The WMI has organized the Solid-State Colloquium of the Faculty of Physics in WS 2017/2018, SS 2018, and WS 2018/2019. The detailed program can be found on the WMI webpage: http://www.wmi.badw-muenchen.de/teaching/Seminars/fkkoll.html.

Staff

Staff of the Walther-Meißner-Institute

Director
Prof. Dr. Rudolf Gross

Deputy Director
Priv.-Doz. Dr. habil. Hans Hübl

Technical Director
Dr. Achim Marx

The deputy director, the technical director and the elected representative of the scientific staff (Dr. Matthias Opel) are members of the WMI Executive Committee and support the director in the management of WMI.

Administration/Secretary's Office
Ludwig Ossiander
Emel Dönertas

Scientific Staff
Dr. Matthias Althammer
Dr. Andreas Baum
Priv.-Doz. Dr. habil. Frank Deppe
Prof. Dr. Andreas Erb
Dr. Kirill Fedorov
Dr. Stephan Geprägs
Priv.-Doz. Dr. habil. Rudolf Hackl
Dr. Mark Kartsovnik
Dr. Matthias Opel
Dr. Natalie Segercrantz
Dr. Nynke Vlietstra
Dr. Mathias Weiler
M. Sc. Michael Fischer
M. Sc. Luis Flacke
M. Sc. Daniel Jost
M. Sc. Lukas Liensberger
M. Sc. Stefan Pogorzalek
M. Sc. Gabriele Rager
M. Sc. Michael Renger
M. Sc. Philip Schmidt
M. Sc. Daniel Schwienbacher
M. Sc. Stefan Weichselbaumer
M. Sc. Tobias Wimmer
M. Sc. Eduard Xie

Technical Staff
Peter Binkert
Thomas Brenninger, M.Sc.
Dieter Guratzsch
Astrid Habel
Dipl.-Ing. (FH) Josef Höss
Sebastian Kammerer
Christoph Kastl
Robert Müller
Jan Naundorf
Georg Nitschke
Christian Reichlmeier
Alexander Rössl
Andreas Russo
Harald Schwaiger
Helmut Thies

Assistants
Sybilla Plöderl
Maria Botta

Permanent Guests
Dr. Werner Biberacher
Prof. Dr. Dietrich Einzel
Dr. Kurt Uhlig
Prof. Dr. B.S. Chandrasekhar
Prof. Dr. Anton Lerf

Guest Researchers

1. Dr. Werner Biberacher
   permanent guest
2. Prof. Dr. B.S. Chandrasekhar
   permanent guest
3. Prof. Dr. Dietrich Einzel
   permanent guest
4. Prof. Dr. Anton Lerf
   permanent guest
5. Dr. Kurt Uhlig
   permanent guest
6. Dr. Aisha Aqeel, Universität Regensburg, Regensburg, Germany
   15. 01. - 20. 01. 2018
7. Prof. Vladimir Zverev, Institute of Solid Physics, Chernogolovka, Russia
   19. 03. - 22. 04. 2018
8. Dr. Nedad Lazarevic, University of Belgrade, Belgrade, Serbia
   25. 04. - 10. 05. 2018, 13. 07. - 05. 08. 2018
9. Prof. T.P. Devereaux, Stanford Institute of Materials and Energy Science (SIMES), Stanford University, Stanford, USA
   06. 06. - 10. 06. 2018
10. Dr. Brain Moritz, Stanford Institute of Materials and Energy Science (SIMES), Stanford University, Stanford, USA
    15. 06. - 25. 06. 2018
11. MSc. Ana Milosovjevic, University of Belgrade, Belgrade, Serbia
    13. 07. - 25. 07. 2018
12. Dr. Akashdeep Kamra, Norwegian University, Trondheim, Norway
    16. 07. - 20. 07. 2018
13. Paul Rosenberger, Forschungszentrum Jülich, Jülich, Germany
    30. 07. - 03. 08. 2018
14. Qiming Chen, Tsinghua University, Beijing, China
    13. 08. - 15. 08. 2018
15. Matti Partanen, Aalto University, Aalto, Finland
    27. 08. - 30. 08. 2018
16. Ei Shigematsu, Kyoto University, Kyoto, Japan
    01. 07. - 13. 08. 2018, 28. 09. - 26. 10. 2018
17. Dr. Toni Helm, Max-Planck-Institut für Chemische Physik fester Stoffe, Dresden, Germany
    03. 09. - 06. 09. 2018
18. Prof. Zoran Popovic, University of Belgrade, Belgrade, Serbia
    26. 11. - 05. 12. 2018

Scientific Advisory Board & Executive Committee

Scientific Advisory Board

According to the statutes of the Bavarian Academy of Sciences and Humanities (BAdW) the Scientific Advisory Board evaluates the quality of the scientific work of Walther-Meißner-Institute (WMI) and gives advice to its Executive Committee to provide scientific quality assurance. The Scientific Advisory Board regularly reports to the Research Committee of BAdW.

The members of the Scientific Advisory Board include members of BAdW with appropriate scientific background, representatives of the two Munich universities (TUM and LMU), as well as leading national and international scientists. They are appointed by the Section III "Naturwissenschaften, Mathematik, Technikwissenschaften" of BAdW for five years. The director of WMI is a consultive member of the WMI Scientific Advisory Board. The Scientific Advisory Board is headed by a chairperson and deputy chairperson. They are elected by the Section III "Naturwissenschaften, Mathematik, Technikwissenschaften" of BAdW for five years at the suggestion of the members of the WMI Scientific Advisory Board. The chairperson of the Scientific Advisory Board must be a member of BAdW.

The present members of the WMI Scientific Advisory Board are:

- **Vollhardt, Dieter**, chairman (BAdW, University of Augsburg)
- **Abstreiter, Gerhard**, deputy chairman (BAdW, Technical University of Munich)
- **Bloch, Immanuel** (BAdW, LMU Munich and Max-Planck-Institute of Quantum Optics)
- **Bühler-Paschen, Silke** (Technical University of Vienna)
- **Finley, Jonathan** (Technical University of Munich)
- **Gross, Rudolf**, consultive member (BAdW, Technical University of Munich)
- **Hänsch, Theodor** (BAdW, LMU Munich and Max-Planck-Institute of Quantum Optics)
- **Schwoerer, Markus** (BAdW, University of Bayreuth)
- **Wallraff, Andreas** (ETH Zurich)
- **Weiss, Dieter** (University of Regensburg)
- **Zinth, Wolfgang** (BAdW, LMU Munich)

Executive Committee

The Walther-Meißner-Institute is headed by the scientific director who is responsible for the development and implementation of the research program. He holds a full professor position at one of the Munich universities (TUM or LMU). He is appointed in a joint process of the respective university and BAdW. The director is supported by the deputy director, the technical director and an elected representative of the scientific staff. They are appointed by the Section III "Naturwissenschaften, Mathematik, Technikwissenschaften" of BAdW for five years at the suggestion of the members of the WMI Scientific Advisory Board.

The present members of the WMI Executive Committee are:

- **Gross, Rudolf**, director
- **Hübl, Hans**, deputy director
- **Marx, Achim**, technical director
- **Opel, Matthias**, representative of the scientific staff

Contact:

Walther–Meißner–Institut
Bayerische Akademie der Wissenschaften
Walther–Meißner–Str. 8
D - 85748 Garching
GERMANY

Phone: +49 – (0)89 289 14201
Fax: +49 – (0)89 289 14206
E–mail: Sekretariat@wmi.badw.de

www.wmi.badw.de

Published by:

Walther–Meißner–Institut
Walther–Meißner–Str. 8, D - 85748 Garching
December 2018